

SPACE- AND ENERGY-DEPENDENT NOISE ANALYSIS  
USING MODAL EXPANSIONS

A THESIS

Presented to

The Faculty of the Graduate Division

by

David Dean Ebert

In Partial Fulfillment  
of the Requirements for the Degree  
Doctor of Philosophy  
in the School of Nuclear Engineering

Georgia Institute of Technology

December, 1971

SPACE- AND ENERGY-DEPENDENT NOISE ANALYSIS  
USING MODAL EXPANSIONS

Date approved by Chairman:

*Jan 16 1972*

In presenting the dissertation as a partial fulfillment of the requirements for an advanced degree from the Georgia Institute of Technology, I agree that the Library of the Institute shall make it available for inspection and circulation in accordance with its regulations governing materials of this type. I agree that permission to copy from, or to publish from, this dissertation may be granted by the professor under whose direction it was written, or, in his absence, by the Dean of the Graduate Division when such copying or publication is solely for scholarly purposes and does not involve potential financial gain. It is understood that any copying from, or publication of, this dissertation which involves potential financial gain will not be allowed without written permission.

7/25/68

## ACKNOWLEDGMENTS

The research work described herein would not have been possible without the support and assistance of many individuals and organizations. Dr. Joseph D. Clement, serving as my thesis advisor, provided much technical assistance throughout the entire course of this investigation. Special thanks are extended to Dr. Weston M. Stacey, Jr. of Argonne National Laboratory for initiating me to the subject matter of this thesis and for his continuing interest and help. Dr. Lawrence J. Gallaher provided many helpful suggestions in particular areas of this work. I would also like to thank Drs. W. Waverly Graham, III and John M. Kallfelz in addition to Drs. Clement, Stacey, and Gallaher for serving on my reading committee. The very careful review of the manuscript by Dr. Geoffrey G. Eichholz is greatly appreciated. Dr. Carlyle J. Roberts, past Director of the School of Nuclear Engineering, not only generously lent financial support but kept my morale from sagging too low. Some financial support was given to me by Dr. Merlin D. Peterson at the Argonne Center for Educational Affairs. The computer time provided by the Rich Electronic Computer Center is acknowledged.

I am most grateful to my friends Drs. Donald N. Bridges and Gabriel H. Weaver and Messrs. Anthony J. Foltman, John P. Renier, and J. Martin Reynolds for their help and interest in this work. I would particularly like to express my sincere gratitude to Mr. Reynolds for the great amount of time and energy expended in helping me understand and use his Fast

Fourier Transform Routine.

The encouragement which I received early in this work from Drs. Norbert J. Ackermann, Anthony R. Buhl, James C. Robinson, and Dominique P. Roux of Oak Ridge National Laboratory, Dr. James R. Sheff of Battelle and Dr. Richard A. Danofsky of Iowa State University is gratefully appreciated. The continuing interest of Drs. Ackermann and Danofsky throughout the entire thesis effort has been very encouraging. I would also like to extend my thanks to Dr. Robert W. Albrecht of the University of Washington and Dr. Paul M. Ebert of Bell Telephone Laboratory for their enlightening discussions on some aspects of this work. The assistance of Drs. D. Stegmann and M. Edelmann in procuring data on the Argonaut Reactor Karlsruhe is also acknowledged.

I am very indebted to Dr. John A. Burke of Knolls Atomic Power Laboratory and Dr. Roger A. Rydin, formerly of KAPL and now at the University of Virginia, for their assistance in supplying and helping me analyze and interpret the KAPL noise data. I would have only "half a thesis" without their and Knolls Atomic Power Laboratory's effort. In addition, the critical review and resulting discussions of the manuscript by Dr. Rydin helped greatly in clarifying a number of complicated points.

I thank Mrs. Maggie Luebs of Argonne National Laboratory for the generous donation of her spare time in typing the first draft of this thesis and Mrs. Lydia Geeslin who did a very precise job in typing the final draft. Mr. George Rothe did a fine job of drawing many of the figures.

This work was chiefly supported by an Atomic Energy Commission

Traineeship with the assistance of a Graduate Research Assistantship.

Lastly, I extend my most deep appreciation to my parents who kept faith in me through this seemingly unending period of study.

## TABLE OF CONTENTS

	Page
ACKNOWLEDGMENTS. . . . .	ii
LIST OF TABLES . . . . .	viii
LIST OF ILLUSTRATIONS. . . . .	ix
SUMMARY. . . . .	xiv
Chapter	
I. INTRODUCTION. . . . .	1
II. HISTORICAL DEVELOPMENT OF NOISE THEORIES AND EXPERIMENTS FOR ZERO-POWER REACTORS . . . . .	8
Background and Definitions. . . . .	8
Differential Methods. . . . .	12
Integral Methods. . . . .	14
The Noise-Equivalent-Source Method. . . . .	16
The Quantum-Liouville Method. . . . .	19
III. THEORETICAL DEVELOPMENT . . . . .	21
Fundamental Assumptions . . . . .	22
Time- and Frequency-Domain Relations. . . . .	22
Modal Expansion Approximation . . . . .	28
Covariance	
Variance	
Cross-Covariance	
Auto-Covariance	
Cross-Power-Spectral-Density	
Auto-Power-Spectral-Density	
Point Reactor Approximation . . . . .	33
Covariance	
Variance	
Cross-Covariance	
Auto-Covariance	
Cross-Power-Spectral-Density	
Auto-Power-Spectral-Density	
Discussion. . . . .	36

## TABLE OF CONTENTS (Continued)

Chapter	Page
IV. EXACT SOLUTION OF THE COHERENCE FUNCTION. . . . .	38
Reactor Diagrams and Nuclear Constants. . . . .	38
Method of Solution and Results. . . . .	46
Absolute Magnitudes of the Exact Coherence Function	
Phase Angles of the Exact Coherence Function	
Discussion. . . . .	66
V. MODAL APPROXIMATION OF THE COHERENCE FUNCTION . . . . .	71
Method of Solution and Results. . . . .	72
Two-Mode Expansion Approximation. . . . .	94
Null Frequency Conditions	
Reactor Parameter Extraction Methods	
Eigenvalue Separation	
Effective Delayed Neutron Fraction and Neutron Generation Time	
Discussion. . . . .	110
VI. INTERPRETATION OF THE NOISE EXPERIMENTS . . . . .	115
Fast Fourier Transformation Procedure and Results . . . . .	115
Reactor Parameter Extraction and Results. . . . .	119
Discussion. . . . .	128
VII. CONCLUSIONS . . . . .	132
VIII. RECOMMENDATIONS . . . . .	137
APPENDICES . . . . .	141
A. BASIC RELATIONS OF RANDOM NOISE THEORY. . . . .	142
Average or Mean . . . . .	142
Variance. . . . .	142
Covariance. . . . .	143
Modified Coefficient of Correlation . . . . .	143
Auto-Covariance . . . . .	143
Gross-Covariance. . . . .	144
Auto-Correlation Function . . . . .	144
Gross-Correlation Function. . . . .	144
Auto-Power-Spectral-Density . . . . .	145
Cross-Power Spectral-Density. . . . .	145
Coherence Function. . . . .	145

## TABLE OF CONTENTS (Concluded)

Appendices	Page
B. MODAL EXPANSION APPROXIMATIONS OF SPACE- ENERGY-TIME REACTOR KINETICS. . . . .	146
Modal Expansion Approximations. . . . .	148
Natural Modes	
Omega Modes	
Lambda Modes	
Discussion. . . . .	154
C. MODAL EXPANSION APPROXIMATION OF THE GREEN'S FUNCTION. . . . .	155
D. DERIVATION OF THE POINT REACTOR COVARIANCE. . . . .	159
E. EXACT SOLUTION OF THE GREEN'S FUNCTION IN ONE-DIMENSIONAL REACTOR GEOMETRY . . . . .	162
F. GENERATION OF THE EIGENVALUES AND EIGENVECTORS. . . . .	168
G. FAST FOURIER TRANSFORM. . . . .	173
Discrete Time and Frequency Relationships . . . . .	173
Digital Computations and the FFT. . . . .	179
H. PHASE ANGLE INVESTIGATION . . . . .	183
BIBLIOGRAPHY . . . . .	188
VITA . . . . .	199

## LIST OF TABLES

Table	Page
1. ARK Nuclear Constants . . . . .	44
2. SHA Core 35A' Nuclear Constants . . . . .	47
3. Results of a Biorthogonality Check on Some Modified Omega Modes of the SHA Core 35A' . . . . .	82
4. Results of a Biorthogonality Check on Some Lambda Modes of the SHA Core 35A' . . . . .	82
5. Results of a Finality Check on Some Lambda Modes of the SHA Core 35A'. . . . .	83
6. Results of a Biorthogonality Check on Some Modified Omega Modes of the ARK . . . . .	83
7. Results of a Biorthogonality Check on Some Lambda Modes of the ARK . . . . .	84
8. Results of a Finality Check on Some Lambda Modes of the ARK. . . . .	84
9. Calculated Terms for Some Expansion Modes of the SHA Core 35A'. . . . .	105
10. Calculated Terms for Some Expansion Modes of the ARK. . . . .	106
11. Summary of the Noise Results. . . . .	125

## LIST OF ILLUSTRATIONS

Figure	Page
1. Typical Coherence Function Plot for a Coupled Core Reactor. . . . .	19
2. Detailed Schematic of the SHA Core 35A' . . . . .	40
3. Detailed Schematic of the Two-Slab ARK. . . . .	41
4. One-Dimensional Representation of the SHA Core 35A'. . . . .	42
5. One-Dimensional Representation of the Two-Slab ARK . . . . .	42
6. Calculated Fast and Thermal Fluxes in the Two-Slab ARK. . . . .	45
7. Calculated and Measured Fast and Thermal Fluxes in the SHA Core 35A'. . . . .	45
8. Exact $ R^{(2,2)}(x_1, -x_1, \omega) $ for the SHA Core 35A'-Varying Symmetric Detector Separation Distances . . . . .	50
9. Exact $ R^{(2,2)}(x_1, -x_1, \omega) $ for the ARK-Varying Symmetric Detector Separation Distances . . . . .	50
10. Exact $ R^{(2,2)}(x_1, x_1, \omega) $ for the SHA Core 35A'-Asymmetric Detector Locations $-x_1 = -72.5$ cm; $x_j =$ Variable . . . . .	53
11. Exact $ R^{(2,2)}(x_1, x_1, \omega) $ for the SHA Core 35A'-Asymmetric Detector Locations $-x_1 = -52.5$ cm; $x_j =$ Variable . . . . .	53
12. Exact $ R^{(2,2)}(x_1, x_1, \omega) $ for the SHA Core 35A'-Asymmetric Detector Locations $-x_1 = -37.5$ cm; $x_j =$ Variable . . . . .	54
13. Exact $ R^{(2,2)}(x_1, x_1, \omega) $ for the SHA Core 35A'-Asymmetric Detector Locations $-x_1 = -12.5$ cm; $x_j =$ Variable . . . . .	54

## LIST OF ILLUSTRATIONS (Continued)

Figure	Page
14. Exact $ R^{(2,2)}(x_i, x_j, \omega) $ for the SHA Core 35A'- Asymmetric Detector Locations $x_i = -2.5$ cm; $x_j =$ Variable . . . . .	55
15. Exact $ R^{(2,2)}(x_i, x_j, \omega) $ for the ARK-Asymmetric Detector Locations $x_i = -92.5$ cm; $x_j =$ Variable . . . . .	55
16. Exact $ R^{(2,2)}(x_i, x_j, \omega) $ for the ARK-Asymmetric Detector Locations $x_i = -32.5$ cm; $x_j =$ Variable . . . . .	56
17. Exact $ R^{(2,2)}(x_i, x_j, \omega) $ for the ARK-Asymmetric Detector Locations $x_i = -2.5$ cm; $x_j =$ Variable. . . . .	56
18. Exact $ R^{(2,2)}(x_i, x_j, \omega) $ for the SHA Core 35A'- Selected Frequencies and Asymmetric Detector Locations $x_i = -52.5$ cm; $x_j =$ Variable. . . . .	58
19. Exact $ R^{(2,2)}(x_i, x_j, \omega) $ for the SHA Core 35A'- Selected Frequencies and Asymmetric Detector Locations $x_i = -72.5$ cm; $x_j =$ Variable. . . . .	58
20. Exact $ R^{(2,2)}(x_i, x_j, \omega) $ for the ARK-Selected Frequencies and Asymmetric Detector Locations- $x_i = -32.5$ cm; $x_j =$ Variable. . . . .	59
21. Exact $ R^{(2,2)}(x_i, x_j, \omega) $ for the ARK-Selected Frequencies and Asymmetric Detector Locations- $x_i = -92.5$ cm; $x_j =$ Variable. . . . .	59
22. Exact $\theta R^{(1,2)}(x_i, x_i, \omega)$ for the SHA Core 35A'- $x_i =$ Variable . . . . .	62
23. Exact $\theta R^{(1,2)}(x_i, x_i, \omega)$ for the ARK- $x_i =$ Variable. . . . .	62
24. Exact $\theta R^{(2,2)}(x_i, x_j, \omega)$ for the SHA Core 35A'- Asymmetric Detector Locations $x_i = -72.5$ cm; $x_j =$ Variable . . . . .	64
25. Exact $\theta R^{(2,2)}(x_i, x_j, \omega)$ for the SHA Core 35A'- Asymmetric Detector Locations $x_i = -12.5$ cm; $x_j =$ Variable . . . . .	64
26. Exact $\theta R^{(2,2)}(x_i, x_j, \omega)$ for the ARK-Asymmetric Detector Locations $x_i = -92.5$ cm; $x_j =$ Variable . . . . .	65

## LIST OF ILLUSTRATIONS (Continued)

Figure	Page
27. Exact $\Theta R^{(2,2)}(x_1, x_1, \omega)$ for the ARK-Asymmetric Detector Locations— $x_1 = -32.5$ cm; $x_j =$ Variable . . . . .	65
28. Exact $\Theta R^{(2,2)}(x_1, x_1, \omega)$ for the SHA Core 35A'- Selected Frequencies and Detector Locations— $x_1 = -72.5$ cm; $x_j =$ Variable. . . . .	67
29. Exact $\Theta R^{(2,2)}(x_1, x_1, \omega)$ for the ARK-Selected Frequencies and Detector Locations— $x_1 = -92.5$ cm; $x_j =$ Variable . . . . .	67
30. Fundamental Thermal Eigenfunctions—SHA Core 35A' . . . . .	75
31. First Harmonic Thermal Eigenfunctions—SHA Core 35A' . . . . .	75
32. Second Harmonic Thermal Eigenfunctions— SHA Core 35A' . . . . .	76
33. Third Harmonic Thermal Eigenfunctions— SHA Core 35A' . . . . .	76
34. Fourth Harmonic Thermal Eigenfunctions— SHA Core 35A' . . . . .	77
35. Fifth Harmonic Thermal Eigenfunctions— SHA Core 35A' . . . . .	77
36. Fundamental Thermal Eigenfunctions—ARK. . . . .	78
37. First Harmonic Thermal Eigenfunctions—ARK . . . . .	78
38. Second Harmonic Thermal Eigenfunctions—ARK. . . . .	79
39. Third Harmonic Thermal Eigenfunctions—ARK . . . . .	79
40. Fourth Harmonic Thermal Eigenfunctions—ARK. . . . .	80
41. Fifth Harmonic Thermal Eigenfunctions—ARK . . . . .	80
42. $2\lambda$ Mode $ R^{(2,2)}(x_1, -x_1, \omega) $ for the SHA Core 35A'- Varying Symmetric Detector Separation Distances . . . . .	86
43. $2\omega$ Mode $ R^{(2,2)}(x_1, -x_1, \omega) $ for the SHA Core 35A'- Varying Symmetric Detector Separation Distances . . . . .	86

## LIST OF ILLUSTRATIONS (Continued)

Figure		Page
44.	$2\lambda$ Mode $ R^{(2,2)}(x_1, -x_1, \omega) $ for the ARK-Symmetric Detector Separation Distance. . . . .	87
45.	$2\omega$ Mode $ R^{(2,2)}(x_1, -x_1, \omega) $ for the ARK-Symmetric Detector Separation Distance. . . . .	87
46.	$6\lambda$ Mode $ R^{(2,2)}(x_1, -x_1, \omega) $ for the SHA Core 35A'-Varying Symmetric Detector Separation Distances . . . . .	88
47.	$6\omega$ Mode $ R^{(2,2)}(x_1, -x_1, \omega) $ for the SHA Core 35A'-Varying Symmetric Detector Separation Distances . . . . .	88
48.	$6\lambda$ Mode $ R^{(2,2)}(x_1, -x_1, \omega) $ for the ARK-Symmetric Detector Separation Distance. . . . .	89
49.	$6\omega$ Mode $ R^{(2,2)}(x_1, -x_1, \omega) $ for the ARK-Symmetric Detector Separation Distance. . . . .	89
50.	$2\lambda$ Mode $ R^{(2,2)}(x_1, x_j, \omega) $ for the SHA Core 35A'-Asymmetric Detector Locations $-x_1 = -48.5$ cm; $x_j =$ Variable . . . . .	90
51.	$2\omega$ Mode $ R^{(2,2)}(x_1, x_j, \omega) $ for the SHA Core 35A'-Asymmetric Detector Locations $-x_1 = -48.5$ cm; $x_j =$ Variable . . . . .	90
52.	$6\lambda$ Mode $ R^{(2,2)}(x_1, x_j, \omega) $ for the SHA Core 35A'-Asymmetric Detector Locations $-x_1 = -48.5$ cm; $x_j =$ Variable . . . . .	91
53.	$6\omega$ Mode $ R^{(2,2)}(x_1, x_j, \omega) $ for the SHA Core 35A'-Asymmetric Detector Locations $-x_1 = -48.5$ cm; $x_j =$ Variable . . . . .	91
54.	$2\lambda$ Mode $ R^{(2,2)}(x_1, x_j, \omega) $ for the ARK-Asymmetric Detector Locations $-x_1^j = -43.5$ cm; $x_j =$ Variable . . . . .	92
55.	$2\omega$ Mode $ R^{(2,2)}(x_1, x_j, \omega) $ for the ARK-Asymmetric Detector Locations $-x_1^j = -43.5$ cm; $x_j =$ Variable . . . . .	92
56.	$6\lambda$ Mode $ R^{(2,2)}(x_1, x_j, \omega) $ for the ARK-Asymmetric Detector Locations $-x_1^j = -43.5$ cm; $x_j =$ Variable . . . . .	93
57.	$6\omega$ Mode $ R^{(2,2)}(x_1, x_j, \omega) $ for the ARK-Asymmetric Detector Locations $-x_1^j = -43.5$ cm; $x_j =$ Variable . . . . .	93

## LIST OF ILLUSTRATIONS (Concluded)

Figure		Page
58.	Spatial Weighting Function $a^{(2)}(x_1)$ --SHA Core 35A' . . . . .	99
59.	Spatial Weighting Function $a^{(2)}(x_1)$ --ARK . . . . .	100
60.	Measured $ MR(x_1, -x_1, \omega) $ for Several SHA Cores-- $x_1 = -77.5$ cm . . . . .	118
61.	Measured Values of the APSD's and Noise Ratios for Several SHA Cores . . . . .	121
62.	Exact and Measured Values of $ R^{(2,2)}(x_1, -x_1, \omega) $ -- ARK-- $x_1 = -42.5$ cm . . . . .	124
63.	Fast Fourier Transform Flowchart of the KAPL Data . . . . .	180

## SUMMARY

The subject of this dissertation lies in the area of space- and energy-dependent neutron noise analysis, which in turn falls within the field of reactor kinetics. The objective of this investigation has been fourfold:

1. to indicate the interrelation between time- and frequency-domain noise techniques,

2. to demonstrate how modal approximations of the neutron noise follow from the manner in which the Green's function or transfer matrix is approximated,

3. to derive an exact solution and several modal approximations of the coherence function in one-dimensional coupled core reactor models, and investigate their characteristics with changing core and detector conditions,

4. to postulate and utilize methods by which some important dynamic reactor parameters can be inferred from the measured coherence function or modified coefficient of correlation in zero-power coupled core reactors.

The interrelation between time- and frequency-domain noise techniques, which still retain the space- and energy-dependence, was shown in a direct manner by starting with the formulation of the covariance. The Green's function or transfer matrix was involved in each noise technique investigated. Modal formulations of the noise techniques were demonstrated

to be dependent upon the manner in which the Green's function or transfer matrix was approximated. The point reactor noise approximation was shown to result when the fundamental prompt decay mode was dominant.

A one-dimensional exact solution of the coherence function was derived to serve as a standard of comparison for the modal approximations and to investigate the nature of the coherence function as the core and detector conditions changed. It was found that the absolute value of the coherence function decreases as a reactor becomes more decoupled, and that the value of the coherence function "sink" or "null" frequency is very sensitive to the degree of coupling and location of the detectors. It was demonstrated that the local thermal neutron lifetime could be inferred from plots of the coherence function phase angle only when the local neutron leakage was small.

Modal approximations of the exact solution in one-dimensional geometry were derived. For detector locations external to the decoupling region, the two-mode expansion approximation was observed to compare well with the exact solution in loosely coupled reactor models. Using these two-mode approximations, methods were postulated by which the eigenvalue separation (a measure of the spatial coupling), neutron generation time, and the effective delayed neutron fraction could be inferred by interpretation of the measured zero-power reactor coherence function or modified coefficient of correlation. These methods were applied to extract the above parameters from frequency-domain noise measurements from the Solid Homogeneous Assembly at Knolls Atomic Power Laboratory and an Argonaut type reactor at the Karlsruhe Research Center. Results obtained using

these methods compared favorably with other experimental interpretations and with direct calculations. In general, the quality of the results decreased as the reactors were made more tightly coupled.

## CHAPTER I

### INTRODUCTION

All phenomena in nature exhibit random fluctuations about a mean value. The neutron population density existing in a steady state nuclear reactor is no exception to this general rule. Since the neutron population density variation results from the sum of the effects of the various processes involved, a measurement of this quantity provides a means whereby some dynamic characteristics of a reactor may be inferred.

Neutron detectors are used to measure the local neutron population density and their response rates also fluctuate about a mean value. These fluctuations are commonly referred to as "noise," and the interpretation of this "noise" is called noise analysis. The detector noise will vary with location in large heterogeneous reactor cores where the neutron population density variation and neutron energy spectrum changes with position. Any noise analysis method used to infer global dynamic characteristics of a reactor must take this spatial-spectral change into account. It is for this reason that it is important to study the space- and energy-dependent noise in reactors which exhibit this dependence. Coupled core reactors, by definition, fall within this category.

The terminology used in reactor noise analysis has borrowed heavily from the disciplines of communications and statistics. The very word "noise" itself originated from the electrical "noise" present in varying

amounts in communication channels.<sup>1</sup> Although at first considered a nuisance, it was later realized that useful information could be found in the noise. Use has been found for noise analysis in other fields, such as resolving binary star systems in astronomy,<sup>2</sup> detection of the natural frequencies found in the brain waves of humans and other animals,<sup>3</sup> the analysis of ocean waves in oceanography,<sup>4</sup> and the detection of reflections in seismic records in the field of geology,<sup>5</sup> to mention only a few.

Although one of the aims of noise analysis in reactor technology is to extract useful information on reactor dynamics, this may often be done with more ease by other well known methods. Pulsed neutron, pile oscillator, and rod drop techniques all possess the ability to measure the dynamic parameters of a reactor. Easy interpretation of the resulting data is characteristic of these methods. However, they all have one common disadvantage, that of perturbing the reactor from its normal operating conditions. The beauty of noise analysis lies in its non-perturbing character. Special procedures outside the normal operation routine need not be undertaken in the procurement of noise data. Other advantages offered by noise analysis are:

1. existing instrumentation and equipment may normally be used, whereas in pulsed neutron and pile oscillator methods special equipment is needed,
2. complex phenomena, such as the variance in the number of neutrons per fission, sometimes require noise analysis as one of their modes of investigation, and
3. considerable precedent now exists in monitoring for reactor

stability by noise analysis.

Much work has been devoted to the development of experimental techniques to measure reactor noise and many mathematical models have been presented to predict and interpret the observed noise. The noise signal is composed of fluctuations which are Poisson and non-Poisson in character. If the neutrons were born independently of one another, uncorrelated by location or time of birth, the detector noise would be entirely Poisson distributed.

In fact, however, neutrons are born together, correlated as to location and time of birth, in fission events and in some other processes occurring in a reactor. This correlation in the neutron birth process leads to [detector] fluctuations which are non-Poisson in character. Moreover, these [non-Poisson] fluctuations can be observed and they reveal important properties of the multiplication process.<sup>6</sup>

Historically, the first reactor dynamic parameter to be inferred by noise techniques was the prompt neutron decay constant, in work conducted at Los Alamos.<sup>7-10</sup> Though this parameter, as well as others, can be easily obtained by other techniques, it was of interest in the development of noise analysis to demonstrate some practical applications. The variance in the number of neutrons per fission, sometimes called the Diven parameter,<sup>11</sup> was also measured during this time.<sup>8</sup> The next parameters to be measured by noise analysis were the subcritical reactivity<sup>12</sup> and the absolute power level of low power reactors.<sup>13</sup> Noise analysis has been applied to various different types of measuring devices in power reactors.<sup>14</sup> Attempts have been made to interpret the statistical correlations of several different types of detectors, such as gamma<sup>15-17</sup> and pressure detectors,<sup>18</sup> in an effort to understand the dynamic character-

istics of the entire system. Recently, Ackermann et al.<sup>19</sup> have indicated a noise method by which the neutron lifetime may be determined independently of the delayed neutron fraction.

Very recently, work has been undertaken in an effort to describe and interpret the neutron noise in zero-power coupled core reactors, in both the time- and frequency-domain.<sup>20-29</sup> These investigations were carried out, for the most part, independently of each other and generally for different reasons. In one case,<sup>20,29</sup> the major objective was to develop analytical and experimental methods, in the time domain, by which the spatial coupling could be predicted. A spatial coupling parameter, called the eigenvalue separation, is important in predicting xenon oscillations,<sup>30</sup> flux tiltability of the reactor core when subjected to local reactivity perturbations, and nodal space-time kinetics coupling parameters. Other noise analysis work in the frequency- and time-domain<sup>21,27,28</sup> was undertaken as part of the fast reactor development program being undertaken by the United States and West Germany. The time-domain work of Borgwaldt et al.<sup>21</sup> was concerned with the study of the coupling effects in moderator-reflected fast assemblies. Seifritz and Albrecht,<sup>27,28</sup> on the other hand, studied coupling parameters in a thermal reactor using a simple frequency-domain model. Likewise, the group at Iowa State University<sup>22-26</sup> has proposed several simple to complicated frequency-domain models to describe some rather curious features of the space-dependent noise in a thermal coupled core reactor.

As previously mentioned, the recent time and frequency domain work has developed more or less independently from each other, although the

results are closely related and the techniques complementary. The manner in which the space- and energy-dependence has been treated in both methods appears to be fragmented. Also, the curious and interesting features of each method have not been explained or related to the other method. Finally, it appears that the techniques to infer some reactor parameters from the measured time domain noise may be applied in the frequency domain with little modification and perhaps some improvement.

To this end, the following four objectives have been undertaken in this dissertation work:

1. to indicate the interrelation between the time- and frequency-domain noise techniques,
2. to demonstrate how modal approximations of the space- and energy-dependent noise follow from the manner in which the Green's function or transfer matrix is approximated,
3. to derive an exact solution and several modal approximations of the noise in one-dimensional coupled core reactor models and investigate their characteristics with changing core and detector conditions, and
4. to postulate and utilize methods by which some important dynamic reactor parameters can be inferred from the measured detector noise in zero-power coupled core reactors.

The work described in this dissertation was undertaken for several reasons: Firstly, to date there exists no comprehensive space- and energy-dependent noise theory which shows the interrelation between time- and frequency-domain methods. From the literature, it appears that

time- and frequency-domain noise methods have been developed independently from each other and that both schools have ignored the applicable work done in space-time (and energy) kinetics. Secondly, it is important to give future experimenters involved in coupled core work insight on how best to perform some experiments. Also, a clear understanding of some of the dynamic properties of coupled cores is gained when interpreted in light of the noise models. Lastly, some important reactor parameters which have not been measured yet are obtained by the methods presented herein. These parameters are the effective delayed neutron fraction ( $\bar{\beta}$ ) and the neutron generation time ( $\Lambda_{00}$ ). In addition, the eigenvalue separation obtained by the time-domain analysis of Rydin et al.<sup>20</sup> is shown to be obtained also by a frequency-domain analysis.

A comprehensive historical background discussion of zero-power reactor noise theories is presented in Chapter II. This is undertaken in an effort to put the rest of the dissertation in the proper perspective. Chapter III is concerned with the development of several space- and energy-dependent noise techniques (variances, correlation functions, and power spectra) starting with an expression for the covariance which was derived by Borgwaldt and Stegemann<sup>31</sup> and Harris.<sup>6</sup> This was undertaken in order to indicate the close interrelation of these various techniques. It is found that the Green's function or transfer matrix is used in each one of these methods. The modal approximation form of the above methods is found to follow from the manner in which the Green's function or transfer matrix is approximated. The common point reactor formulation of these methods results when the prompt neutron decay mode dominates.

A one-dimensional exact solution of the space- and energy-dependent noise is derived in Chapter IV to serve as a standard of comparison for the modal approximations and to provide a means to investigate the nature of the noise as the core and detector conditions change. Another type of solution of the space- and energy-dependent noise, called the modal approximation, is developed in Chapter V. Using the special case of the modal scheme, called the two-mode approximation, methods are developed by which reactor dynamic parameters may be extracted from noise measurements. The methods developed in Chapter V are applied with fairly good success in Chapter VI.

## CHAPTER II

### HISTORICAL DEVELOPMENT OF NOISE THEORIES AND EXPERIMENTS

#### FOR ZERO-POWER REACTORS

##### Background and Definitions

Many noise theories for zero-power reactors, both in the time- and frequency-domain have been developed rather independently from each other. It is the purpose of this chapter to present a brief review of these various theories and to classify them as to type. It has been observed by Seifritz and Stegemann<sup>32</sup> that all existing noise theories fall into four separate categories:

1. differential methods,
2. integral methods,
3. noise equivalent source method, and
4. the quantum-Liouville method.

Dragt,<sup>33</sup> on the other hand, has condensed the above four groups into only two; the autonomous and the Green's function approaches. Likewise, Uhrig<sup>34</sup> has only two categories which he calls the microscopic and macroscopic approaches. The microscopic and autonomous approaches are equivalent and include both the differential and quantum-Liouville methods listed above. Also, the macroscopic and Green's function techniques may be thought to be identical and they include the integral and noise equivalent source methods.

As mentioned earlier, very little interaction between the various theoretical developments has taken place. Theories within each category have started with simple, space- and energy-independent models and progressed, with time, to take into account space- and energy-dependence. There are advantages and disadvantages with each of the different methods. The integral and noise equivalent source methods tend to be easier to comprehend and are more directly applicable to the interpretation of experimental results. However, these methods require a more intuitive feel for the problem and are not as rigorous as the differential and quantum-Liouville approaches. For the most part, workers in the reactor noise field have applied their skills to the development of more elegant theories, in attempts to describe the noise space- and energy-dependence, rather than trying to infer any dynamic reactor parameters from the measured noise. Only recently has this situation changed, as evidenced by papers presented at the recent American Nuclear Society Meeting.<sup>35</sup>

In order to better understand the ensuing discussion in this chapter and the next, a number of terms and equations used in the discussions are defined or described in alphabetical order.

Auto-Covariance--the time lag function which results when a detector's response rate is correlated with itself as a function of time displacement.

Auto-Power-Spectral-Density (APSD)--the lag time Fourier transform of the auto-covariance.

Chapman-Kolmogoroff Equation--an equation relating the neutron transition probabilities of Markoff processes from one state to another as an integral product of two earlier transition probabilities.

Coherence Function--a type of normalized CPSD which is quite useful in coupled core noise analysis work. It is defined as the CPSD divided by the square root of the product of each detector's APSD.

Covariance--the expected value of the product of the fluctuations of two different detector response rates. It is similar to the variance, but involves two detectors.

Cross-Covariance--the time lag function which results when one detector's response rate is correlated with another as a function of time displacement.

Cross-Power-Spectral-Density (CPSD)--the lag time Fourier transform of the cross-covariance.

Eigenvalue Separation ( $\Delta(1/K_1)$ )--a quantity which gives an indication of the degree of coupling within a reactor core. If  $\Delta(1/K_1) \cong 2\% \Delta K/K$ , the core is termed loosely coupled, and if  $\Delta(1/K_1) > 2\% \Delta K/K$ , the core is termed tightly coupled.

Ergodic Processes--processes whose time averages are equal to their ensemble averages.

Fokker-Planck Equation--the probability generating function form of the Kolmogoroff equation. The first order moment of this equation yields the transport equation or its approximations and the second order moment gives the correlation equations.

Green's Function--the time, space, and energy dependent neutron density due to an impulse of source neutrons of some energy and spatial location that was introduced at some initial time.

Kolmogoroff Equation--the Chapman-Kolmogoroff equation for stationary processes. This equation may be subdivided into forward or backward parts depending on whether one is dealing with forward or backward Markoff processes.

Langevin Equation--an integro-differential equation which describes the statistical nature of the neutron interactions. It may be thought of as the statistical version of the transport equation.

Markoff Processes--short-memory processes in which the condition of a neutron is determined by the most recent past interaction.

Modified Coefficient of Correlation (MCC)--the time-domain equivalent of the coherence function. It is defined as the ratio of the covariance divided by the product of each detector's standard deviation.

Null Frequency--that frequency (if any) where the absolute value of the coherence function vanishes.

Probability Generating Function--a particular type of mathematical transformation of the transition probabilities.

Quantum-Liouville Equation--a statistical description of the neutron probability distributions. This equation is closely related to the Langevin equation.

Rossi- $\alpha$  Method--a particular noise method by which the prompt neutron decay constant is obtained by observing the slope of the auto- or cross-covariance.

Schottky Formula--an equation originally developed to calculate the electron noise in a temperature-limited electronic diode. In reactor noise analysis it is used to calculate the driving noise source called the noise equivalent source.

Sink Frequency--that frequency (if any) where the absolute value of the coherence function reaches a local minimum.

Stationary Processes--processes whose statistics are not affected by a shift in the time origin.

Variance--the expected value of the square of the fluctuations of a detector's response rate. It is the square of the standard deviation.

Variance-to-Mean--a particular noise method by which the prompt neutron decay constant is obtained by observing the change in the ratio of the variance divided by the mean as the detector's gate time is increased.

The nature of the neutron noise problem is to attempt a prediction of the statistical variation of the neutron population as indicated by a detector, sensitive to some neutron energy, at any position within a reactor. The adjunct problem, which is more difficult, is that, once an adequate prediction is in hand, can any reactor parameters be extracted from the measured noise? In light of this background information and the definitions, the various noise analysis approaches are outlined along the lines presented by Seifritz and Stegemann.<sup>32</sup>

#### Differential Methods

The first differential reactor noise theory was proposed in 1946 by Courant and Wallace<sup>36</sup> to estimate the neutron detector standard deviation observed in an operating reactor. They started with the forward Kolmogoroff equation to establish a set of differential equations for the conditional probability distributions of neutron counts. A point reactor model with delayed neutrons was used but the effect of detector insertion was not taken into account properly. Several years later Frisch and

Littler,<sup>37</sup> using the same Kolmogoroff equation formalism but treating only prompt neutrons, correctly treated the detector. This theory<sup>37</sup> was constructed to account for the disturbing noise in a pile oscillator experiment.

Up to then the space and energy effects had been neglected. In 1958, Raievski<sup>38</sup> took a one-velocity homogeneous reactor model and divided the reactor volume into a number of cells. Starting from the differential equation for the probability generating function, where the transitions of neutrons from one space cell to another were taken into account, he derived corrections to the point reactor theory. Neutron slowing-down was included approximately in the statement that the thermal neutrons produced by fission spread out uniformly, within a sphere about the fission source, to a radius equal to the slowing-down length.

Matthes<sup>39,40</sup> extended Raievski's work by treating the space- and energy-dependence using a multigroup Green's function approach. By integrating corresponding products of Green's functions over the reactor volume he obtained correction factors with respect to the results of point reactor theory. Later Matthes<sup>41</sup> rederived his previous results starting from the Kolmogoroff equation, producing a very general formalism for treating fluctuations in neutron fields. Matthes<sup>42</sup> showed the close relation between the backward Kolmogoroff equation and the concept of neutron importance. A general set of theories was produced by Dalles<sup>42-47</sup> using the Fokker-Planck and Langevin approaches, but he only took the detector into account in one of his papers.<sup>46</sup> The Fokker-Planck and Schottky formulation was incorporated by Blaquièrè.<sup>48-50</sup> Hurwitz<sup>51</sup> and Kozik<sup>52,53</sup>

used the binary or doublet neutron density in their developments. Finally, using a forward Kolmogoroff equation approach, Stacey<sup>54</sup> calculated space-energy- and time-dependent variances, covariances, and correlation functions for low source start-up problem models.

### Integral Methods

Reactor noise work first started at Los Alamos in 1944 when de Hoffmann<sup>9,10</sup> proposed the first integral method to describe the magnitude of the reactor fluctuations. The reactor was described by a point model which neglected delayed neutrons. The starting point in treating the neutron fluctuation was to pursue the events in a neutron's lifetime by means of the theory of branching processes and correlation measures which were borrowed from the theory of general stochastic processes. The results of this treatment produced integral equations for the probability distributions of the neutron densities. In addition to de Hoffmann's early work, two other papers were published<sup>8,12</sup> in which the variance-to-mean and the Rossi- $\alpha$  methods were postulated. These four publications formed the nucleus for many others that followed and that are particularly well suited for use by experimentalists.

Pál<sup>55</sup> presented a complex analytical theory based on essentially the backwards Kolmogoroff theory for branching processes. In a later paper, Pál<sup>56</sup> used the generating function method to establish a probability distribution of neutron counts in a certain time interval that could be used in calculating the neutron variance. Starting with a modified Boltzmann equation, Borgwaldt and Sanitz<sup>57</sup> attacked the space- and energy-dependent problem and calculated binary densities of neutrons by taking

into account two detectors. A similar technique was employed by Bell<sup>58</sup> who published his results in 1965.

In 1965, Borgwaldt and Stegemann<sup>31</sup> presented a unified noise theory based on the Green's function and branching processes approach. From a basic formula, which in principle contains the space-energy- and angular-dependence, expressions for the variance and covariance were derived. Specializing to a point reactor model, relations between the variance-to-mean, Rossi- $\alpha$ , and power-spectra techniques were shown. At the same time Harris<sup>6</sup> and later Dragt<sup>33</sup> calculated correction factors for the point reactor model. Harris et al.<sup>59</sup> have recently retained the capabilities for treating the space- and energy-dependent time domain problems by using natural modal expansions. Rydin et al.<sup>20</sup> have applied Harris's<sup>6,59</sup> work to loosely coupled core reactors.

Following the line of references 6 and 31, Borgwaldt, Murley, and Sanitz<sup>21</sup> presented a theory which was applied to a Rossi- $\alpha$  experiment in a fast reflected reactor system. In 1967, Williams,<sup>60</sup> following the procedure suggested by Bell and Pál, started with the backward equation for the probability generating function to obtain a general formalism accounting for slowing-down effects, delayed neutrons, and detector geometry. He evaluated simple working expressions for the variance, the correlation function in the time-domain, and the power-spectra in the frequency-domain. Recently Williams<sup>61</sup> used the Fokker-Planck formalism to deduce the neutron density probability distribution with a random source excitation. At the same time, Williams and Cassell<sup>62</sup> derived expressions for the cross-power-spectral-density in a uniform infinite medium using one-speed transport theory.

Starting with the probability balance equation written in terms of the probability generating function formalism and with the solutions satisfying the sourceless forward Kolmogoroff equation, Vaurio and Jauko<sup>63</sup> developed a two-group model for reactor noise in an effort to evaluate slowing-down parameters. Another approach for evaluating the two-energy group diffusion parameters by correlating fast and thermal neutron detectors has been provided by Bulavin.<sup>64</sup>

The complete distribution of neutron counts for a stationary system has been calculated by Zolotukhin and Mogil'ner at first wrongly<sup>65</sup> and later correctly.<sup>66</sup> Moments of higher order were considered later by Dragt,<sup>67</sup> Furuhashi,<sup>68</sup> and Borgwaldt,<sup>69</sup> who evaluated third-order moments of neutron counts in a reactor due to threefold correlation of the detected neutrons.

Recently Congdon and Albrecht<sup>70</sup> treated theoretically the problem of the effective detector efficiency for the analysis of correlation experiments in large reactor systems. Zolotar<sup>71</sup> used a Monte Carlo scheme to calculate the spatial corrections to the point reactor model. His results compared well with those calculated by using the one-mode Boltzmann model of Bell.<sup>58</sup>

#### The Noise-Equivalent-Source Method

This approach was first formulated by Cohn<sup>72</sup> for a uniform reactor and later<sup>73</sup> for a reflected reactor. It starts with the familiar equations for the point (or two point) reactor kinetic model but with the addition of a stochastic (noise-equivalent) source. This source is computed by means of the Schottky<sup>74</sup> formula. The resulting equation to be

solved is called the Langevin equation and has been extensively used in the study of Brownian motion and in stellar dynamics.<sup>2,75</sup> This approach has the advantage over the other methods in that it is applicable to power reactor work,<sup>14</sup> if the noise-equivalent source can be specified. Moore<sup>76,77</sup> showed that the correlated part of the noise spectrum is proportional to the square modulus of the zero-power reactor transfer function. Several years later, Moore<sup>78</sup> proposed a space-dependent theory where both the input and output correlation functions were expanded in spatial eigenfunctions.

Sheff and Albrecht<sup>79-82</sup> extended Cohn's theory to space-dependent problems using the method of images<sup>83</sup> borrowed from the theory of heat conduction in solids. They looked at space effects in several different geometrically shaped reactor models and showed that the input noise source is not white when delayed neutron effects are included. In 1969, Sheff<sup>84</sup> extended his theory to include energy-dependence by casting the Langevin equation in matrix form. This technique has also been used by Ackermann et al.<sup>19</sup> in their two-group point reactor noise theory. They have shown that the thermal neutron lifetime may be measured independently of the effective delayed neutron fraction by using the two-group approach. A two point, one-group noise theory was adopted by Hendrickson and Murphy<sup>22</sup> to describe the behavior of the cross-power-spectral-density. Akcasu and Osborn<sup>85</sup> have developed a general space- and energy-dependent noise theory using the Langevin technique and the eigenfunction expansion modes of the Boltzmann operator. They established the connection between the Langevin technique and the quantum-Liouville approach. Johnson, Macdonald, and

Cohn<sup>86-88</sup> have calculated the space- and energy-dependent noise using a standard static diffusion theory code.<sup>89</sup> They could only treat problems at low frequencies due to convergence properties of the static algorithm.

A further extension of Cohn's work has been achieved by Otsuka, Saito, and Iijima<sup>90-93</sup> who justified the Green's function approach. Iijima,<sup>90</sup> Ukai,<sup>94</sup> and Furuhashi<sup>95</sup> have presented space-dependent formulae for the Rossi- $\alpha$  experiments. They showed that some modification is necessary for the well known formula based on the point reactor model even if the system is sufficiently small.

Danofsky,<sup>23,24</sup> Betancourt,<sup>25</sup> and Nagy<sup>26</sup> have formulated a one-dimensional, space-dependent noise theory, based on modal expansions, in an attempt to describe the null or sink frequencies observed in the CPSD or coherence function experimental results. A nodal treatment along the lines of Hendrickson's approach<sup>22</sup> has been presented by Albrecht and Seifritz<sup>27,28</sup> to describe the observed sink or null frequencies in coupled core reactors. The nature of this particular problem may be seen in Figure 1, which shows the magnitude of the coherence function for a typical coupled core reactor. As will be shown later, the shape of the coherence function is very dependent on the coupling characteristics of the core and the spatial location of the detectors. As the reactor becomes more loosely coupled, the value of the coherence function decreases at low frequencies. Also, the sink or null frequency decreases as the reactor becomes more loosely coupled. It is because of the occurrence of a sink or null frequency that one is enabled to extract some important reactor parameters. Detailed discussions of these points will be undertaken in

later chapters.

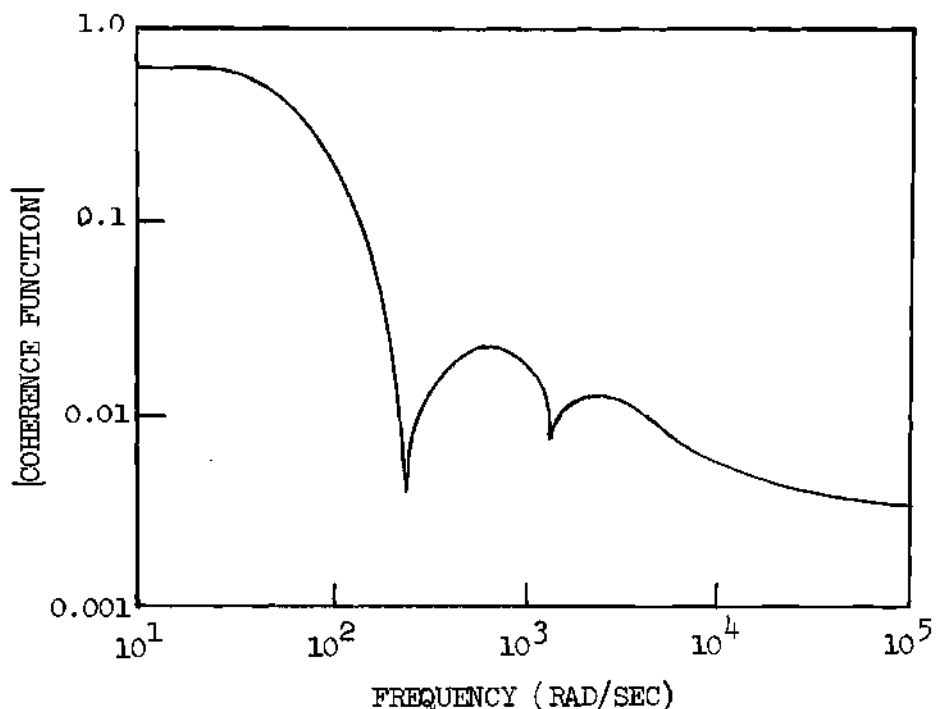


Figure 1. Typical Coherence Function Plot for a Coupled Core Reactor

#### The Quantum-Liouville Method

Lastly, a special technique for the treatment of stochastic neutron fluctuations has been developed which differs considerably from the preceding theories. Osborn, Yip, Natelson, and Shure<sup>96-100</sup> borrowed the Liouville equation from quantum mechanics to give a statistical description of the probability distribution (or doublet density) of the  $\alpha$ -particles occurring in a detector when neutrons react with the filling gas. This technique is intimately related to corresponding ones used in the theory of plasmas. In a relatively simple way this method allows for

the effects of infinite and finite geometry reactor models, detector size, and delayed neutrons. The interrelation between this approach and the Langevin technique has been established.<sup>85,99</sup>

Some new ideas, outside the scope of these classifications, for considering specific questions in reactor noise analysis have been presented by Albrecht and Seifritz.<sup>101</sup> Fundamental concepts of information and communication theory (e.g., entropy, channel capacity, equivocation, prevarication, mutual information, etc.) have been introduced in order to show the applicability of these concepts to the analysis of the statistical fluctuations in the neutron density in nuclear reactors.

## CHAPTER III

### THEORETICAL DEVELOPMENT

Of the four noise methods described in the previous chapter, only the Integral and Noise Equivalent Source methods are easily applied to the prediction and description of the measured noise. For this reason, their applications and interrelations are studied in this work.

Little developmental interaction has taken place between the Integral Noise methods, which use the time-domain as their frame of reference and the frequency-domain Noise Equivalent Source methods, even though they both involve the use of the Green's or transfer function. Also, within each method, the manner in which the space-dependence is approximated (nodal or modal) has developed independently. The task of this chapter is to show the interrelation of the time- and frequency-domain noise methods and to indicate how the space- and energy-dependence approximations follow according to the manner in which the Green's or transfer function is approximated. The point reactor noise approximation, both in the frequency- and time-domain is shown to result from using a special case of the Green's or transfer function approximation.

The groundwork for the next several chapters is presented within this chapter. The equation from which the one-dimensional (1D) exact or analytical solution of the space- and energy-dependent coherence function (SECF) is derived (Chapter IV) is presented here. Also covered is the basic methodology used in obtaining the 1D modal expansion approximation

of the SECF (Chapter V), and the MCC, which in turn are used to extract reactor parameters from experimental data (Chapter VI).

### Fundamental Assumptions

A number of necessarily restrictive assumptions must be stated before proceeding. It is assumed that the thermal reactor contains only one type of fissionable material and has the properties of stationarity and ergodicity. Also, it is assumed that the reactor is either critical at a low power or slightly subcritical with a source which emits uncorrelated Poisson distributed neutrons. Furthermore, it is implied that there are one or two noiseless, immediate-response absorption type (e.g.,  $B^{10}$ ) detectors of arbitrary geometry to indicate the state of the reactor in their vicinity. Since in this analysis we are only interested in reactor time responses on the order of the prompt neutron decay half-life, the time (but not the magnitude) effects of delayed neutrons are ignored.

### Time- and Frequency-Domain Relations

Borgwaldt and Stegemann<sup>31</sup> and Harris<sup>6,59</sup> have derived an expression for the covariance (defined in Appendix A) between two neutron detectors. The result of these derivations is written as

$$\sigma^2(\rho_i, \rho_j, T) = \frac{1}{T^2} \int_{\text{reactor}} d\rho_1' \int_{\text{reactor}} d\rho_2' \int_0^T dt_2 \int_0^T dt_1 \quad (3.1)$$

$$\times VW(t_1, t_2) D(\rho_i, \rho_1', t_1 - t_0) S_2(\rho_1', \rho_2') D(\rho_j, \rho_2', t_2 - t_0) ,$$

where

$$VW(t_1, t_2) = \int_{-\infty}^{t_1} dt_0 V(t_2 - t_1) + \int_{-\infty}^{t_2} dt_0 W(t_1 - t_2) , \quad (3.2)$$

and

$$D(\rho_i, \rho', t) = \int_{\text{detector-i}} d\rho \sum_{\text{detector-i}}(\rho) g(\rho, \rho', t) , \quad (3.3)$$

$$V(\xi) = \begin{cases} 1 & \text{when } \xi \geq 0 \\ 0 & \text{when } \xi < 0 \end{cases} , \quad W(\xi) = \begin{cases} 1 & \text{when } \xi > 0 \\ 0 & \text{when } \xi \leq 0 \end{cases} . \quad (3.4)$$

The symbol  $\sigma^2(\rho_i, \rho_j, T)$  represents the covariance between the detection rates of two neutron detectors which occupy phase space (position and velocity)  $\rho_i$  and  $\rho_j$ .  $T$  is the detection time interval, or also called the detector gate time.  $\rho_1'$  and  $\rho_2'$  represent the phase space of the stochastic source neutron and  $S_2(\rho_1', \rho_2')$  is the binary pair (correlated fission neutrons) production rate.  $D(\rho_i, \rho', t)$  is the neutron detector response rate sensitive to  $\rho_i$  phase space neutrons at time  $t$  after a source neutron of phase space  $\rho'$  is introduced into the system at zero initial time. The detector response rate is closely tied to the Green's function as shown in equation (3.3). In this equation,  $g(\rho, \rho', t)$  is the  $\rho$  phase space neutron flux at time  $t$  after a  $\rho'$  phase space neutron is introduced into the system at time zero.  $\sum(\rho)$  is the detector response cross section.

The variance follows directly from the expression for the covariance (see Appendix A) and may be represented as

$$\sigma^2(\rho_i, \rho_i, T) = \frac{\bar{D}_i}{T} + \frac{1}{T^2} \int_{\text{reactor}} d\rho_1' \int_{\text{reactor}} d\rho_2' \int_0^T dt_2 \int_0^T dt_1 \quad (3.5)$$

$$\times VW(t_1, t_2) D(\rho_i, \rho_1', t_1 - t_0) S_2(\rho_1', \rho_2') D(\rho_i, \rho_2', t_2 - t_0) .$$

$\bar{D}_i$  is the time averaged detection rate of the  $i^{\text{th}}$  detector. The first term on the right-hand side of the variance arises from the fact that each registered reaction releases a trivial synchronized response in a single detector. That is, every count is correlated with itself in a single neutron detector for a variance type measurement.

Expressions for the cross- and auto-covariances (see Appendix A) follow directly from equations (3.1) and (3.5), respectively

$$C(\rho_i, \rho_j, T, \tau) = \frac{1}{T^2} \int_{\text{reactor}} d\rho_1' \int_{\text{reactor}} d\rho_2' \int_0^T dt_2 \int_0^T dt_1 VW(t_1, t_2) \quad (3.6)$$

$$\times D(\rho_i, \rho_1', t_1 - t_0 + \gamma_1(\tau)) S_2(\rho_1', \rho_2') D(\rho_j, \rho_2', t_2 - t_0 + \gamma_2(\tau))$$

and

$$C(\rho_i, \rho_i, T, \tau) = \frac{\bar{D}_i}{T} \Delta(T, \tau) + \frac{1}{T^2} \int_{\text{reactor}} d\rho_1' \int_{\text{reactor}} d\rho_2' \int_0^T dt_2 \int_0^T dt_1 \quad (3.7)$$

$$\times VW(t_1, t_2) D(\rho_i, \rho_1', t_1 - t_0 + \gamma_1(\tau)) S_2(\rho_1', \rho_2') D(\rho_i, \rho_2', t_2 - t_0 + \gamma_2(\tau)) .$$

The functions  $\gamma_1(\tau)$  and  $\gamma_2(\tau)$  are the lead or lag times, respectively

$$\gamma_1(\tau) = \begin{cases} |\tau| & \text{when } \tau \leq 0 \\ 0 & \text{when } \tau > 0 \end{cases}, \quad \gamma_2(\tau) = \begin{cases} 0 & \text{when } \tau \leq 0 \\ \tau & \text{when } \tau > 0 \end{cases}. \quad (3.8)$$

A function  $\Delta(T, \tau)$  is proposed which represents the time overlap of the lag or lead of the time displacement

$$\Delta(T, \tau) = \begin{cases} 0 & \text{when } |\tau| > T \\ \frac{T - |\tau|}{T} & \text{when } |\tau| \leq T \end{cases}. \quad (3.9)$$

This function arises because the trivial synchronized response in a single detector does not occur if the lag (or lead) time is greater than the gate time.

The expression for the detector response rate  $D(\rho, \rho', \xi + \tau)$  in equations (3.6) and (3.7) may be represented in a different form

$$D(\rho, \rho', \xi + \tau) = f(\rho, \xi) D(\rho, \rho', \tau). \quad (3.10)$$

The function  $f(\rho, \xi)$  is a scaling factor which is equal to one when  $\xi$  equals zero, and less than one for  $\xi$  greater than zero.

Equations (3.6) and (3.7) may therefore be rewritten as

$$C(\rho_i, \rho_j, T, \tau) = U(\rho_i, \rho_j, T) \int_{\text{reactor}} d\rho_1' \int_{\text{reactor}} d\rho_2' D(\rho_i, \rho_1', \gamma_1(\tau)) \quad (3.11) \\ \times S_2(\rho_1', \rho_2') D(\rho_j, \rho_2', \gamma_2(\tau)),$$

$$C(\rho_i, \rho_i, T, \tau) = \frac{\bar{D}_i \Delta(T, \tau)}{T} + U(\rho_i, \rho_i, T) \int_{\text{reactor}} d\rho_1' \int_{\text{reactor}} d\rho_2' \quad (3.12)$$

$$\times D(\rho_i, \rho_1', \gamma_1(\tau)) S_2(\rho_1', \rho_2') D(\rho_i, \rho_2', \gamma_2(\tau)) ,$$

where  $U(\rho_i, \rho_j, T)$  is defined as

$$U(\rho_i, \rho_j, T) = \frac{1}{T^2} \int_0^T dt_2 \int_0^T dt_1 VW(t_1, t_2) f(\rho_i, t_1 - t_0) f(\rho_j, t_2 - t_0) . \quad (3.13)$$

Fourier transforming equations (3.11) and (3.12) result in the following equations for the cross- and auto-power-spectral-density, respectively

$$\hat{\Phi}(\rho_i, \rho_j, T, \omega) = U(\rho_i, \rho_j, T) \int_{\text{reactor}} d\rho_1' \int_{\text{reactor}} d\rho_2' D(\rho_i, \rho_1', \omega)^* \quad (3.14)$$

$$\times S_2(\rho_1', \rho_2') D(\rho_j, \rho_2', \omega) ,$$

and

$$\hat{\Phi}(\rho_i, \rho_i, T, \omega) = \frac{\bar{D}_i}{T} \Delta(T, \omega) + U(\rho_i, \rho_i, T) \int_{\text{reactor}} d\rho_1' \int_{\text{reactor}} d\rho_2' \quad (3.15)$$

$$\times D(\rho_i, \rho_1', \omega)^* S_2(\rho_1', \rho_2') D(\rho_i, \rho_2', \omega) ,$$

where  $\Delta(T, \omega)$  and  $D(\rho, \rho', \omega)$  are the Fourier transforms of  $\Delta(T, \tau)$  and  $D(\rho, \rho', \tau)$ , respectively.

Equations (3.1), (3.5), (3.6), and (3.7) are representative of the Integral Noise methods and equations (3.14) and (3.15) are representative of the Noise Equivalent Source method. Notice that in both methods the

space- and energy-dependence is retained explicitly through the flux response or Green's functions  $g(\rho, \rho', t)$ ,  $g(\rho, \rho', \tau)$ , or  $g(\rho, \rho', \omega)$ . The particular manner in which the Green's function is approximated (nodal or modal) will determine the spatial form of the noise analysis method.

The Green's function,  $g(\rho, \rho', t)$ , is the solution to the inhomogeneous diffusion equation

$$B(\rho, t)g(\rho, \rho', t) = \delta(\rho - \rho')\delta(t) , \quad (3.16)$$

where  $B(\rho, t)$  is the diffusion operator and  $\delta(\rho - \rho')$  and  $\delta(t)$  are Dirac deltas. In general, the exact solution of equation (3.16) is not possible, thereby necessitating some approximation. The usual procedure in time-dependent multigroup diffusion theory problems is to use the method of weighted residuals,<sup>102</sup> of which the modal expansion, synthesis, nodal, and quasistatic methods are subsets.<sup>30</sup> The same type of procedure may be undertaken to approximate the solution of equation (3.16).

It was decided that time-synthesis modal expansions (see Appendix B for a description of the time-synthesis modal approximations applied to space-time kinetics problems) would be used to approximate the Green's function. This technique was used because of its potential for interpreting some of the dynamic characteristics of coupled core reactors. That is, when the Green's function is approximated by some particular types of time-synthesis expansion modes, reactor dynamic information may be extracted from noise measurements (both in the time- and frequency-domain). Two specific types of expansion modes were considered. One group of functions, called the lambda modes, are eigenfunctions of the static neu-

tron diffusion balance operator. The other group of functions, called the modified omega modes, are eigenfunctions of the prompt neutron diffusion balance operator. These expansion modes were considered because of their ease of computation and applicability to the problem at hand. Another group of modal approximations, called the natural modes (eigenfunctions of the prompt and delayed neutron diffusion balance operator), also could have been used. They were not used because they are difficult to calculate.

Presented in the next section is the derivation of the noise analysis expressions using the time-synthesis modal expansion approximation of the Green's function. It will be shown that the ordinary point reactor noise form results when only a one mode expansion is assumed to be sufficient. This was the procedure carried out by Borgwaldt and Stegemann.<sup>31</sup> Harris<sup>6,59</sup> retained the higher harmonic modes in his theoretical derivation of the variance and covariance, but in his expansions he used only the natural modes.

#### Modal Expansion Approximation

In order to obtain the modal approximation forms of the noise analysis expressions explicitly, it is necessary to assume some approximation of the diffusion equation. For the rest of this section we will be working with the two-group prompt diffusion theory in three dimensional space. Spatial variables are designated as  $r$ . Two by two matrix operators and functions are designated with a double arrow affixed above the quantity, and 2x1 column vector functions have single arrows over them.

It is shown in Appendix C that the Green's function flux response

may be approximated by the following finite modal expansion

$$\vec{g}(r, r', t) \cong \sum_{n=0}^N \frac{e^{\omega_n t} \vec{\psi}_n(r) \vec{\psi}_n^{+T}(r')}{\langle \vec{\psi}_n, \vec{V}^{-1} \vec{\psi}_n \rangle}, \quad N = 0, 1, 2, \dots \quad (3.17)$$

$\vec{g}(r, r', t)$  is the Green's function matrix

$$\vec{g}(r, r', t) \equiv \begin{bmatrix} g^{(1,1)}(r, r', t) & g^{(1,2)}(r, r', t) \\ g^{(2,1)}(r, r', t) & g^{(2,2)}(r, r', t) \end{bmatrix}, \quad (3.18)$$

where  $g^{(k,l)}(r, r', t)$  is the  $k^{\text{th}}$  group flux response at point  $r$ , time  $t$  after one  $l^{\text{th}}$  group source neutron is introduced at point  $r'$ .  $\vec{\psi}_n(r)$  is the  $n^{\text{th}}$  order expansion vector function (see Appendix B) and  $\vec{\psi}_n^{+T}(r')$  is the  $n^{\text{th}}$  order transpose of the adjoint expansion vector function.  $\omega_n$  is the  $n^{\text{th}}$  order prompt neutron decay constant or eigenvalue. The bracketed term in the denominator represents the scalar inner product

$$\langle \vec{\psi}_n, \vec{V}^{-1} \vec{\psi}_n \rangle \equiv \int_{\text{reactor}} dr \vec{\psi}_n^{+T}(r) \vec{V}^{-1} \vec{\psi}_n(r), \quad (3.19)$$

where  $\vec{V}^{-1}$  is the diagonal matrix of inverse velocities

$$\vec{V}^{-1} \equiv \begin{bmatrix} 1/v^{(1)} & 0 \\ 0 & 1/v^{(2)} \end{bmatrix} \quad (3.20)$$

The superscript numbers indicate the energy groups.

It will be further assumed that only thermal fissions are occurring and that the fission neutrons are all born in the fast group. With these assumptions, the binary pair source rate ( $\vec{S}_2$ ) is seen to be<sup>31</sup>

$$\vec{S}_2(r_1', r_2') = \chi_2 \bar{\nu}_p^2 \delta(r_1' - r_2') \sum_f^{(2)}(r_1') \bar{\phi}^{(2)}(r_1') \begin{bmatrix} 1 & 0 \\ 0 & 0 \end{bmatrix}, \quad (3.21)$$

where  $\chi_2$  is the Diven<sup>11</sup> parameter,  $\bar{\nu}_p$  is the average number of prompt neutrons per fission,  $\sum_f^{(2)}$  is the thermal fission cross section, and  $\bar{\phi}^{(2)}(r_1')$  is the thermal flux distribution.

### Covariance

The elements of the covariance matrix for the model at hand are found by making use of equations (3.1), (3.17), and (3.21)

$$\begin{aligned} \sigma^2(k, l)(r_i, r_j, T) &= \frac{1}{T^2} \int_{\text{reactor}} dr_1' \int_{\text{reactor}} dr_2' \int_0^T dt_1 \int_0^T dt_2 VW(t_1, t_2) \quad (3.22) \\ &\times \int_{\text{det-i}} dr \sum_{\text{det-i}}^{(k)}(r) \sum_{n=0}^N \frac{e^{\omega_n(t_1-t_0)} \psi_n^{(k)}(r) \psi_n^{(1)+}(r_1')}{\langle \vec{\psi}_n, \vec{V}^{-1} \vec{\psi}_n \rangle} \\ &\times \chi_2 \bar{\nu}_p^2 \delta(r_1' - r_2') \sum_f^{(2)}(r_1') \bar{\phi}^{(2)}(r_1') \\ &\times \int_{\text{det-j}} dr \sum_{\text{det-j}}^{(l)}(r) \sum_{m=0}^N \frac{e^{\omega_m(t_2-t_0)} \psi_m^{(l)}(r) \psi_m^{(1)+}(r_2')}{\langle \vec{\psi}_m, \vec{V}^{-1} \vec{\psi}_m \rangle} \end{aligned}$$

The meaning of  $\sigma^2(k, l)(r_i, r_j, T)$  is the covariance of detector rates for a detection time  $T$  between the  $i^{\text{th}}$  detector located at  $r_i$  sensitive to the  $k^{\text{th}}$  group of neutrons and the  $j^{\text{th}}$  detector located at  $r_j$  which is sensitive to the  $l^{\text{th}}$  group of neutrons.

Equation (3.22) may be written in a more compact form as

$$\sigma^2(k, l)(r_i, r_j, T) = \sum_{n=0}^N \sum_{m=0}^N C_{nm} D_n^{(k)}(r_i) D_m^{(l)}(r_j) G_{nm}(T) , \quad (3.23)$$

where

$$C_{nm} \equiv \int_{\text{reactor}} dr_i' \frac{\chi_e \bar{v}^2 \sum_f^{(2)} (r_i') \bar{\phi}^{(2)}(r_i') \psi_n^{(1)}(r_i') + (r_i') \psi_m^{(1)}(r_i')}{\langle \bar{\psi}_n, \bar{V}^{-1} \bar{\psi}_n \rangle \langle \bar{\psi}_m, \bar{V}^{-1} \bar{\psi}_m \rangle} \quad (3.24)$$

$$D_n^{(k)}(r_i) \equiv \int dr \sum_{\det-i}^{(k)} (r) \psi_n^{(k)}(r) , \quad (3.25)$$

$$D_m^{(l)}(r_j) \equiv \int dr \sum_{\det-j}^{(l)} (r) \psi_m^{(l)}(r) , \quad (3.26)$$

$$G_{nm}(T) \equiv \frac{\left[ \frac{\omega_n T + 1 - e^{-\omega_n T}}{(\omega_n T)^2} + \frac{\omega_m T + 1 - e^{-\omega_m T}}{(\omega_m T)^2} \right]}{\omega_n + \omega_m} . \quad (3.27)$$

The form of the covariance in equation (3.23) is identical with that of Harris et al.<sup>59</sup> and Rydin et al.<sup>20</sup> except that they considered a correlated non-Poisson distributed spontaneous fission source.

### Variance

The variance is readily obtained using equations (3.5) and (3.23)

$$\sigma^2(k,k)(r_i, r_i, T) = \frac{\bar{D}_i}{T} + \sum_{n=0}^N \sum_{m=0}^N C_{nm} D_n^{(k)}(r_i) D_m^{(k)}(r_i) G_{nm}(T) . \quad (3.28)$$

### Cross-Covariance

By combining equations (3.6) and (3.23), the cross-covariance is obtained

$$C^{(k,l)}(r_i, r_j, T, \tau) = \begin{cases} \sum_{n=0}^N \sum_{m=0}^N C_{nm} D_n^{(k)}(r_i) D_m^{(l)}(r_j) G_{nm}(T) e^{\omega_m \tau} , & \text{when } \tau \geq 0 \\ \sum_{n=0}^N \sum_{m=0}^N C_{nm} D_n^{(k)}(r_i) D_m^{(l)}(r_j) G_{nm}(T) e^{-\omega_n \tau} , & \text{when } \tau \leq 0 . \end{cases} \quad (3.29)$$

### Auto-Covariance

In a similar manner, combining equations (3.7) and (3.28), the auto-covariance is obtained

$$C^{(k,k)}(r_i, r_i, T, \tau) = \quad (3.30)$$

$$\begin{cases} \frac{\bar{D}_i}{T} \Delta(T, \tau) + \sum_{n=0}^N \sum_{m=0}^N C_{nm} D_n^{(k)}(r_i) D_m^{(k)}(r_i) G_{nm}(T) e^{\omega_m \tau} , & \text{when } \tau \geq 0 \\ \frac{\bar{D}_i}{T} \Delta(T, \tau) + \sum_{n=0}^N \sum_{m=0}^N C_{nm} D_n^{(k)}(r_i) D_m^{(k)}(r_i) G_{nm}(T) e^{-\omega_n \tau} , & \text{when } \tau \leq 0 . \end{cases}$$

### Cross-Power-Spectral-Density

Fourier transforming the cross-covariance results in the cross-power-spectral-density expression

$$\hat{\Phi}^{(k, \ell)}(r_i, r_j, T, \omega) = \sum_{n=0}^N \sum_{m=0}^N C_{nm} D_n^{(k)}(r_i) D_m^{(\ell)}(r_j) G_{nm}(T) H_{nm}(\omega) \quad (3.31)$$

where

$$H_{nm}(\omega) = \frac{\omega_m + \omega_n}{(\omega_m - i\omega)(\omega_n + i\omega)} \quad (3.32)$$

and  $i$  is the imaginary number,  $\sqrt{-1}$ .

### Auto-Power-Spectral-Density

Fourier transforming the auto-covariance results in an expression for the auto-power-spectral-density

$$\hat{\Phi}^{(k, k)}(r_i, r_i, T, \omega) = \frac{\bar{D}_i}{T} \Delta(T, \omega) + \sum_{n=0}^N \sum_{m=0}^N C_{nm} D_n^{(k)}(r_i) D_m^{(k)}(r_i) G_{nm}(T) H_{nm}(\omega) \quad (3.33)$$

### Point Reactor Approximation

The one-group, point reactor expression for the neutron noise is usually derived starting with the point reactor kinetic equations. A slightly different approach is followed here in order to relate the general modal method to the point reactor case.

Suppose that the time varying spatial neutron flux distribution can be well described by the fundamental mode eigenfunction (see Appendix B). In this event the modal approximation of the Green's function flux response has only one term (see Appendix C)

$$g(r, r', t) \cong \frac{ve^{\omega_0 t} \psi_0(r) \psi_0(r')}{\int_{\text{reactor}} dr' \psi_0(r') \psi_0(r')} \quad (3.34)$$

which is just the scalar analogy of equation (3.17). When the expansion function  $\psi_0$  is the lambda eigenfunction, the following point reactor relation holds

$$\omega_0 = \frac{1 - \bar{\beta} - 1/K_{\text{eff}}}{\Lambda_{00}} = \frac{\rho - \bar{\beta}}{\Lambda_{00}} = \frac{K_{\text{eff}}(1 - \bar{\beta}) - 1}{l} . \quad (3.35)$$

$\omega_0$  is the prompt decay constant,  $\Lambda_{00}$  is the neutron generation time,  $l$  is the neutron lifetime,  $\bar{\beta}$  is the effective delayed neutron fraction, and the other quantities have their usual definitions.

The binary pair production rate for the model at hand is given by,

$$S_2(r_1', r_2') = \chi_2 \bar{v}_p^2 \sum_f^{(2)} (r_1') \phi^{(2)}(r_1') \delta(r_1' - r_2') . \quad (3.36)$$

### Covariance

The covariance is found by the proper modification of equation (3.22)

$$\sigma^2(r_i, r_j, T) = C_{00} D_0(r_i) D_0(r_j) G_{00}(T) . \quad (3.37)$$

Performing all the integrations and mathematical operations shown in Appendix D, the covariance can be expressed as

$$\sigma^2(r_i, r_j, T) = P \left( \frac{eK_{\text{eff}}}{l} \right)^2 \chi_2 \frac{1}{\omega_0} \left[ \frac{\omega_0 T + 1 - e^{-\omega_0 T}}{(\omega_0 T)^2} \right] . \quad (3.38)$$

This is identical with the results of Borgwaldt and Stegemann.<sup>31</sup>  $P$  is the reactor power level and  $\epsilon$  is the detector efficiency. There is no space-dependence in equation (3.38) because the reactor is assumed to respond as an entire unit. The variables  $r_i$  and  $r_j$  are therefore just to indicate that there are two physically separate detectors in the reactor.

### Variance

An expression for the variance may be obtained directly from the covariance with the addition of the trivial correlated component

$$\sigma^2(r_i, r_i, T) = \frac{P\epsilon}{T} + P \left( \frac{\epsilon K_{eff}}{\beta} \right)^2 \chi_2 \frac{1}{\omega_0} \left[ \frac{\omega_0 T + 1 - e^{-\omega_0 T}}{(\omega_0 T)^2} \right]. \quad (3.39)$$

### Cross-Covariance

Introduction of a lag or lead time ( $\tau$ ) into the covariance expression yields the cross-covariance

$$C(r_i, r_j, T, \tau) = P \left( \frac{\epsilon K_{eff}}{\beta} \right)^2 \chi_2 \frac{1}{\omega_0} \left[ \frac{\omega_0 T + 1 - e^{-\omega_0 T}}{(\omega_0 T)^2} \right] e^{-\omega_0 |\tau|}. \quad (3.40)$$

### Auto-Covariance

The auto-covariance results with addition of the trivial correlated portion to the cross-covariance

$$C(r_i, r_i, T, \tau) = \frac{P\epsilon}{T} \Delta(T, \tau) + P \left( \frac{\epsilon K_{eff}}{\beta} \right)^2 \chi_2 \frac{1}{\omega_0} \left[ \frac{\omega_0 T + 1 - e^{-\omega_0 T}}{(\omega_0 T)^2} \right] e^{-\omega_0 |\tau|}. \quad (3.41)$$

### Cross-Power-Spectral-Density

Fourier transformation of the cross-covariance gives the cross-

power-spectral-density

$$\hat{\Phi}(r_i, r_j, T, \omega) = P \left( \frac{\epsilon K_{eff}}{\ell} \right)^2 \chi_2 \left[ \frac{\omega_0 T + 1 - e^{-\omega_0 T}}{(\omega_0 T)^2} \right] \left( \frac{2}{\omega_0^2 + \omega^2} \right). \quad (3.42)$$

### Auto-Power-Spectral-Density

The auto-power-spectral-density arises from the Fourier transformation of the auto-covariance

$$\hat{\Phi}(r_i, r_i, T, \omega) = \frac{P\epsilon}{T} \Delta(T, \omega) + P \left( \frac{\epsilon K_{eff}}{\ell} \right)^2 \chi_2 \left[ \frac{\omega_0 T + 1 - e^{-\omega_0 T}}{(\omega_0 T)^2} \right] \left( \frac{2}{\omega_0^2 + \omega^2} \right). \quad (3.43)$$

### Discussion

It is apparent from equations (3.38) - (3.43) that the same type of reactor parameter information is available in the various point reactor noise analysis methods. The most common quantity which is extracted from point reactor noise measurements is the prompt neutron decay constant  $\omega_0$ , and, therefore, the subcritical reactivity. If the variance or covariance is plotted against detection time  $T$ , or if the cross-covariance or auto-covariance is plotted against lag time  $\tau$ , or if the CPSD or APSF is plotted against the frequency  $\omega$ , the prompt decay constant is determined by interpretation of the various graphs in the light of the appropriate equation. The subcritical reactivity is determined by use of the well known relationship

$$\rho(\$) = 1 - \omega_0 / \omega_0^{\text{critical}}. \quad (3.44)$$

The other quantities like the detector efficiency, absolute power level, and the Diven parameter can at least, in principle, be measured by applying one or the other type of noise analysis formulations provided that enough other information about the reactor is known. In general, better accuracy is obtained in experiments using two separated detectors rather than a single detector. The reason for this is that detector related correlated events appear in single detector measurements (equations (3.39), (3.41), and (3.43)) but not in the two detector measurements ((3.38), (3.40), and (3.42)). It should also be mentioned that equations (3.38) - (3.43) represent only the fluctuating portion of noise analysis measurements. In an actual noise measurement a term equal to  $(P\epsilon)^2$  is present and must be subtracted to obtain the appropriate quantity of interest. As a consequence of this, it is usually desirable to perform measurements with detectors of high efficiency at very low power levels.

Additional information, over and above the one-group, point reactor noise analysis methods may result if more energy groups and/or modal expansions are retained. Ackermann et al.<sup>19</sup> observed that, if the two-group dependence is retained for the point reactor model, the neutron lifetime can be inferred from the CPSD independently of the delayed neutron fraction. Seifritz and Albrecht<sup>27,28</sup> were able to obtain nodal reactivities and other coupling parameters when they interpreted coherence function measurements by a one-group, two node approximation. Rydin et al.<sup>20</sup> were able to find the eigenvalue separation in a loosely coupled core assuming a three-group, two-lambda mode expansion approximation of the MCC.

## CHAPTER IV

## EXACT SOLUTION OF THE COHERENCE FUNCTION

An exact or analytical<sup>103</sup> solution of the space- and energy-dependent coherence function for one-dimensional representations of two coupled core reactors was undertaken for the following reasons:

1. to serve as a standard of comparison with the modal approximations of the coherence function (developed in Chapter V),
2. to investigate how the shape of the coherence function changes with changing detector locations and core properties, and
3. to give an indication as to what detector locations and core properties are necessary to produce a sink or null frequency in the coherence function.

Reactor Diagrams and Nuclear Constants

One-dimensional representations of the tightly coupled Argonaut<sup>104</sup> type reactor, called the ARK<sup>28</sup> (for the Argonaut Reactor Karlsruhe), and the loosely coupled SHA Core 35A<sup>20</sup> (for the Solid Homogeneous Assembly) were postulated for use in the exact solution of the coherence function.

The SHA is a critical assembly at Knolls Atomic Power Laboratory in Schenectady, New York of the type in which the core can be separated into two sections for loading and shut-down. Each section consists of an assembly of fuel-moderator blocks and reflector blocks stacked on a movable bed. A general description of the SHA facility is given in reference

105, while the physical properties of the SHA-I type fuel are given in reference 106. Since each core is quite long compared to its transverse dimensions, the kinetic behavior can be closely approximated by a one-dimensional model. In order to make the reactor loosely coupled, a slab of polyethylene of varying thickness was introduced at the center vertical plane.

A detailed schematic of a SHA core (SHA Core 35A') is shown in Figure 2. The  $B^{10}F_3$  detector banks used in the experiments were located at opposite ends of the core.

The ARK is a research reactor at the Karlsruhe Nuclear Research Center in Karlsruhe, West Germany. The reactor is cylindrical in shape with graphite located in the center and outer annulus with fuel in between. Some of the fuel elements may be removed at symmetric locations to form a slab configuration.<sup>28</sup> Because each half-core in the slab configuration is rather long compared to its transverse dimensions, it can also be approximated by a one-dimensional model. The physical arrangement and type of material in the reactor produce a tightly coupled core.

A detailed schematic of the two slab ARK core is shown in Figure 3. The  $He_3$  detectors, used in the experiments, were located near the outer diameter of the fuel in symmetric locations.

The one-dimensional representations of the SHA Core 35A' and the ARK used in the exact computation of the coherence function are given in Figures 4 and 5, respectively. The appropriate macroscopic constants for the two reactor models were obtained in different ways. Constants used in the ARK coherence function calculations were taken directly from the work

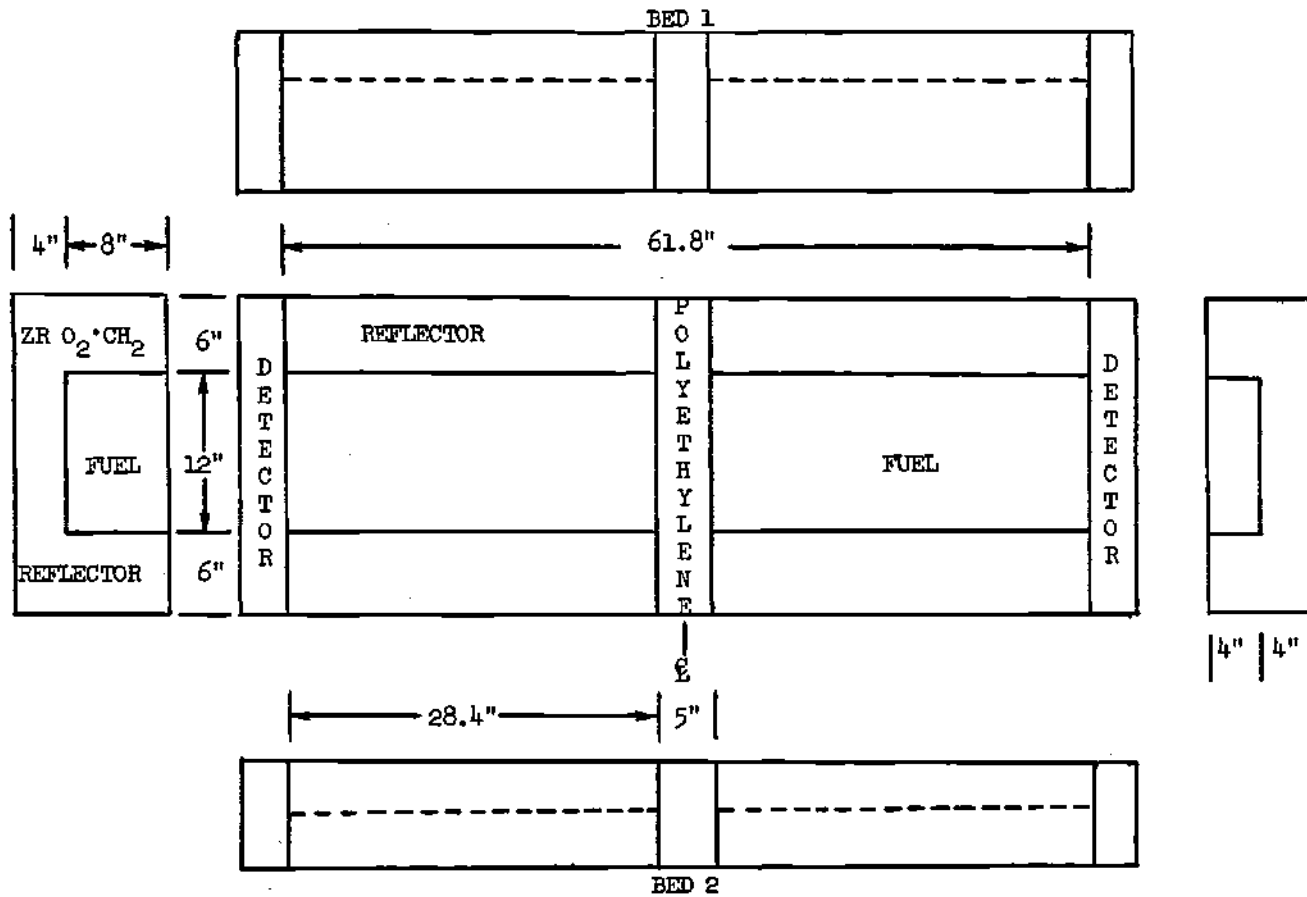


Figure 2. Detailed Schematic of the SHA Core 35A'

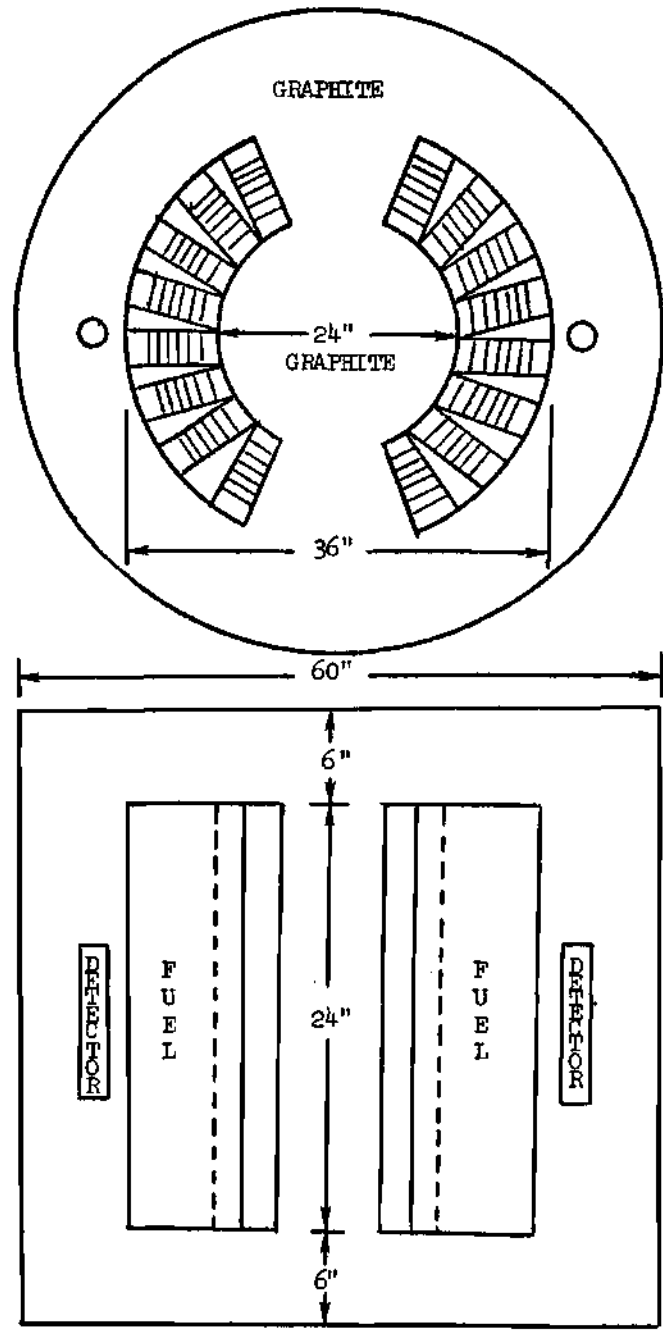


Figure 3. Detailed Schematic of the Two-Slab ARK

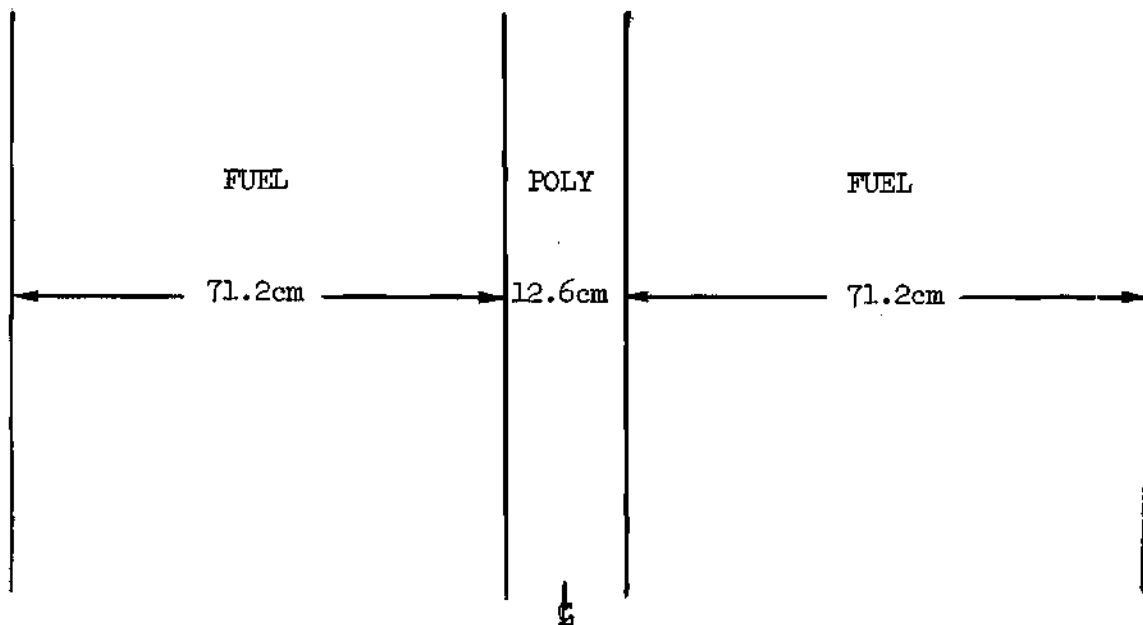


Figure 4. One-Dimensional Representation of the SHA Core 35A'

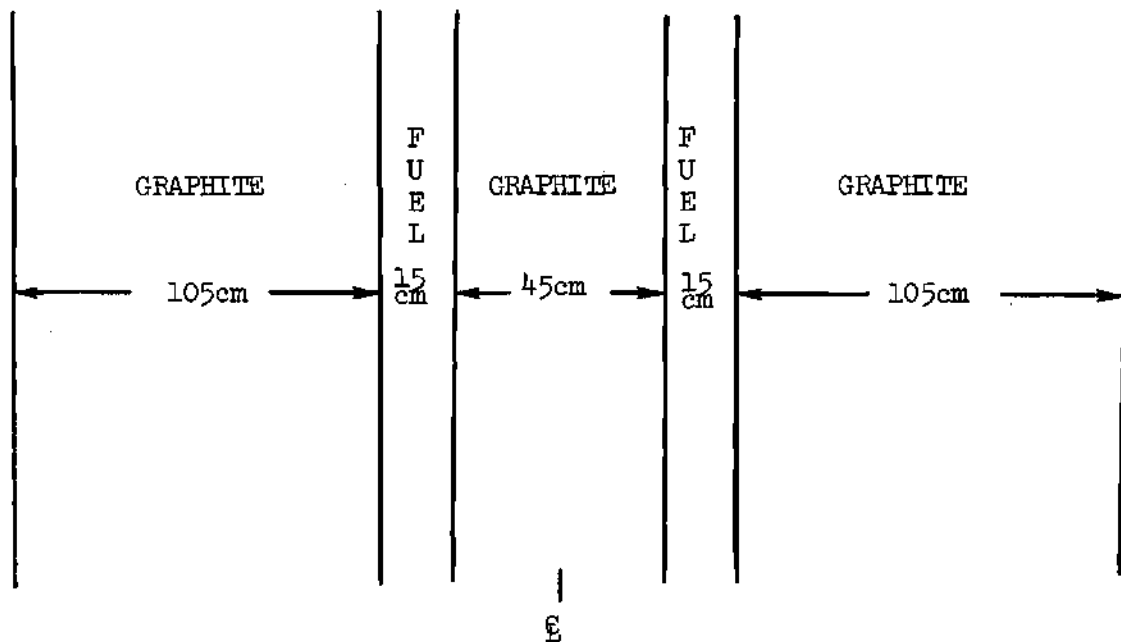


Figure 5. One-Dimensional Representation of the Two-Slab ARK

of Danofsky<sup>23</sup> or Kussmaul.<sup>107</sup> These nuclear constants are tabulated in Table 1. Using the given ARK nuclear constants in the statics neutron diffusion theory computer routine EXTERMINATOR-II,<sup>89</sup> the computed two-group fluxes and  $k_{\text{eff}}$  were in excellent agreement with those calculated by Danofsky,<sup>23</sup> as may be seen in Figure 6.

Macroscopic nuclear constants for the SHA Core 35A' were computed using an iterative interchange between the fast cross section numerical code FORM,<sup>108</sup> the thermal cross section code TEMPEST-II,<sup>109</sup> and the statics diffusion theory routine EXTERMINATOR-II.<sup>89</sup> The iterative strategy was initiated by inputting the fuel and poly atom number densities<sup>105,106</sup> into FORM and TEMPEST-II. The light element moderation option was used in the TEMPEST-II calculations. Initial estimates of the transverse and regional longitudinal bucklings were used in both codes. Resulting macroscopic cross sections were used in a 1D version of EXTERMINATOR-II to calculate the fast and thermal fluxes. Regional longitudinal bucklings were recomputed from the computed flux shapes and used in the cross section codes to compute new macroscopic cross sections. The above procedure was repeated until no change in the flux shapes was observed from one iteration to the next. From this point on, the cross section routines were no longer utilized.

The last stages of the iterative process consisted of varying the macroscopic down-scattering cross section  $(\sum \sigma_{s,2}^{(1,2)})$  in the poly region and adjusting the overall transverse buckling  $(B_T^2)$  to obtain the best possible agreement with the foil activation measurements and the experimental value of  $k_{\text{eff}}$ .<sup>118</sup> Final values of the nuclear constants used in the coherence

Table 1. ARK Nuclear Constants

Nuclear Constant	Definition	Graphite	Fuel
$D^{(1)}$ (cm)	fast diffusion coefficient	1.016	1.23
$D^{(2)}$ (cm)	thermal diffusion coefficient	0.840	0.189
$\Sigma^{(1,2)}$ ( $\text{cm}^{-1}$ )	fast scattering cross section	0.00276	0.0267
$\Sigma^{(1)}$ ( $\text{cm}^{-1}$ )	fast absorption cross section	0.00	0.00
$\Sigma^{(2)}$ ( $\text{cm}^{-1}$ )	thermal absorption cross section	0.00024	0.0908
$\nu \Sigma_f^{(2)}$ ( $\text{cm}^{-1}$ )	# neutrons per fission X fission cross section	0.00	0.122
$B_T^2$ ( $\text{cm}^{-2}$ )	transverse buckling	0.00216	0.00216
$v^{(1)}$ (cm/sec)	fast velocity	$4.36 \times 10^8$	$4.36 \times 10^8$
$v^{(2)}$ (cm/sec)	thermal velocity	$2.2 \times 10^5$	$2.2 \times 10^5$
$\bar{\beta}$	effective delayed neutron fraction	0.00	0.0076

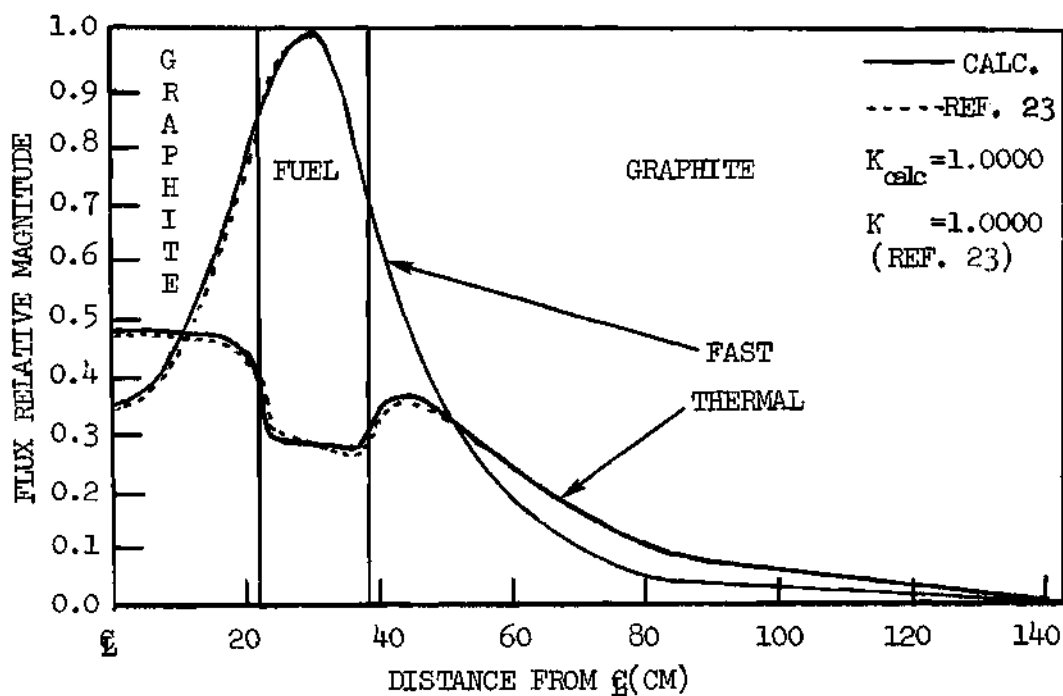


Figure 6. Calculated Fast and Thermal Fluxes in the Two-Slab ARK

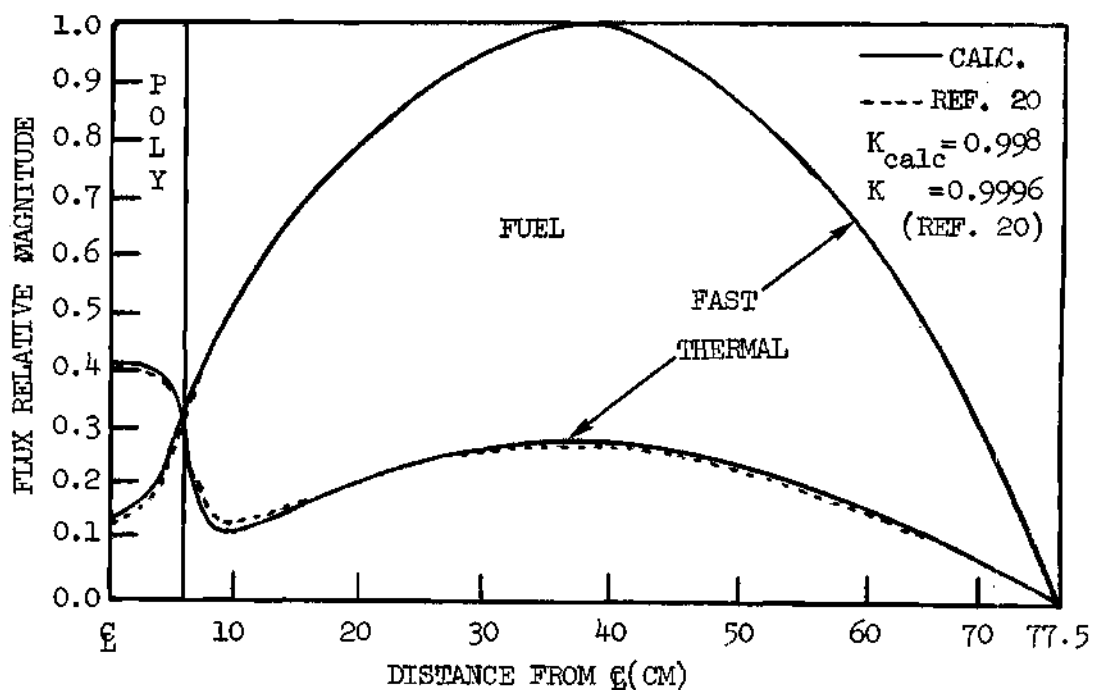


Figure 7. Calculated and Measured Fast and Thermal Fluxes in the SHA Core 35A'

function calculations of the SHA Core 35A' are listed in Table 2. A comparison of the computed fluxes and the appropriate foil activations and the values of  $k_{\text{eff}}$  are presented in Figure 7. The  $^{55}\text{Mn}$  foil activations were assumed to be proportional to the thermal flux and the  $^{115}\text{In}$  activations proportional to the fast flux. The above assumptions are fairly good in the highly thermalized SHA Core 35A'. That is, the epithermal activation contribution to the  $^{55}\text{Mn}$  activity is small and the 1.5 eV resonance activation peak accounts for almost all of the  $^{115}\text{In}$  activity (assuming that the foils were Cd covered). To a good approximation, the flux spatial distribution at 1.5 eV is proportional to the fast flux in the SHA Core 35A'.<sup>153</sup>

The above modeling procedure did not take into account the variation of the transverse leakage from one part of the core to the other, nor the transport and spectral effects as considered by Rydin et al.<sup>20</sup> The adjustment of quantities other than  $\sum^{(1,2)}$  in the poly and the overall  $B_T^2$  could have been undertaken with perhaps more physical justification. However, it was concluded that the SHA Core 35A' model was adequate for this work because not only did the computed and experimental flux shapes and  $k_{\text{eff}}$  agree well, but also the computed and experimentally determined value of eigenvalue separation compared favorably (see Chapter VI). The good agreement in the later value was the most difficult to attain in this work and the most crucial to compute accurately.

#### Method of Solution and Results

The exact solution of the one-dimensional, two-group coherence function was constructed<sup>103</sup> by combining the definition of the coherence

Table 2. SHA Core 35A' Nuclear Constants

Nuclear Constant	Definition	Poly	Fuel
$D^{(1)}$ (cm)	fast diffusion coefficient	1.033	1.142
$D^{(2)}$ (cm)	thermal diffusion coefficient	0.135	0.354
$\Sigma^{(1,2)}$ ( $\text{cm}^{-1}$ )	fast scattering cross section	0.0572	0.0186
$\Sigma^{(1)}$ ( $\text{cm}^{-1}$ )	fast absorption cross section	0.0004	0.0025
$\Sigma^{(2)}$ ( $\text{cm}^{-1}$ )	thermal absorption cross section	0.0185	0.0648
$\nu \Sigma_f^{(2)}$ ( $\text{cm}^{-1}$ )	# neutrons per fission X fission cross section	0.00	0.1113
$B_T^2$ ( $\text{cm}^{-2}$ )	transverse buckling	0.0069	0.0069
$v^{(1)}$ (cm/sec)	fast velocity	$4.36 \times 10^8$	$4.36 \times 10^8$
$v^{(2)}$ (cm/sec)	thermal velocity	$2.2 \times 10^5$	$2.2 \times 10^5$
$\bar{\beta}$	effective delayed neutron fraction	0.00	0.0078

function (Appendix A), the exact solution of the Green's response or transfer function (Appendix E), and the forms of the auto- and cross-power-spectral densities (equations (3.15) and (3.14)). By assuming that the detectors subtend a very small region (point detector approximation) and that the product of the frequency and detection time is much less than one ( $\omega T \ll 1$ ), the auto- and cross-power-spectral-density for the models at hand are, respectively

$$\begin{aligned} \hat{\Phi}^{(k,k)}(x_i, x_i, T, \omega) &= \bar{D}_i^{(k)} + U^{(k,k)}(x_i, x_i, T) \\ &\times \int_{\text{reactor}} dx' \sum_{\text{det-i}}^{(k)} (x_i) g^{(k,1)}(x_i, x', \omega) \chi_{\text{e}}^* \bar{V}_p^{(2)} \sum_f^{(2)}(x') \hat{\Phi}^{(2)}(x') \\ &\times \sum_{\text{det-i}}^{(k)} (x_i) g^{(k,1)}(x_i, x', \omega) , \end{aligned} \quad (4.1)$$

and

$$\begin{aligned} \hat{\Phi}^{(k,l)}(x_i, x_j, T, \omega) &= U^{(k,l)}(x_i, x_j, T) \\ &\times \int_{\text{reactor}} dx' \sum_{\text{det-i}}^{(k)} (x_i) g^{(k,1)}(x_i, x', \omega) \chi_{\text{e}}^* \bar{V}_p^{(2)} \sum_f^{(2)}(x') \hat{\Phi}^{(2)}(x') \\ &\times \sum_{\text{det-j}}^{(l)} (x_j) g^{(l,1)}(x_j, x', \omega) . \end{aligned} \quad (4.2)$$

$U^{(k,l)}$  is a function which, in principle, may be evaluated; however, it cancels out when the coherence function is expressed

$$R^{(k, \ell)}(x_i, x_j, \omega) = \frac{\hat{\phi}^{(k, \ell)}(x_i, x_j, \omega)}{\sqrt{[\hat{\phi}^{(k, k)}(x_i, x_i, \omega) - \bar{D}_i^{(k)}][\hat{\phi}^{(\ell, \ell)}(x_j, x_j, \omega) - \bar{D}_j^{(\ell)}]}} \quad (4.3)$$

$$= \int_{\text{reactor}} dx' |g^{(k, 1)}(x_i, x', \omega)|^2 \sum_f^{(2)} (x') \hat{\phi}^{(2)}(x') |g^{(\ell, 1)}(x_j, x', \omega)|^2 \sum_f^{(2)} (x') \hat{\phi}^{(2)}(x')$$

$$\left\{ \int_{\text{reactor}} dx' |g^{(k, 1)}(x_i, x', \omega)|^2 \sum_f^{(2)} (x') \hat{\phi}^{(2)}(x') \right. \\ \left. \times \int_{\text{reactor}} dx' |g^{(\ell, 1)}(x_j, x', \omega)|^2 \sum_f^{(2)} (x') \hat{\phi}^{(2)}(x') \right\}^{\frac{1}{2}}$$

where  $g^{(k, \ell)}(x, x', \omega)$  is the exact solution of the Green's function (see Appendix E).

The integrals in equation (4.3) were computed using the trapezoidal rule on intervals of one centimeter and summing over the model dimensions. This process was repeated for several different detector pair locations and many frequencies. Results of these calculations are shown in Figures 8-29.

#### Absolute Magnitudes of the Exact Coherence Function

Absolute magnitudes of the symmetrically located, two thermal detector coherence functions for the SHA Core 35A' and ARK models are given in Figures 8 and 9, respectively. For small detector separations, the coherence function is always positive for the frequency range of interest, but for large detector separations the coherence passes from

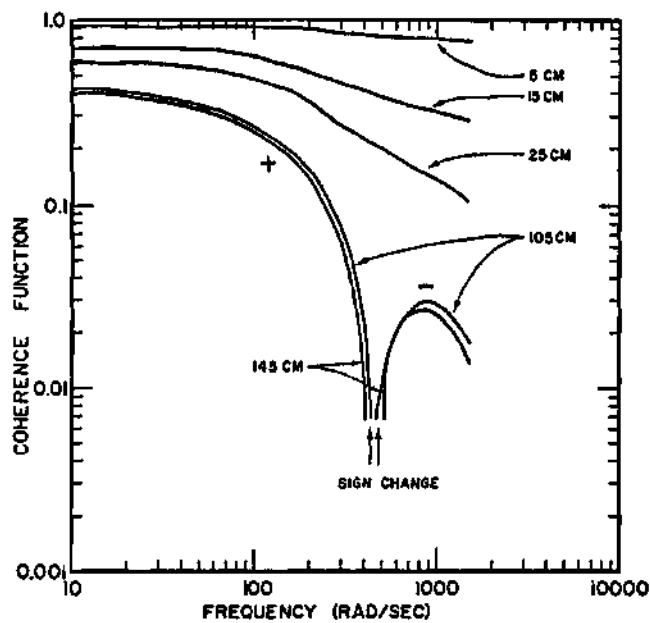


Figure 8. Exact  $|R^{(2,2)}(x_i, -x_i, \omega)|$  for the SHA Core 35A—Varying Symmetric Detector Separation Distances

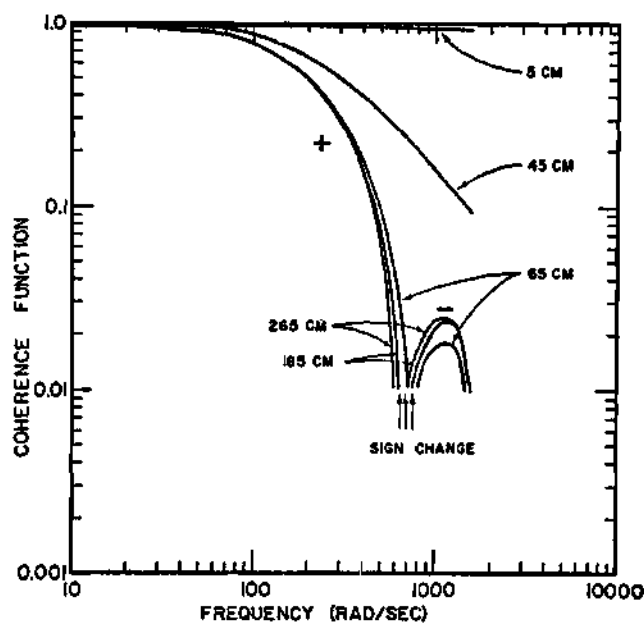


Figure 9. Exact  $|R^{(2,2)}(x_i, -x_i, \omega)|$  for the ARK—Varying Symmetric Detector Separation Distances

positive at low frequencies to negative at higher frequencies. This transition point is called the "null frequency"<sup>27</sup> because the coherence function passes through zero there. It should be noted that, for symmetric reactors and detector locations, the coherence function is real, but for asymmetric detector locations the coherence function is complex. The occurrence of the null frequency is usually ascribed to an interference effect of traveling neutron waves from one core to the other.<sup>22,26-28</sup> This approach is usually taken in conjunction with the two-node model<sup>27</sup> which has incorporated in it a neutron wave traveling time distribution function. It is generally very difficult to evaluate the distribution function, and the wave propagation times tend to be in doubt.<sup>28,110</sup> A simpler approach is taken in this work to explain the null or sink<sup>22,23</sup> frequencies by assuming an interference between the harmonic decay modes of the entire reactor (see Chapter V).

It should be noted that the coherence function at low frequencies (below the null frequency) decreases with increasing detector separations. This seems entirely reasonable when viewed in terms of coupling of one detector with the other. The extent of coupling should depend on the distance in mean free paths from one detector to the other. Viewed in this light and realizing that the mean free paths are much shorter in regions with higher scattering cross sections, the results of Figures 8 and 9 are reasonable at low frequencies where the  $\hat{i}\omega/v^{(2)}$  term (see Appendix E, equation (E.19)) is small in comparison with the absorption cross section. It has been suggested by Harris<sup>6</sup> that the variation of the low frequency coherences might be used to infer the migration length. When the  $\hat{i}\omega/v^{(2)}$

term takes on values on the order of the absorption terms (mainly above the null frequency), the coherence function tends to be less for smaller detector separations than larger separations. The frequency dependent mean free path has to be investigated in this case.

The null frequency tends to increase with decreasing detector separations. This phenomenon may be ascribed to the relative magnitudes of the fundamental to first harmonic values of the decay modes for the given detector placements. Reasoning of this sort is studied in detail in the next chapter.

Finally, it is seen that the coherence function is always smaller in the SHA Core 35A' than in the ARK. This is consistent with the fact that the eigenvalue separation is smaller in the SHA Core 35A' than in the ARK. Again, the reason for this is given in the next chapter.

Everything mentioned above for symmetric detector locations also holds for the asymmetric detector results as shown in Figures 10-17. The exception is that null frequencies are no longer observed but rather sink<sup>22,23</sup> frequencies, due to the fact that the coherence function is now complex, in general. The sink frequency is defined as the frequency where the absolute magnitude of the coherence function (or cross-power-spectral-density) experiences a local minimum. The coherence function in Figures 15 and 16 shows a second sink frequency. This is most likely due to the interference of the fundamental and second harmonic decay modes in the ARK. The SHA Core 35A' coherence function would probably show a similar behavior but the range between the first and second sink would be much greater because of the larger eigenvalue separation between the first and second harmonics.

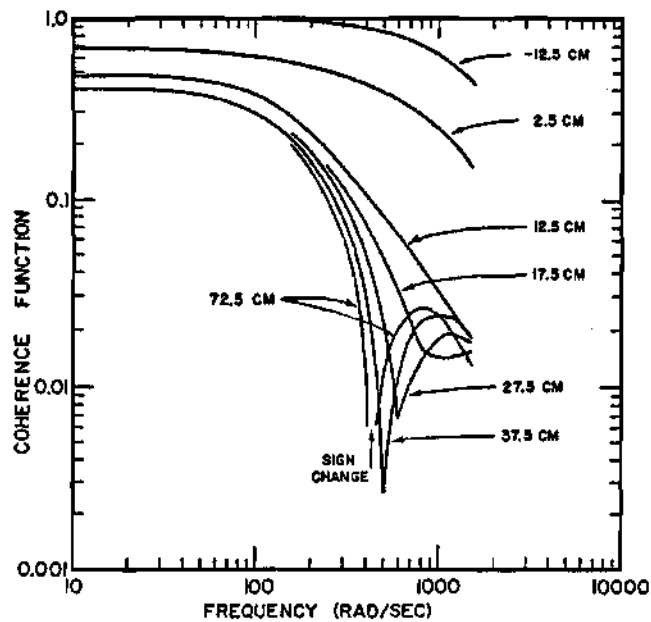


Figure 10. Exact  $|R^{(2,2)}(x_i, x_j, \omega)|$  for the SHA Core 35A1-  
Asymmetric Detector Locations  $x_i = -72.5$  cm;  
 $x_j =$  Variable

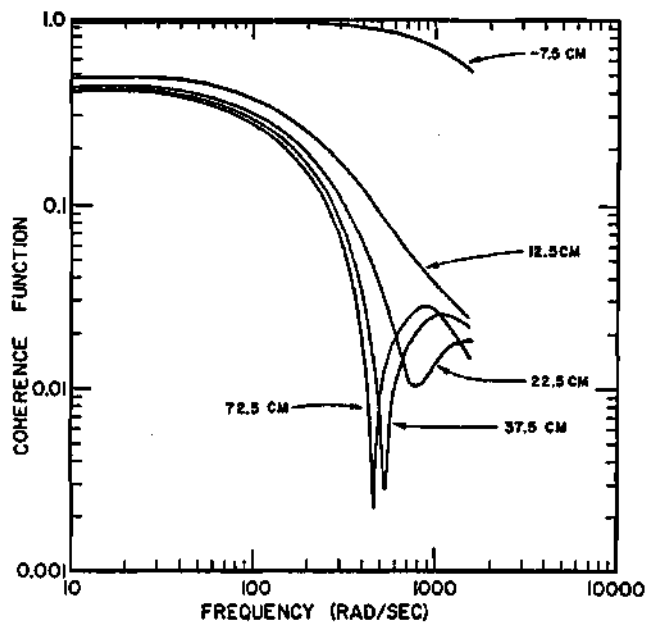


Figure 11. Exact  $|R^{(2,2)}(x_i, x_j, \omega)|$  for the SHA Core 35A1-  
Asymmetric Detector Locations  $x_i = -52.5$  cm;  
 $x_j =$  Variable

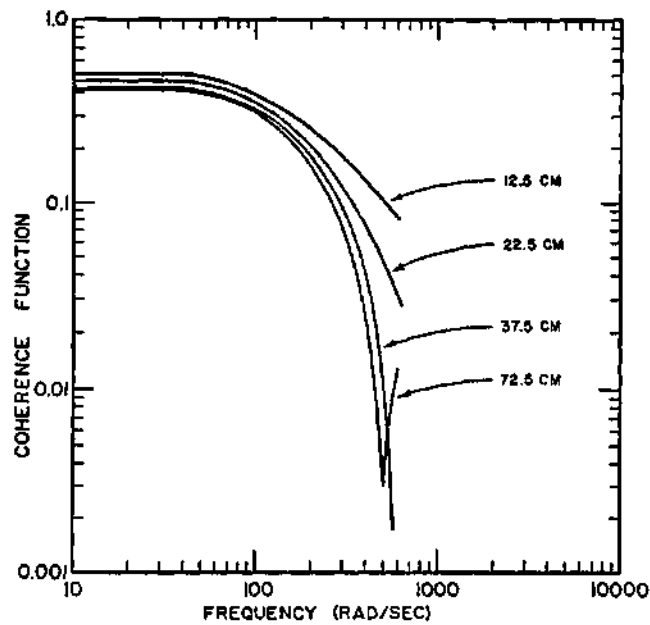


Figure 12. Exact  $|R^{(2,2)}(x_1, x_j, \omega)|$  for the SHA Core 35A'-  
Asymmetric Detector Locations  $-x_1 = -37.5$  cm;  
 $x_j =$  Variable

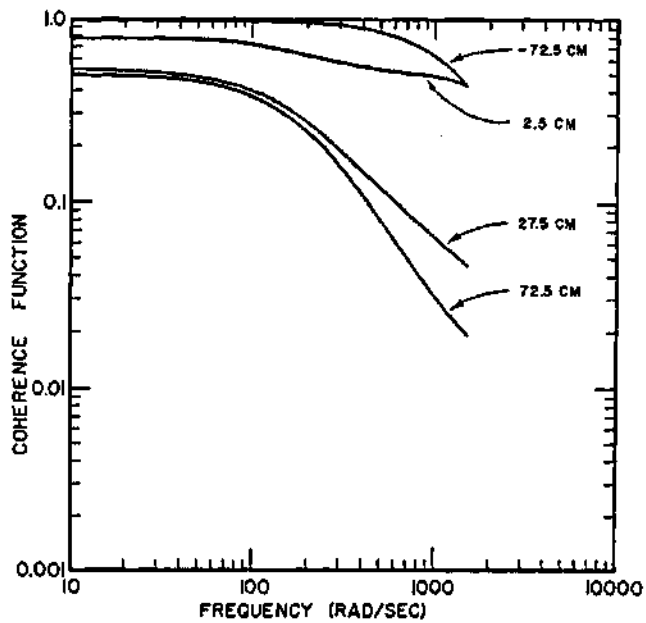


Figure 13. Exact  $|R^{(2,2)}(x_1, x_j, \omega)|$  for the SHA Core 35A'-  
Asymmetric Detector Locations  $-x_1 = -12.5$  cm;  
 $x_j =$  Variable

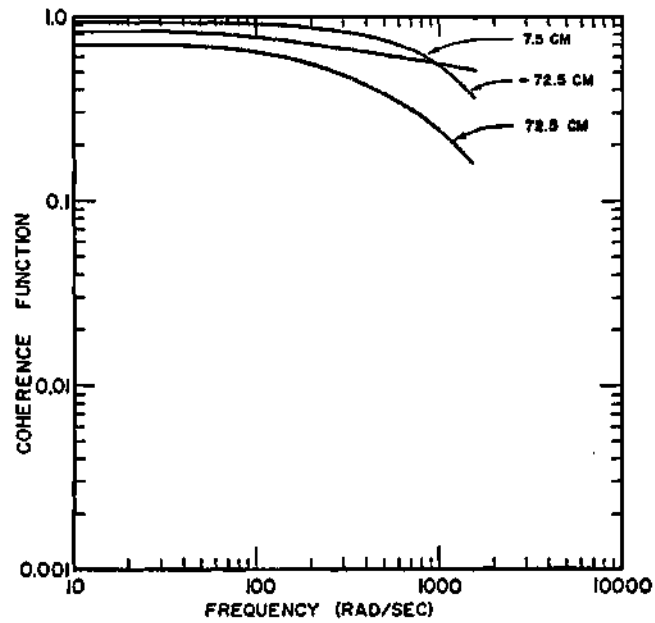


Figure 14. Exact  $|R^{(a,a)}(x_i, x_j, \omega)|$  for the SHA Core 35A'—  
Asymmetric Detector Locations— $x_i = -2.5$  cm;  
 $x_j =$  Variable

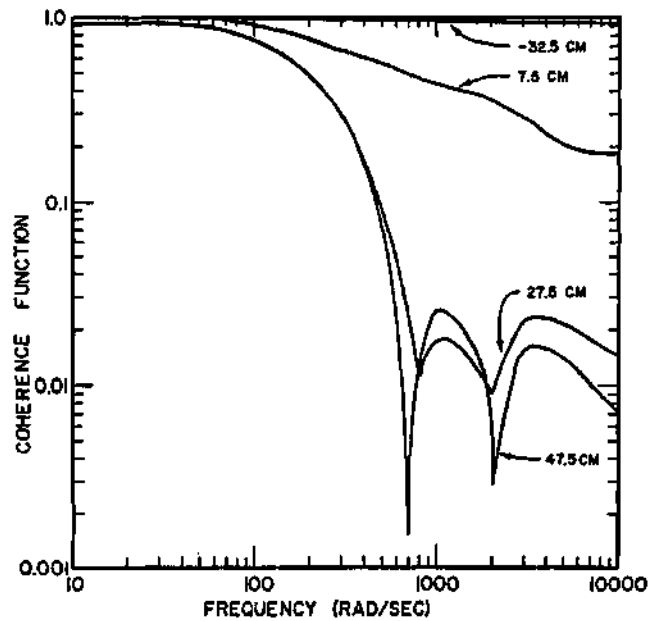


Figure 15. Exact  $|R^{(a,a)}(x_i, x_j, \omega)|$  for the ARK—Asymmetric  
Detector Locations— $x_i = -92.5$  cm;  $x_j =$  Variable

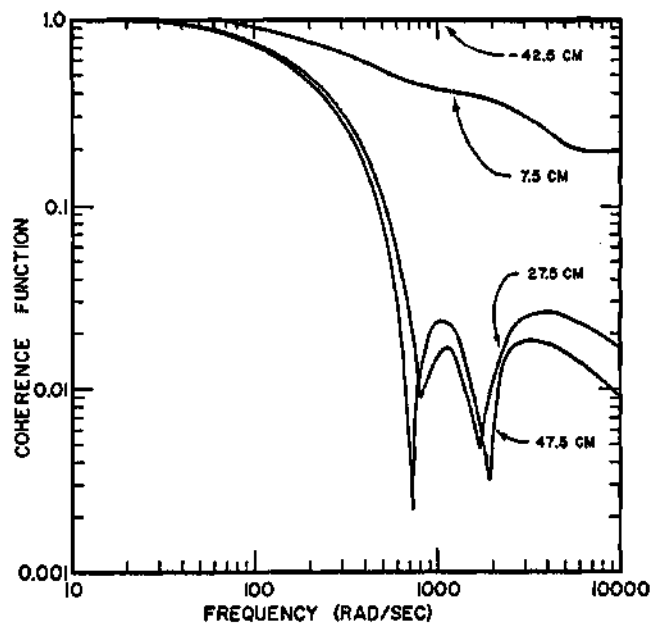


Figure 16. Exact  $|R^{(2,2)}(x_i, x_j, \omega)|$  for the ARK-Asymmetric Detector Locations  $x_i = -32.5$  cm;  $x_j =$  Variable

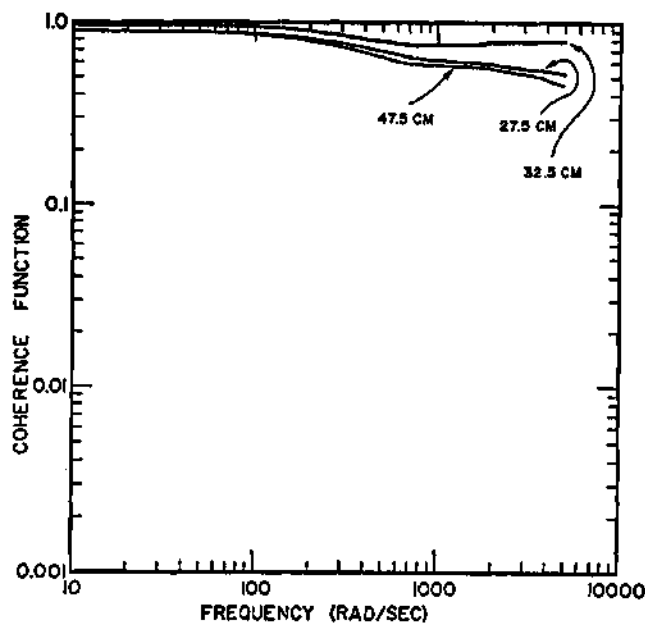


Figure 17. Exact  $|R^{(2,2)}(x_i, x_j, \omega)|$  for the ARK-Asymmetric Detector Locations  $x_i = -2.5$  cm;  $x_j =$  Variable

Detector placement conditions needed to produce a sink or null in the coherence function are vividly demonstrated in Figures 18-21. In these figures, one detector is placed at a fixed location in the left part of the reactor and the other detector is swept across the core. The coherence function at several selected frequencies which bracket the sink frequency is plotted as a function of the second detector's location. The minimum detector pair separation distance to cause a sink and the approximate value of this sink frequency may be inferred from these figures. When one detector is moved from left to right, the first point where two isofrequency lines intersect is the minimum detector distance where a sink can occur. The value of the sink frequency will lie somewhere between these two frequencies. As the detectors are moved further apart, the sink frequency tends to decrease to some asymptotic value. Depth of the sink increases up to the point of symmetry (where the sink becomes a null) and then decreases at lower sink frequencies. The first place where a sink is formed, when one detector is placed far to the left of the decoupling region, is located about 20 centimeters from the polyethylene in the SHA Core 35A' and about 5 centimeters from the decoupling graphite in the case of the ARK.

The coherence functions  $R^{(1,1)}(x_i, x_j, \omega)$ ,  $R^{(1,2)}(x_i, x_j, \omega)$ , and  $R^{(2,1)}(x_i, x_j, \omega)$  were also computed. It was found that the shapes of the absolute values of these various coherence functions were almost identical to  $|R^{(2,2)}(x_i, x_j, \omega)|$ . The phase angles of these several coherence functions were quite different, as will be seen in the next section.

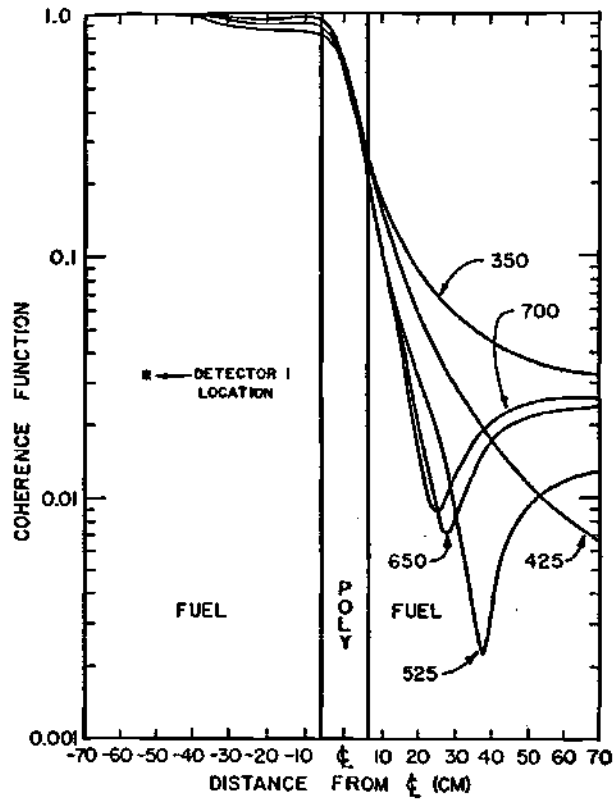


Figure 18. Exact  $|R^{(2,2)}(x_i, x_j, \omega)|$  for the SHA Core 35A'—Selected Frequencies and Asymmetric Detector Locations— $x_i = -52.5$  cm;  $x_j =$  Variable

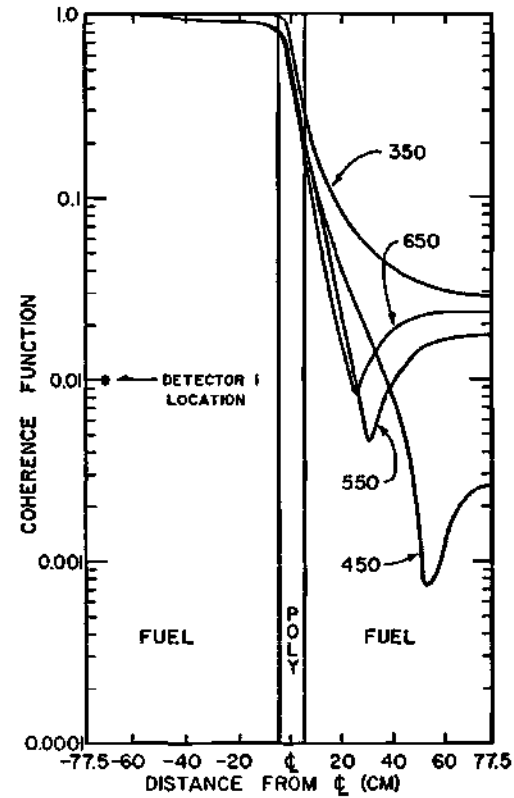


Figure 19. Exact  $|R^{(2,2)}(x_i, x_j, \omega)|$  for the SHA Core 35A'—Selected Frequencies and Asymmetric Detector Locations— $x_i = -72.5$  cm;  $x_j =$  Variable

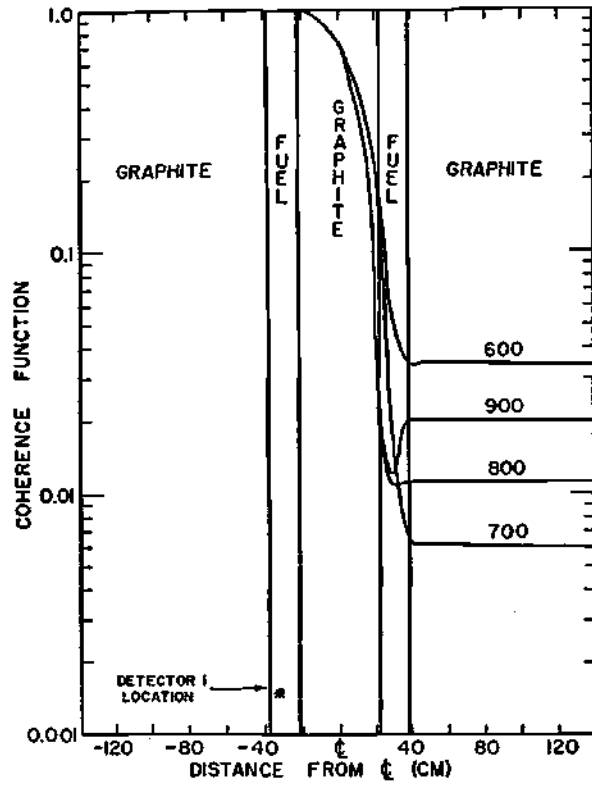


Figure 20. Exact  $|R^{(2,2)}(x_i, x_j, \omega)|$  for the ARK- Selected Frequencies and Asymmetric Detector Locations  $-x_i = -32.5$  cm;  $x_j =$  Variable

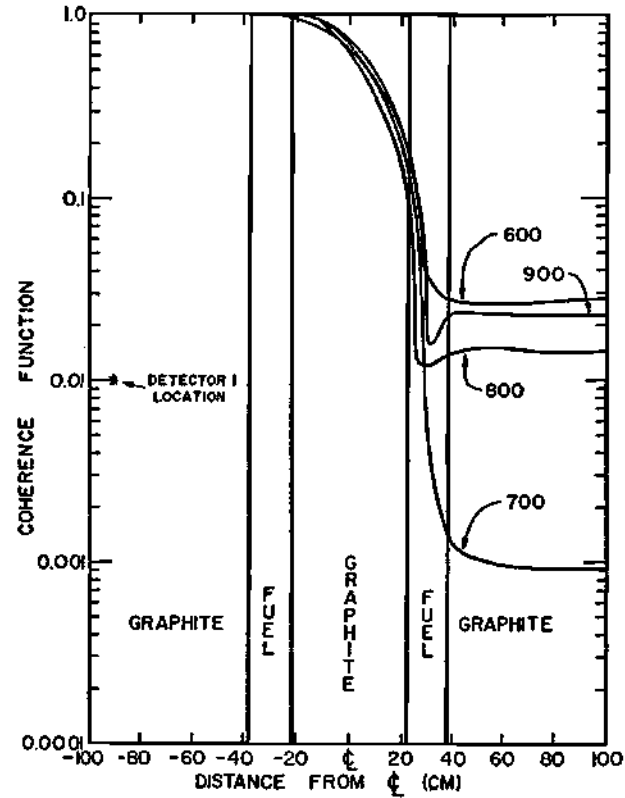


Figure 21. Exact  $|R^{(2,2)}(x_i, x_j, \omega)|$  for the ARK- Selected Frequencies and Asymmetric Detector Locations  $-x_i = -92.5$  cm;  $x_j =$  Variable

### Phase Angles of the Exact Coherence Function

The phase angle values of the CPSD and coherence function are identical because the denominator of equation (4.3) is a real function. Therefore, designating the phase of the coherence function by  $\theta_R^{(k, \ell)}(x_i, x_j, \omega)$  and the phase of the CPSD by  $\theta_{\hat{\Phi}}^{(k, \ell)}(x_i, x_j, \omega)$

$$\theta_{\hat{\Phi}}^{(k, \ell)}(x_i, x_j, \omega) = \tan^{-1} \left[ \frac{\text{Im} \hat{\Phi}^{(k, \ell)}(x_i, x_j, \omega)}{\text{Re} \hat{\Phi}^{(k, \ell)}(x_i, x_j, \omega)} \right] = \theta_R^{(k, \ell)}(x_i, x_j, \omega) . \quad (4.4)$$

It is shown in Appendix H that the CPSD may be expressed as

$$\hat{\Phi}^{(1, z)}(x_i, x_i, \omega) = \frac{\left[ \sum^{(z)} (x_i) - \frac{i\omega}{v(z)} \right] A_{\omega}(x_i) + B_{\omega}(x_i)}{C_{\omega}(x_i)} , \quad (4.5)$$

and

$$\hat{\Phi}^{(z, z)}(x_i, x_j, \omega) = \frac{D_{\omega}(x_i, x_j)}{E_{\omega}(x_i, x_j)} . \quad (4.6)$$

$A_{\omega}(x_i)$ ,  $B_{\omega}(x_i)$ , and  $D_{\omega}(x_i, x_j)$  are complicated functions of the local leakage and the (fast) stochastic source spatial distribution. They are complex functions (real and imaginary components), in general, but the imaginary component is much smaller than the real portion for frequencies below  $\bar{\beta}/\ell$ .  $\ell$  is the thermal neutron lifetime.  $C_{\omega}(x_i)$  is always a real function which is only weakly dependent on frequency below  $\ell^{-1}$  and not dependent on the local leakage.  $E_{\omega}(x_i, x_j)$  is either pure real or weakly complex for frequencies less than  $\ell^{-1}$  and also not a function of the local

leakage. When the detectors are placed in regions of the same type (e.g., both in the graphite but not necessarily the same region),  $E_{\omega}(x_i, x_j)$  is real. When the detectors are located in different types of regions,  $E_{\omega}(x_i, x_j)$  is weakly complex for frequencies below  $l^{-1}$ . It should also be noted that, for contiguous or symmetric detector locations, the numerator in equation (4.6) is pure real and, therefore, the coherence function exhibits zero phase at all frequencies.

The physical implications of Figures 22-29 may be understood by judicious use of equations (4.4) - (4.6). Combination of equations (4.4) and (4.5) lead to the expression

$$\tan\theta_R^{(1,2)}(x_i, x_i, \omega) = \frac{\sum^{(2)}(x_i) \text{Im}A_{\omega}(x_i) - \frac{\omega}{v^{(2)}} \text{Re}A_{\omega}(x_i) + \text{Im}B_{\omega}(x_i)}{\sum^{(2)}(x_i) \text{Re}A_{\omega}(x_i) - \frac{\omega}{v^{(2)}} \text{Im}A_{\omega}(x_i) + \text{Re}B_{\omega}(x_i)} \quad (4.7)$$

If the leakage (both fast and thermal) is small at a given location, equation (4.7) reduces to

$$-\tan\theta_R^{(1,2)}(x_i, x_i, \omega) = \omega l(x_i) \quad (4.8)$$

where  $l(x_i)$  is the local thermal neutron lifetime ( $1/v^{(2)} \sum^{(2)}(x_i)$ ).

Ackermann et al.<sup>19</sup> obtained equation (4.8) by assuming a point reactor model, which by definition has no leakage. Equation (4.7) represents a generalization of the Ackermann method to the space-dependent case.

According to equation (4.8), the slope of the coherence function phase angle is equal to the local thermal neutron lifetime (in low leakage regions). This relationship is well demonstrated in Figures 22 and 23

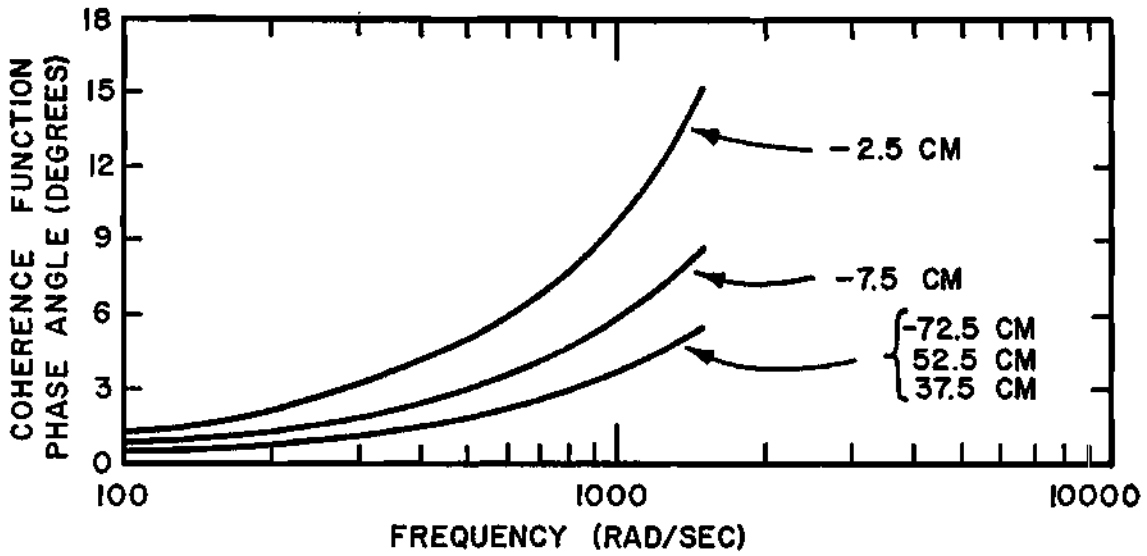


Figure 22. Exact  $\theta R^{(1,2)}(x_i, x_i, \omega)$  for the SHA Core 35A'—  
 $x_i = \text{Variable}$

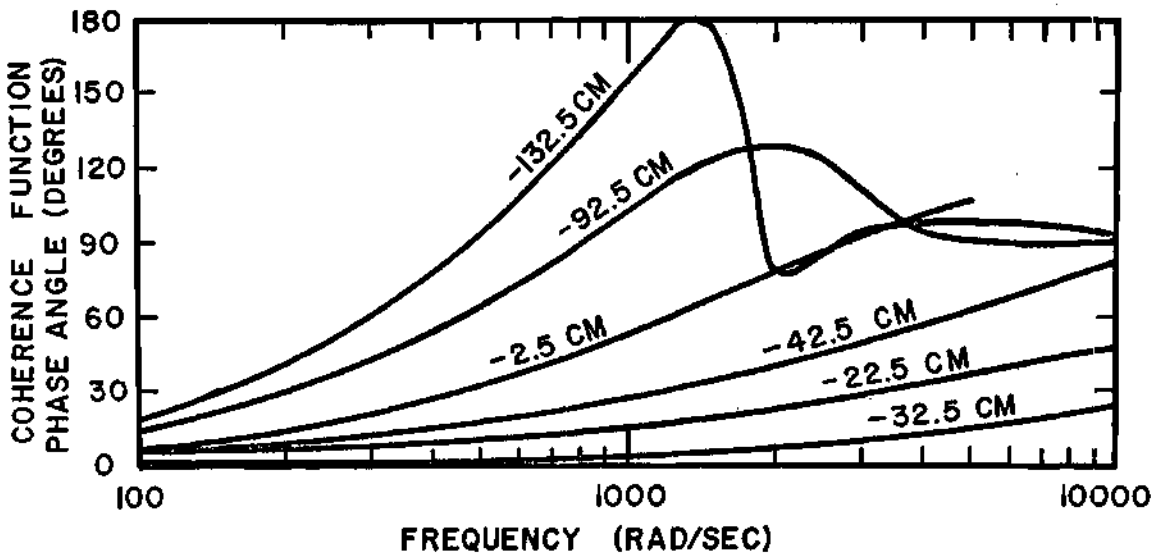


Figure 23. Exact  $\theta R^{(1,2)}(x_i, x_i, \omega)$  for the ARK- $x_i = \text{Variable}$

and has been observed by Penland.<sup>111</sup> The thermal neutron lifetime is longer in the polyethylene and graphite regions of low thermal absorption than in the fuel regions of high thermal neutron absorption. The local lifetimes change within any given material because the leakage (which is not zero in general) changes with position.

At higher frequencies, the complex leakage terms in equation (4.5) become large and the slope of the phase becomes complicated. This is particularly evident in Figure 23. This abrupt change in slope has been experimentally observed by Penland<sup>111</sup> and analytically predicted by Ackermann<sup>112</sup> and Robinson.<sup>113</sup>

The numerator in equation (4.6) tends to dominate at all frequencies considered. As a consequence, the coherence function phase for two thermal neutron detectors is

$$\theta R^{(2,2)}(x_i, x_j, \omega) \cong \tan^{-1} \left[ \frac{\text{Im} D_{\omega}(x_i, x_j)}{\text{Re} D_{\omega}(x_i, x_j)} \right]. \quad (4.8)$$

At low frequencies, the imaginary part of  $D_{\omega}(x_i, x_j)$  is small and the phase is therefore also small, as indicated in Figures 24-27. It is observed that the phase angle tends to be smaller in the SHA Core 35A', at any given frequency, than in the ARK. The reason for this is not entirely clear. It may arise from the fact that the SHA Core 35A' is loosely coupled and the ARK is tightly coupled. It should also be noted that, for certain detector locations, the phase fluctuates widely near the sink frequencies. In this sense, the phase tends to be a more accurate measure of the sink frequency than the absolute magnitude of the coherence function.

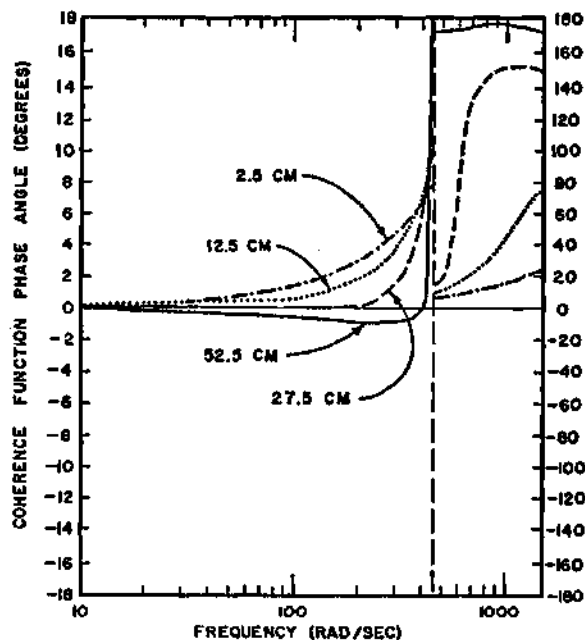


Figure 24. Exact  $\theta R^{(2,2)}(x_i, x_j, \omega)$  for the SHA Core 35A'—  
Asymmetric Detector Locations  $x_i = -72.5$  cm;  
 $x_j =$  Variable

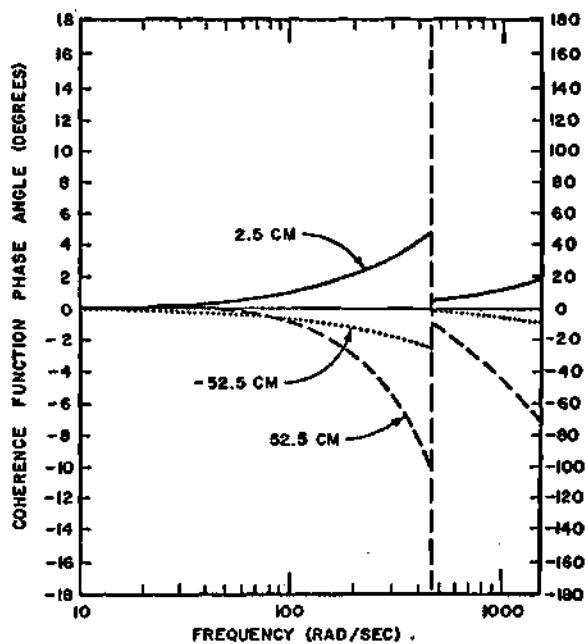


Figure 25. Exact  $\theta R^{(2,2)}(x_i, x_j, \omega)$  for the SHA Core 35A'—  
Asymmetric Detector Locations  $x_i = -12.5$  cm;  
 $x_j =$  Variable

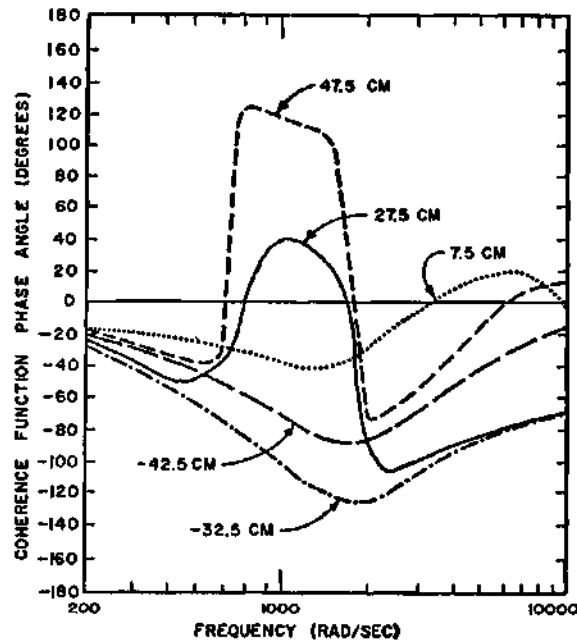


Figure 26. Exact  $\Theta R^{(2,2)}(x_i, x_j, \omega)$  for the ARK-Asymmetric Detector Locations  $x_i = -92.5$  cm;  $x_j =$  Variable

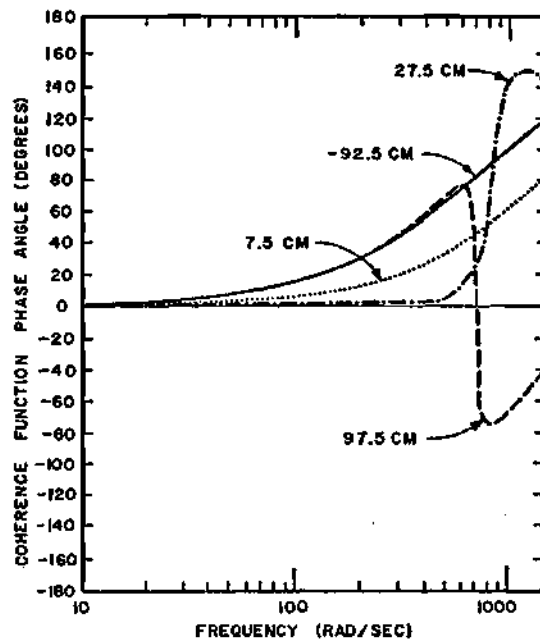


Figure 27. Exact  $\Theta R^{(2,2)}(x_i, x_j, \omega)$  for the ARK-Asymmetric Detector Locations  $x_i = -32.5$  cm;  $x_j =$  Variable

Perhaps the reason for these large fluctuations is due to the interference effects of the fundamental and first harmonic leakage modes (second derivatives of the eigenfunctions).

From Figures 28 and 29 it may be seen that, around the sink frequencies, the real part of equation (4.8) has a dominant role for all detector locations in the SHA Core 35A' but not in the ARK. This probably stems from the previous observation that the phase is generally smaller in the SHA Core 35A'. When the two detectors are at symmetric positions, the imaginary part is zero, and the real part passes from positive to negative to form a null.

#### Discussion

It is apparent from the preceding presentation that the coherence function is a complicated function of the spatial coupling and stochastic source distribution. The spatial coupling, or the number of mean free paths between detectors, is a complex frequency-dependent function. This complex nature arises from the presence of an imaginary (number)  $\hat{i}\omega/v^{(2)}$  absorption cross section (see equations (H.1) and (H.2) in Appendix H) in addition to the normal static destruction operator (i.e., absorption cross section and leakage). At low frequencies, the  $\hat{i}\omega/v^{(2)}$  term is small in comparison with the static destruction operator. Consequently, in this case, the coherence function will assume values which reflect the static coupling. As the frequency is increased, the effective mean free path length decreases, resulting in a smaller spatial coupling. The net effect is a decrease in the coherence function for increasing frequency. However, for frequencies above the sink or null, it appears that the effect of the

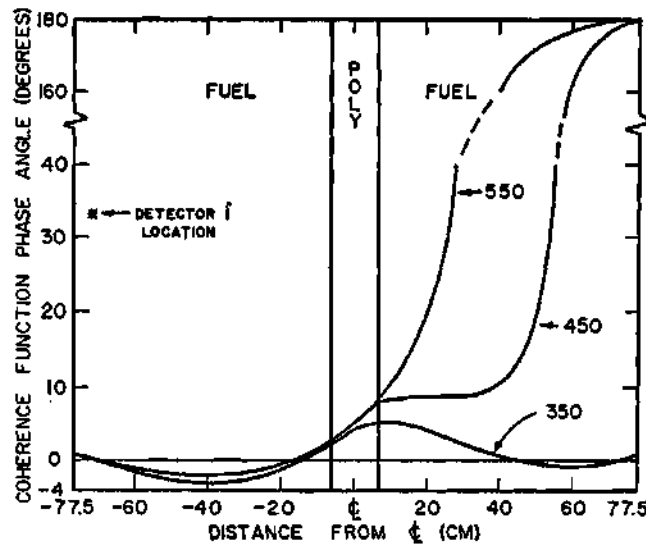


Figure 28. Exact  $\theta R^{(2,2)}(x_i, x_j, \omega)$  for the SHA Core 35A<sup>†</sup>—  
Selected Frequencies and Detector Locations—  
 $x_i = -72.5$  cm;  $x_j =$  Variable

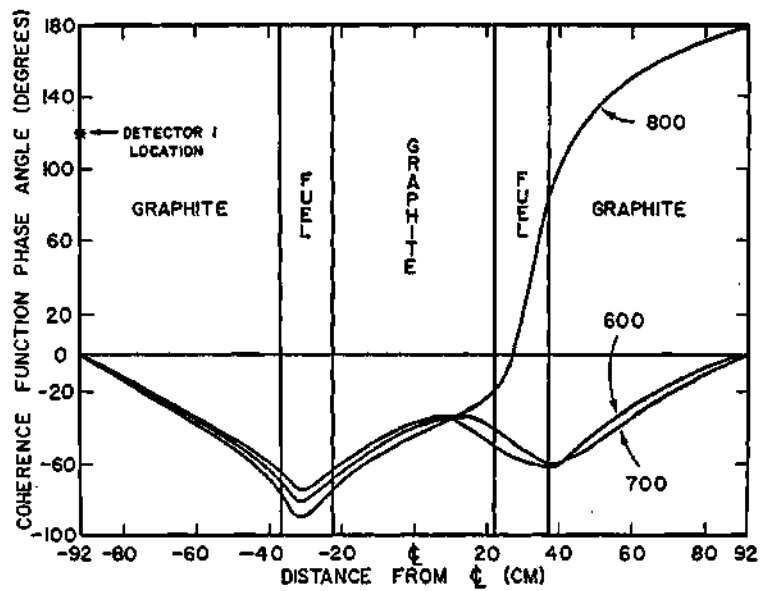


Figure 29. Exact  $\theta R^{(2,2)}(x_i, x_j, \omega)$  for the ARK—Selected  
Frequencies and Detector Locations— $x_i = -92.5$  cm;  
 $x_j =$  Variable

$\hat{i}\omega/v^{(2)}$  term is one of production rather than absorption. The frequency at which this can occur is very dependent on the static core coupling, detector separations, and stochastic source distribution. It is quite difficult to separate one effect from another.

The effects of the  $\hat{i}\omega/v^{(2)}$  absorber are well reflected in the shape of the phase angle. Here the effect of this imaginary absorber is highly dependent on the relative magnitude of the local destruction operator. In this case as before, for frequencies above the sink or null, the effect of the  $\hat{i}\omega/v^{(2)}$  term is that of production.

All the major conclusions of this chapter may be qualitatively explained by use of the frequency dependent spatial coupling and stochastic source spatial distribution concepts. A more quantitative analysis follows in the next chapter. The major conclusions and explanations are listed below.

1. Sink or null frequencies in  $|R^{(z,z)}(x_i, x_j, \omega)|$  occur for certain detector separations and placements and not for others. Sink or null frequencies arise because the net effect of the  $\hat{i}\omega/v^{(2)}$  term changes from that of an absorption to production cross section. It appears that, in principle, sink or null frequencies can appear for any detector separation. However, for detectors located in the decoupling region, the sink or null frequency is most likely very high.

2. For the symmetric reactor models investigated, symmetric thermal neutron detector locations produced real coherence functions and, consequently, null frequencies. Conversely, asymmetric detector locations produced complex coherence functions and, therefore, sink frequencies.

This comes about because the integrated value of one detector's Green's function is equal to the other (see equation (4.3)). Consequently, when the complex conjugate is taken, the CPSD is real and therefore so is the coherence function.

3.  $|R^{(2,2)}(x_i, x_j, \omega)|$  tends to be smaller in the SHA Core 35A' than in the ARK, particularly at low frequencies. The number of frequency dependent mean free paths between detectors is the explanation for this phenomenon.

4. The sink or null frequency increases with decreasing detector separation for a given reactor model. If it is assumed that the sink or null occurs when the two detectors are a certain number of frequency dependent mean free paths apart, then the above conclusion follows. That is, the closer the detectors are, the higher must be the effective destruction probability per unit length of intervening material to produce the same number of mean free paths. This is accomplished by having a higher  $\hat{i}\omega/v^{(2)}$  term in the destruction operator.

5. The value of  $|R^{(2,2)}(x_i, x_j, \omega)|$  at any given frequency decreases with increasing detector separation for frequencies below the sink or null frequency, but increases with increasing detector separation for frequencies above the sink or null frequency. This may be explained by assuming that the  $\hat{i}\omega/v^{(2)}$  term acts as an absorption cross section below the sink or null frequency and a production cross section above it.

6. The relative magnitude of the imaginary to real component of the coherence function (i.e., the phase angle) tends to be smaller in the SHA Core 35A' than in the ARK at low frequencies. This stems from the

fact that the  $\hat{i}\omega/v^{(2)}$  term is relatively small in comparison to the destruction operator in the SHA Core 35A' but not in the ARK.

7. The local thermal neutron lifetime can be inferred from  $\theta R^{(1,2)}(x_i, x_i, \omega)$  only when the local leakage is very small.

## CHAPTER V

## MODAL APPROXIMATION OF THE COHERENCE FUNCTION

Modal approximations of the space- and energy-dependent coherence function (SECF) for 1D representations of two coupled core reactors were undertaken<sup>114</sup> to answer the following questions.

1. How many expansion modes are needed to closely approximate the exact solution?

2. What coupled core reactor characteristics and detector pair placements are necessary for the two-omega ( $2\omega$ ) or the two-lambda ( $2\lambda$ ) mode expansion approximation of the exact solution to be valid?

3. Can the measured coherence function null or sink frequency be interpreted using the  $2\omega$  or  $2\lambda$  mode approximation?

4. Can a method be developed to extract reactor parameters from the measured coherence function when interpreted in the light of the  $2\omega$  or  $2\lambda$  mode approximation?

5. What is the relationship between the MCC<sup>20,59</sup> (see Appendix A) and the coherence function in coupled cores?

Modal and nodal expansion approximations of the space- and energy-dependent noise are characterized as those procedures in which the Green's function or transfer matrix is approximated by a series expansion of trial functions. The type of trial functions chosen for this task is dependent on the nature of the problem under investigation. In this work, the objec-

tives were to use those trial functions whereby some global reactor dynamic parameters could be inferred from the measured noise and to maintain the capability of extension to two-dimensional, multiregion systems. These particular objectives immediately ruled out the use of nodal expansions<sup>22,27</sup> and the natural,<sup>25</sup> Green's function,<sup>23</sup> Helmholtz,<sup>30</sup> and image<sup>79</sup> modal expansion trial functions. However, the lambda and modified omega modal approximations were consistent with the objectives.<sup>114</sup>

### Method of Solution and Results

The same 1D geometrical representations of the SHA Core 35A' and ARK, which were used in the last chapter, are used here (Figures 4 and 5, respectively). Also, the macroscopic constants are the same (SHA Core 35A', Table 1; ARK, Table 2).

Modal approximations of the SECF for the particular two-group, one-dimensional models at hand were arrived at by the use of the coherence function definition (Appendix A), the modal approximations of the Green's response function (Appendix C), the method to produce the eigenvalues and eigenvectors (Appendix F), and finally the form of the auto- and cross-power-spectral-densities (equations (3.33) and (3.31)). Again assuming the point detector approximation, the APSD and CPSD for the models at hand are written, respectively

$$\hat{\phi}(k, k)_{(x_1, x_1, T, \omega)} = \bar{D}_i^{(k)} \frac{\Delta(T, \omega)}{T} \quad (5.1)$$

$$+ \sum_{n=0}^N \sum_{m=0}^N C_{nm} D_n^{(k)}(x_1) D_m^{(k)}(x_1) G_{nm}(T) H_{nm}(\omega) ,$$

and

$$\hat{\phi}^{(k,\ell)}(x_i, x_j, T, \omega) = \sum_{n=0}^N \sum_{m=0}^N C_{nm} D_n^{(k)}(x_i) D_m^{(\ell)}(x_j) G_{nm}(T) H_{nm}(\omega) , \quad (5.2)$$

where

$$\frac{\Delta(T, \omega)}{T} = \frac{2}{(\omega T)^2} [1 - \cos(\omega T)] , \quad (5.3)$$

$$C_{nm} \equiv \int_{\text{reactor}} dx' \frac{\chi_2 \bar{v}_p \sum_f^{(2)} (x') \phi^{(2)}(x') \psi_n^{(1)+}(x') \psi_m^{(1)+}(x')}{\langle \vec{\psi}_n, \vec{\nabla}^{-1} \vec{\psi}_n \rangle \langle \vec{\psi}_m, \vec{\nabla}^{-1} \vec{\psi}_m \rangle} \quad (5.4)$$

$$D_n^{(k)}(x_i) \equiv \sum_{\text{det-i}}^{(k)} (x_i) \psi_n^{(k)}(x_i) , \quad (5.5)$$

$$G_{nm}(T) \equiv \left[ \frac{\omega_n^{T+1} - e^{-\omega_n T}}{(\omega_n T)^2} + \frac{\omega_m^{T+1} - e^{-\omega_m T}}{(\omega_m T)^2} \right] (\omega_m + \omega_n)^{-1} \quad (5.6)$$

$$H_{nm}(\omega) \equiv \frac{(\omega_m + \omega)}{(\omega_n + i\omega)(\omega_m - i\omega)} . \quad (5.7)$$

If it is also assumed that the detection time is small such that  $|\omega T| \ll 1$  and  $|\omega_n T| \ll 1$  for all  $n$  from 0 to  $N$ , then the following approximations hold

$$\frac{\Delta(T, \omega)}{T} \cong 1 , \quad (5.8)$$

and

$$G_{nm}(T) \cong 1/(\omega_m + \omega_n) . \quad (5.9)$$

Using equations (5.1) - (5.9) and the definitions of the coherence function (Appendix A), the modal approximation of the SECF may be written

$$R^{(k, \ell)}(x_i, x_j, \omega) = \quad (5.10)$$

$$\frac{\sum_{n=0}^N \sum_{m=0}^N \frac{C_{nm} \psi_n^{(k)}(x_i) \psi_m^{(\ell)}(x_j)}{(\omega_n + i\omega)(\omega_m - i\omega)}}{\left\{ \left[ \sum_{n=0}^N \sum_{m=0}^N \frac{C_{nm} \psi_n^{(k)}(x_i) \psi_m^{(k)}(x_i)}{(\omega_n + i\omega)(\omega_m - i\omega)} \right] \left[ \sum_{n=0}^N \sum_{m=0}^N \frac{C_{nm} \psi_n^{(\ell)}(x_j) \psi_m^{(\ell)}(x_j)}{(\omega_n + i\omega)(\omega_m - i\omega)} \right] \right\}}$$

The similarity between the CPSD portion of equation (5.10) and the form derived by Akcazu and Osborn<sup>85</sup> from the Langevin formulation should be noted. In the Langevin technique the source terms  $C_{nm}$  are specified from the noise equivalent source procedure<sup>85</sup> which is valid even in power reactors as long as the proper noise equivalent source is specified.

The modified omega and lambda thermal eigenfunctions ( $\psi^{(\omega)}(x)$  and  $\psi^{(\lambda)}(x)$ , respectively), used in the modal approximation, were calculated by the critical determinate method outlined in Appendix F. These modes are plotted in Figures 30-41 for the 1D representations of the SHA Core 35A' and ARK. For each expansion index, they are normalized such that the maximum value is unity. It should be noted that the fundamental lambda and modified omega modes and the first harmonic lambda and modified omega modes have identical shapes in the SHA Core 35A' (Figures 30 and 31) but differ a fair amount in the case of the ARK (Figures 36 and 37). The

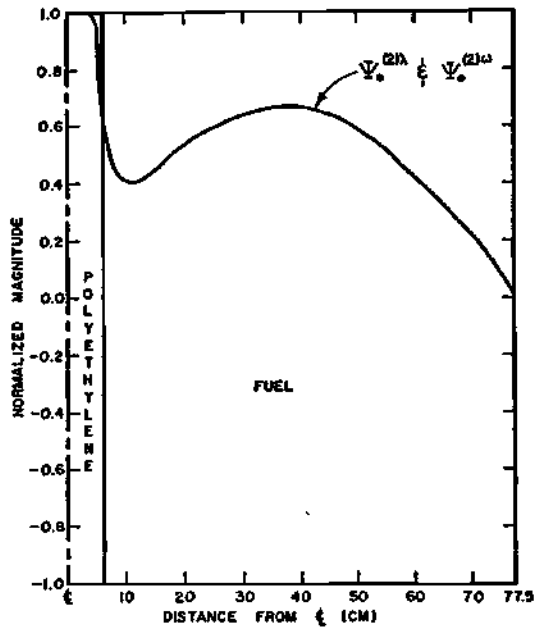


Figure 30. Fundamental Thermal Eigenfunctions—SHA Core 35A'

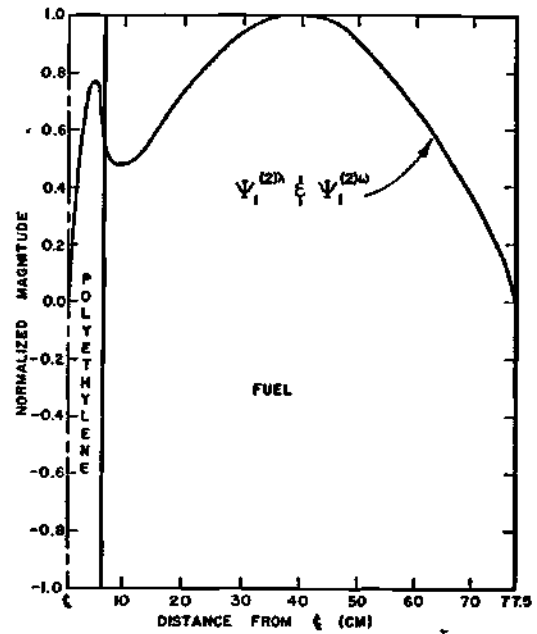


Figure 31. First Harmonic Thermal Eigenfunctions—SHA Core 35A'

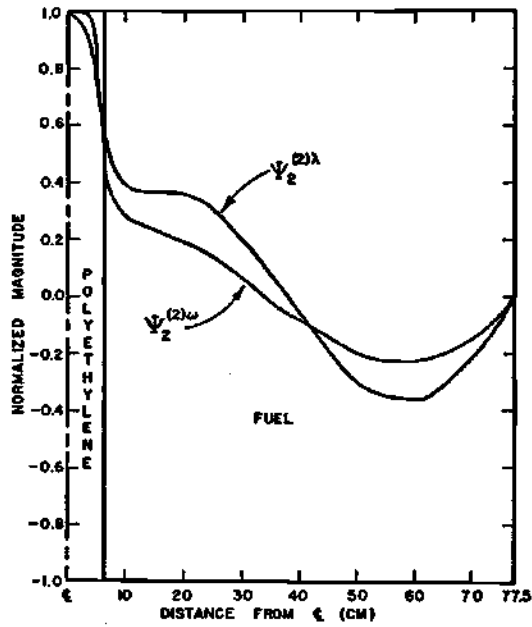


Figure 32. Second Harmonic Thermal Eigenfunctions—SHA Core 35A'

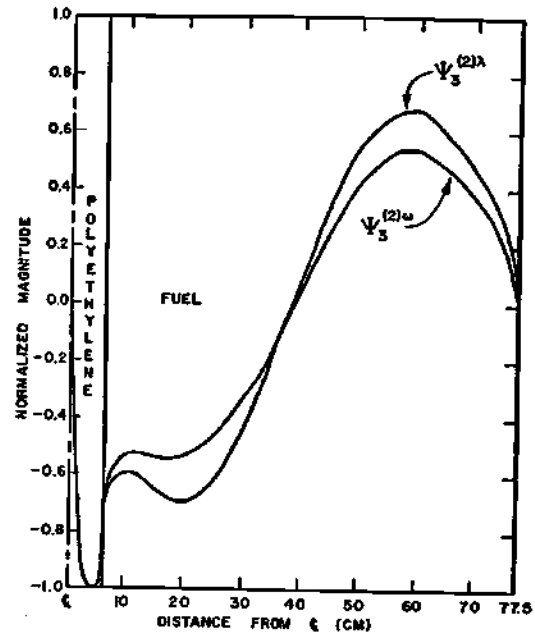


Figure 33. Third Harmonic Thermal Eigenfunctions—SHA Core 35A'

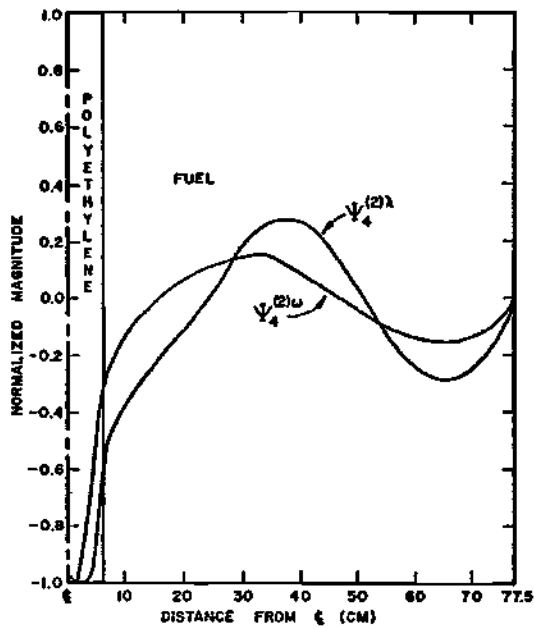


Figure 34. Fourth Harmonic Thermal Eigenfunctions—SHA Core 35A'

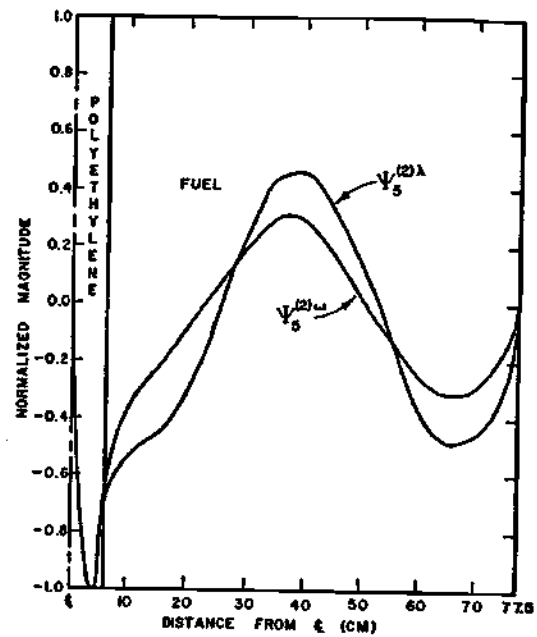


Figure 35. Fifth Harmonic Thermal Eigenfunctions—SHA Core 35A'

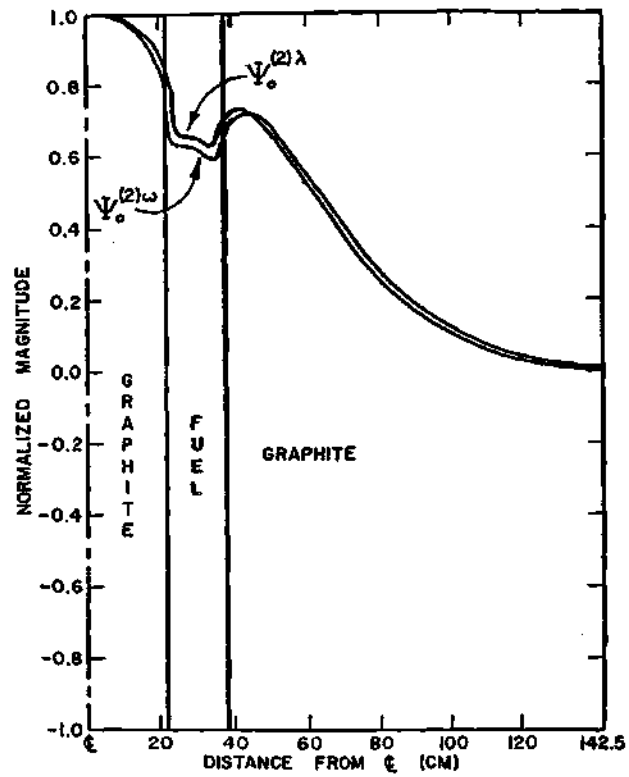


Figure 36. Fundamental Thermal Eigenfunctions-ARK

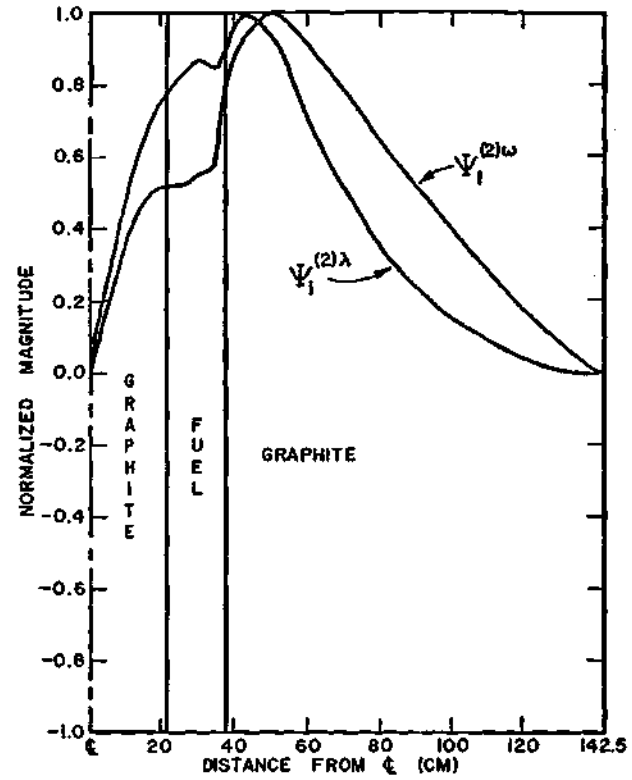


Figure 37. First Harmonic Thermal Eigenfunctions-ARK

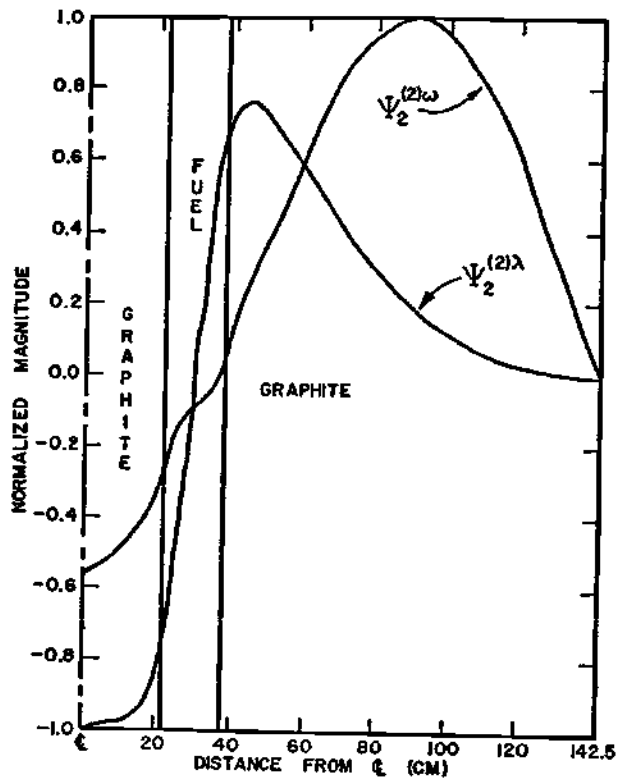


Figure 38. Second Harmonic Thermal Eigenfunctions-ARK

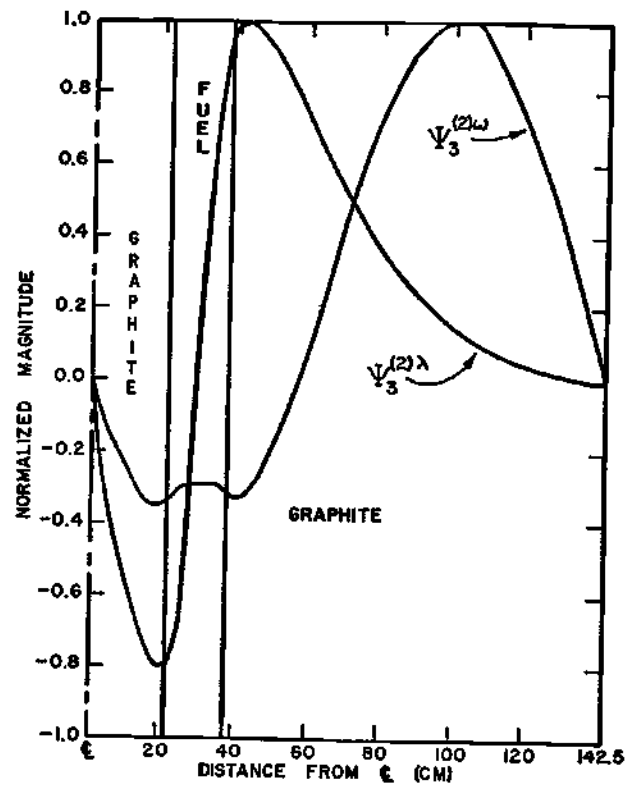


Figure 39. Third Harmonic Thermal Eigenfunctions-ARK

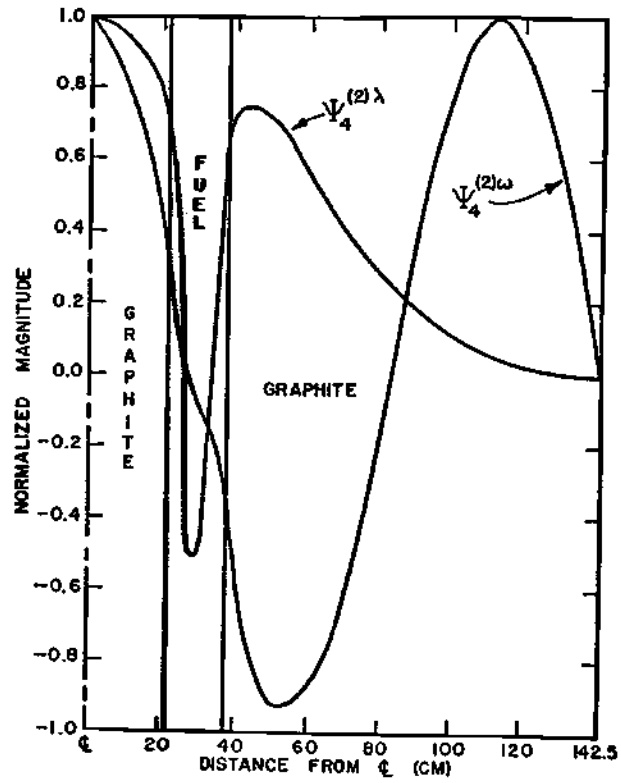


Figure 40. Fourth Harmonic Thermal Eigenfunctions-ARK

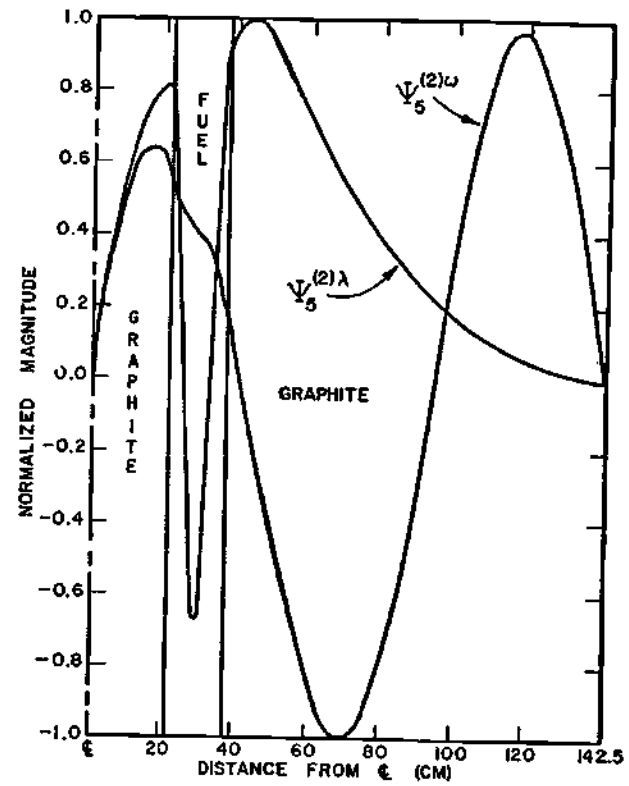


Figure 41. Fifth Harmonic Thermal Eigenfunctions-ARK

reason for this can be seen upon inspection of equations (B.24) and (B.28) in Appendix B. In reactors like the ARK, which have large moderator regions of low absorbing material, the  $\omega_n \vec{V}_n^{-1}$  production operator is not small compared to the destruction operator. This is not the case for the SHA Core 35A', where the moderator region (which is also the fuel region), although large, has a relatively high absorption cross section. The shape difference between the lambda and modified omega modes is also demonstrated in the higher harmonics (Figures 32-35 and 38-41). In the SHA Core 35A' the higher harmonic shapes tend to have the same form, but there is complete lack of similarity in the case of the ARK.

Shape differences are also reflected in the orthogonality properties. Orthogonality properties for the modified omega and lambda modes in the SHA Core 35A' and ARK are presented in Tables 3-8. It is apparent from these tables that both modal types have the required biorthogonality properties<sup>30</sup> (see Appendix B), because the off-diagonal elements are small relative to the diagonal elements. It is also true that the modified omega modes have the property of finality<sup>30,115</sup> (see Appendix B). That is, there is the absence of modal coupling. The finality property was assumed in the derivation of lambda and modified omega approximation of the Green's function (see Appendix C, equations (C.7) and (C.11)). However, the lambda modes do not have the finality property, as indicated in Tables 5 and 8. The deviation from this property is fairly small for the SHA Core 35A' (at most 18% for the first six lambda expansion modes), but quite large for the ARK (up to 96%). The consequence of the above fact is that the lambda mode approximation of the exact coherence function will not be as good as the modified omega mode approximation.

Table 3. Results of a Biorthogonality Check on Some Modified Omega Modes of the SHA Core 35A'

		Normalized Values of $\langle \vec{\psi}_n^w, \vec{\psi}_m^w \rangle$				
n	m → 0	1	2	3	4	5
0	1	0.0034	+	-	+	-
1	-0.0043	1	-	-	+	+
2	0.0108	0.0052	1	0.0028	-0.0034	0.0078
3	0.0088	0.0078	-0.0028	1	-0.0095	0.0099
4	-0.0018	-	+	+	1	-0.0062
5	-	-	+	-	-0.0011	1

Note: + or - denotes that the absolute magnitude is less than 0.001.

Table 4. Results of a Biorthogonality Check on Some Lambda Modes of the SHA Core 35A'

		Normalized Values of $\langle \vec{\psi}_n^\lambda, \vec{\psi}_m^\lambda \rangle$				
n	m → 0	1	2	3	4	5
0	1	0.0055	-	-	+	+
1	-0.005	1	-	-	+	+
2	-	+	1	0.0029	-0.0012	-
3	+	-	0.0016	1	+	-
4	0.0022	-	-0.0028	-	1	-0.0018
5	-	+	-	-	+	1

Note: + or - denotes that the absolute magnitude is less than 0.001.

Table 5. Results of a Finality Check on Some Lambda Modes of the SHA Core 35A'

		Normalized Values of $\langle \vec{\psi}_n^\lambda, \vec{V}^{-1} \vec{\psi}_m^\lambda \rangle$				
n	m → 0	1	2	3	4	5
0	1	0.0053	-0.0233	-	0.0230	+
1	-0.0056	1	-	-0.0068	-	0.0109
2	-0.0872	+	1	0.0029	-0.0616	-
3	+	-0.0256	0.0017	1	+	-0.0216
4	0.1846	+	-0.1317	-	1	-0.0016
5	-	0.0866	-	-0.0449	+	1

Note: + or - denotes that the absolute magnitude is less than 0.001.

Table 6. Results of a Biorthogonality Check on Some Modified Omega Modes of the ARK

		Normalized Values of $\langle \vec{\psi}_n^\omega, \vec{V}^{-1} \vec{\psi}_m^\omega \rangle$				
n	m → 0	1	2	3	4	5
0	1	-	+	-	-	-
1	0.0018	1	-0.0035	0.0021	-	-
2	0.0011	+	1	0.0028	-	-
3	+	+	-0.0031	1	+	-
4	-0.0011	+	-	+	1	-
5	+	-	0.0014	+	-	1

Note: + or - denotes that the absolute magnitude is less than 0.001.

Table 7. Results of a Biorthogonality Check on Some Lambda Modes of the ARK

		Normalized Values of $\langle \vec{\psi}_n^\lambda, \vec{M} \vec{\psi}_m^\lambda \rangle$				
n	m $\rightarrow$ 0	1	2	3	4	5
0	1	+	-	+	0.0018	+
1	+	1	-	-	-	-
2	-0.0014	+	1	0.0031	-0.0015	+
3	+	-0.0015	-0.0026	1	-	+
4	0.0092	+	-	-0.0017	1	0.0613
5	0.0035	-	0.0038	-0.0014	0.0362	1

Note: + or - denotes that the absolute magnitude is less than 0.001.

Table 8. Results of a Finality Check on Some Lambda Modes of the ARK

		Normalized Values of $\langle \vec{\psi}_n^\lambda, \vec{V}^{-1} \vec{\psi}_m^\lambda \rangle$				
n	m $\rightarrow$ 0	1	2	3	4	5
0	1	+	-0.1097	-	0.5746	0.0268
1	+	1	+	-0.2842	0.0085	-0.4945
2	-0.1517	-	1	0.0028	-0.0933	-0.0055
3	+	-0.2972	-0.0038	1	-0.0035	0.2519
4	0.9596	-0.0074	-0.1121	0.0024	1	0.0561
5	0.0747	-0.8267	-0.0050	0.3864	0.0602	1

Note: + or - denotes that the absolute magnitude is less than 0.001.

Various modal approximations of the absolute value of  $R^{(2,2)}(x_i, x_j, \omega)$  are presented in Figures 42-57. Graphs for the symmetric detector locations are given in Figures 42-49. The  $2\lambda$  and  $2\omega$  mode approximations for the SHA Core 35A' (Figures 42 and 43) tend to be in fairly good agreement not only with themselves, but also with the exact solution (Figure 8) for frequencies below and including the null frequency. The  $2\omega$  mode approximation for detector separations of 87 cm in the ARK (Figure 45) agrees well with the exact solution (Figure 9) below the null frequency. The  $2\lambda$  mode approximation in the ARK (Figure 44) led to a low estimate of the null frequency. High frequency structure is not possible with only a two mode expansion. It is necessary to run the expansion to higher orders to obtain this structure, as shown in Figures 46-49. The same low frequency shape is retained with the higher order expansion. No improvement in this frequency range is obtained with more expansion modes. In fact, the quality of the modified omega mode expansion tends to decrease as the modal number increases in the ARK model. This may possibly be explained by the fact that the first harmonic transverse mode eigenvalue falls between the second and third horizontal mode eigenvalues.

For asymmetric detector locations (Figures 50-57) the same general conclusions as in the symmetric cases may be drawn. It takes more than a two-mode expansion to approximate the exact coherence function when one or both of the detectors are located near the reactor centerline. The reason for this may be understood when it is realized that the value of the first harmonic eigenfunction is small near the reactor's center. Consequently, it takes at least three expansion modes to approximate the behavior in this region.

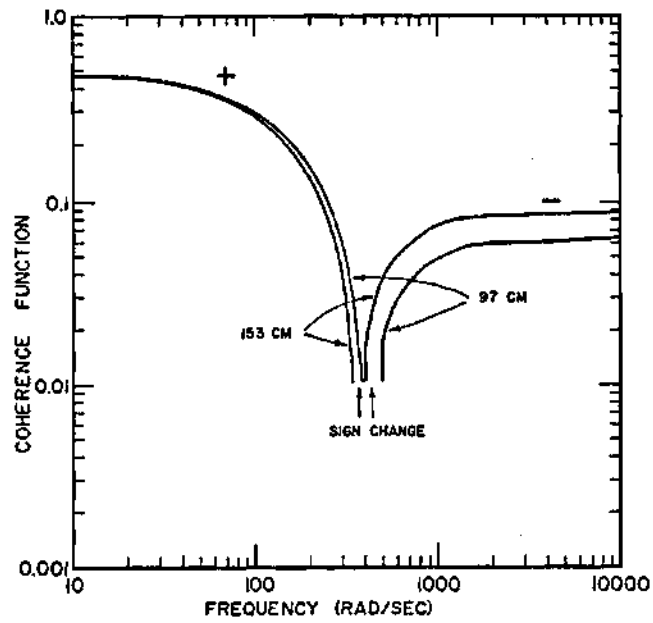


Figure 42.  $2\lambda$  Mode  $|R^{(2,2)}(x_i, -x_i, \omega)|$  for the SHA Core 35A'—  
Varying Symmetric Detector Separation Distances

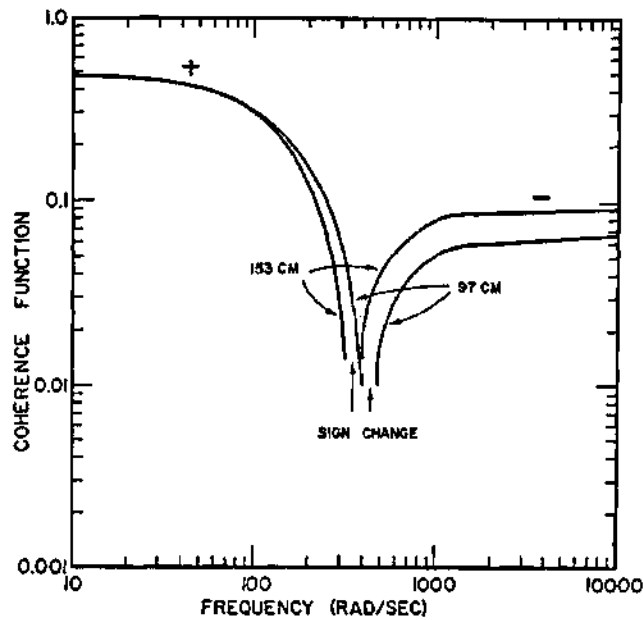


Figure 43.  $2\omega$  Mode  $|R^{(2,2)}(x_i, -x_i, \omega)|$  for the SHA Core 35A'—  
Varying Symmetric Detector Separation Distances

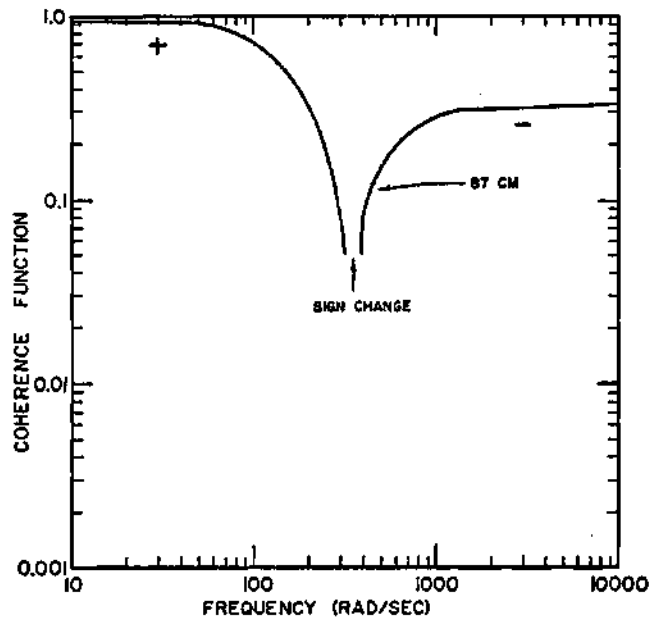


Figure 44.  $2\lambda$  Mode  $|R^{(2,2)}(x_i, -x_i, \omega)|$  for the ARK-Symmetric Detector Separation Distance

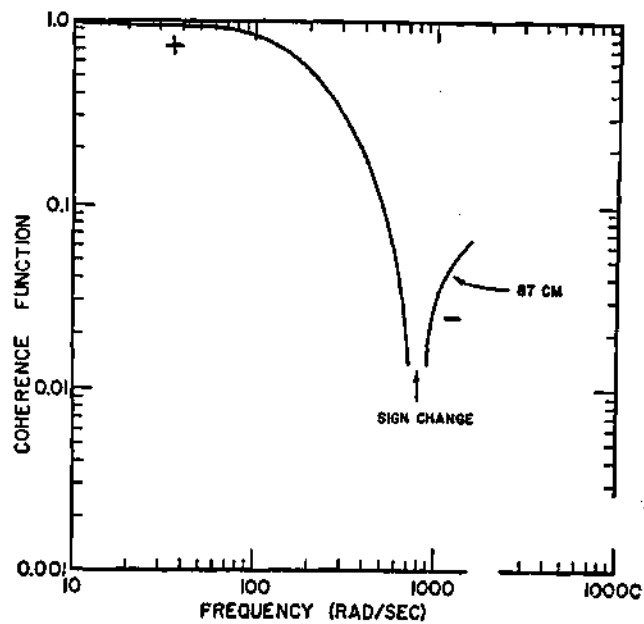


Figure 45.  $2\omega$  Mode  $|R^{(2,2)}(x_i, -x_i, \omega)|$  for the ARK-Symmetric Detector Separation Distance

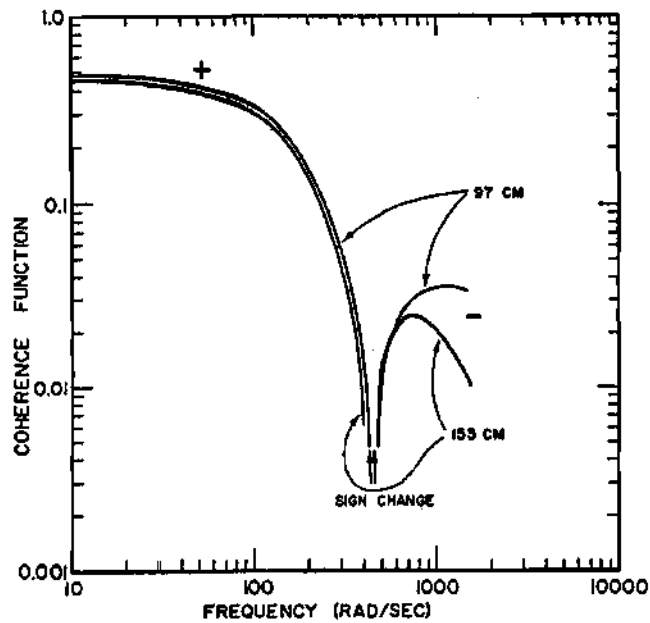


Figure 46.  $6\lambda$  Mode  $|R^{(2,2)}(x_i, -x_i, \omega)|$  for the SHA Core 35A'-  
Varying Symmetric Detector Separation Distances

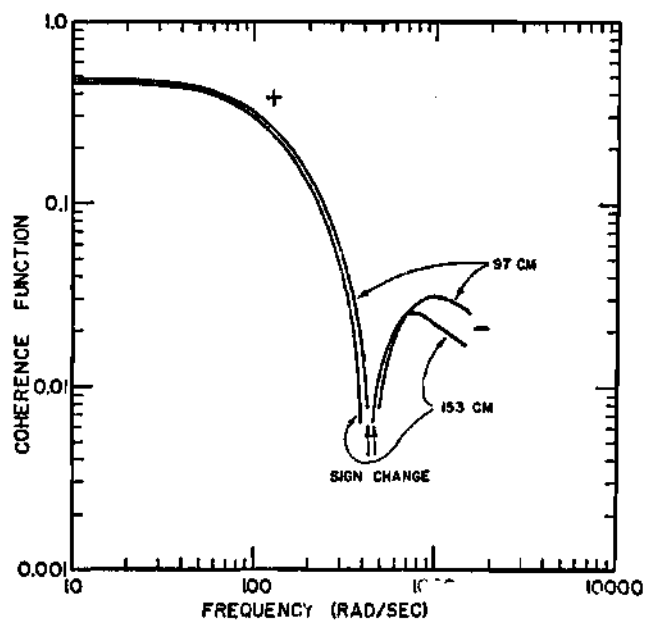


Figure 47.  $6\omega$  Mode  $|R^{(2,2)}(x_i, -x_i, \omega)|$  for the SHA Core 35A'-  
Varying Symmetric Detector Separation Distances

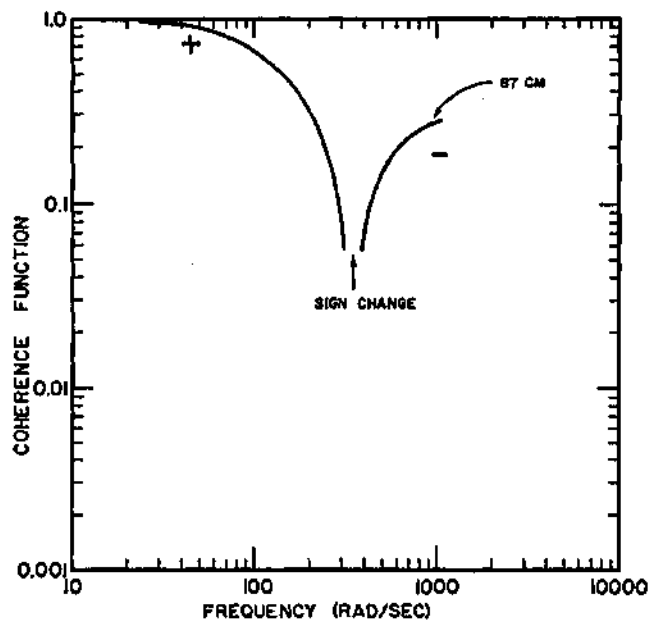


Figure 48.  $6\lambda$  Mode  $|R^{(2,2)}(x_1, -x_1, \omega)|$  for the ARK-Symmetric Detector Separation Distance

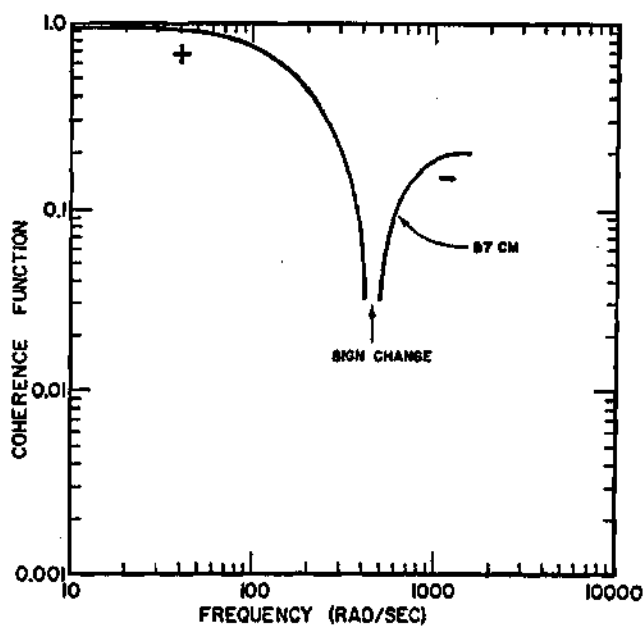


Figure 49.  $6\omega$  Mode  $|R^{(2,3)}(x_1, -x_1, \omega)|$  for the ARK-Symmetric Detector Separation Distance

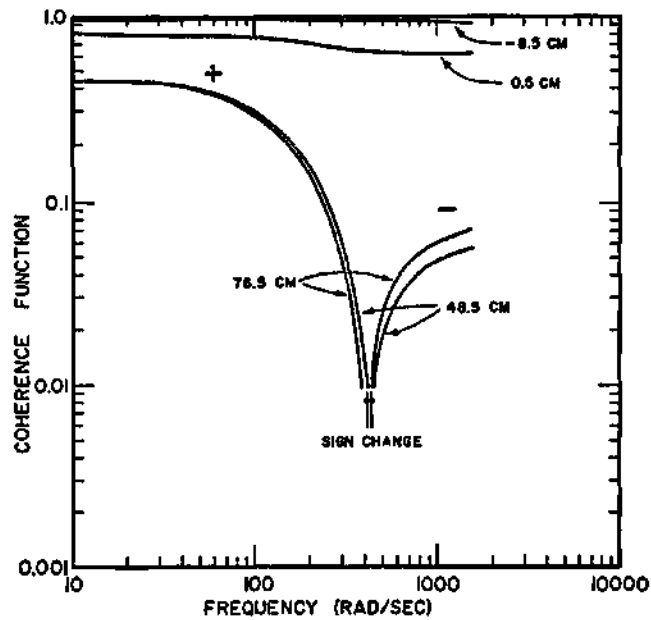


Figure 50.  $2\lambda$  Mode  $|R^{(2,2)}(x_i, x_j, \omega)|$  for the SHA Core 35A'-  
Asymmetric Detector Locations  $x_i = -48.5$  cm;  
 $x_j =$  Variable

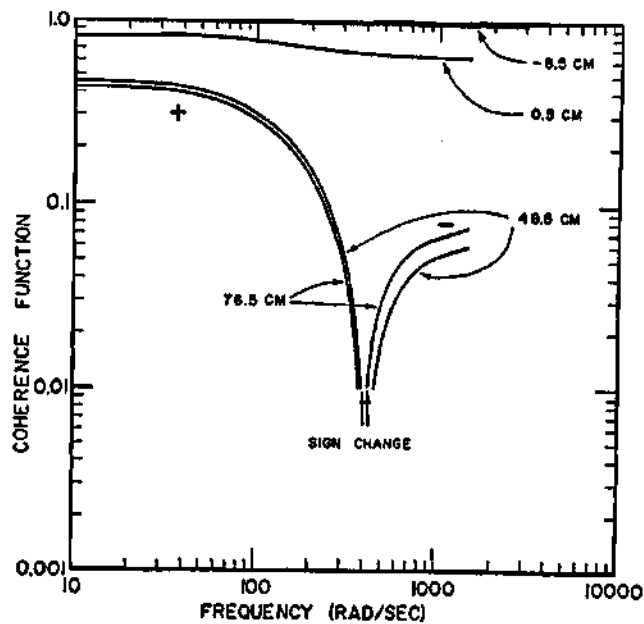


Figure 51.  $2\omega$  Mode  $|R^{(2,2)}(x_i, x_j, \omega)|$  for the SHA Core 35A'-  
Asymmetric Detector Locations  $x_i = -48.5$  cm;  
 $x_j =$  Variable

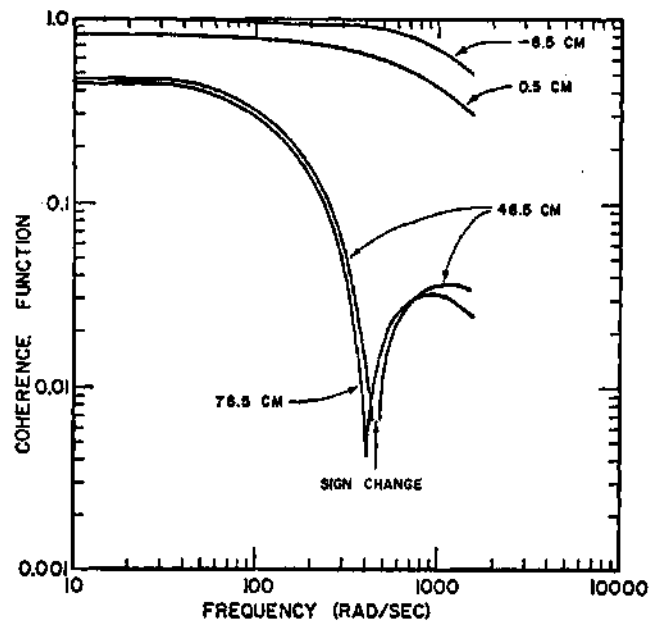


Figure 52.  $6\lambda$  Mode  $|R^{(2,2)}(x_1, x_j, \omega)|$  for the SHA Core 35A'-  
Asymmetric Detector Locations  $x_1 = -48.5$  cm;  
 $x_j =$  Variable

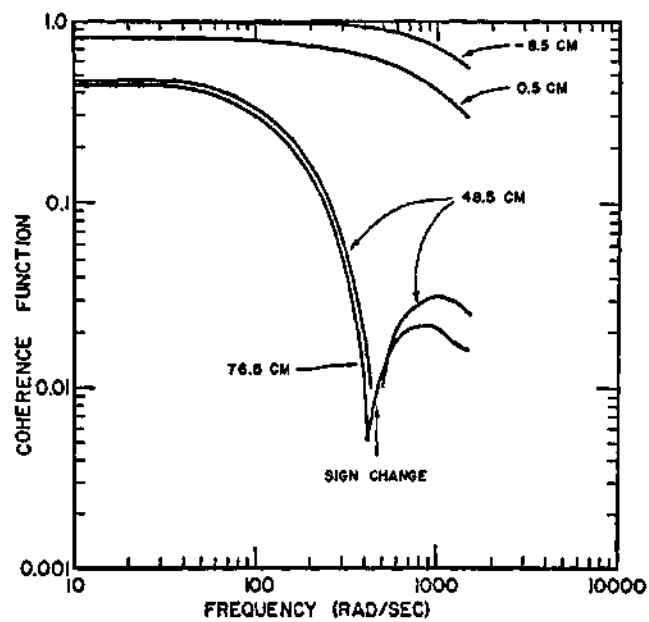


Figure 53.  $6\omega$  Mode  $|R^{(2,2)}(x_1, x_j, \omega)|$  for the SHA Core 35A'-  
Asymmetric Detector Locations  $x_1 = -48.5$  cm;  
 $x_j =$  Variable

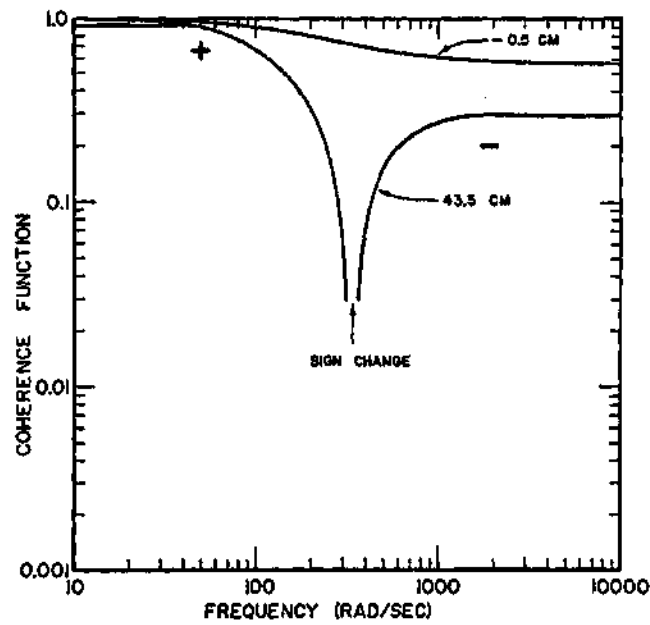


Figure 54.  $2\lambda$  Mode  $|R^{(a,a)}(x_i, x_j, \omega)|$  for the ARK-Asymmetric Detector Locations  $x_i = -43.5$  cm;  $x_j =$  Variable

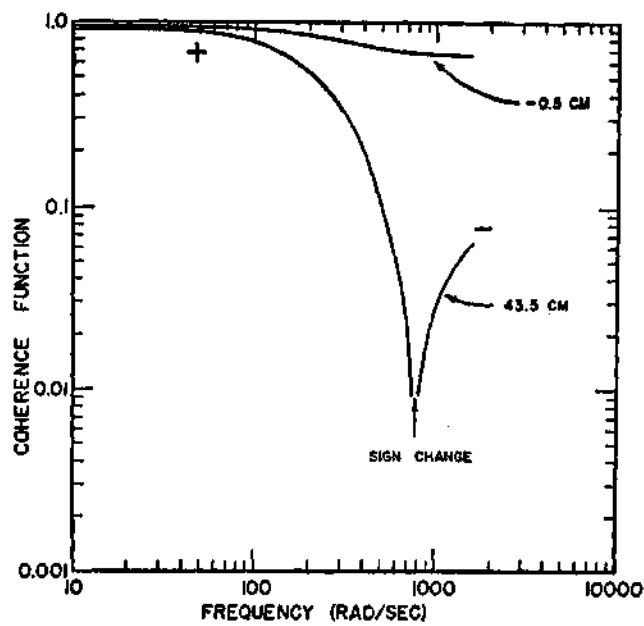


Figure 55.  $2\omega$  Mode  $|R^{(a,a)}(x_i, x_j, \omega)|$  for the ARK-Asymmetric Detector Locations  $x_i = -43.5$  cm;  $x_j =$  Variable

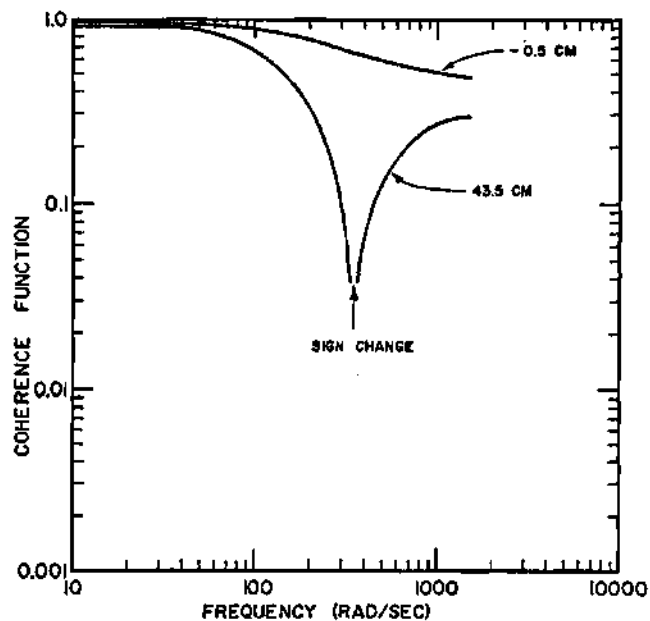


Figure 56.  $6\lambda$  Mode  $|R^{(2,2)}(x_i, x_j, \omega)|$  for the ARK-Asymmetric Detector Locations  $-x_i = -43.5$  cm;  $x_j =$  Variable

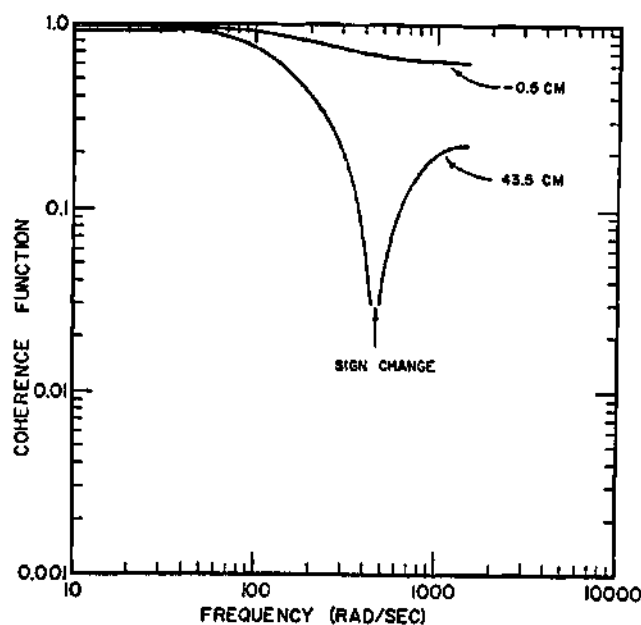


Figure 57.  $6\omega$  Mode  $|R^{(2,2)}(x_i, x_j, \omega)|$  for the ARK-Asymmetric Detector Locations  $-x_i = -43.5$  cm;  $x_j =$  Variable

Agreement between the exact and modal approximations of the thermal-thermal and fast-thermal coherence function phase angles is very poor in both reactor models. The phase angles tend to be very small for all frequencies and detector locations. The reasons for these discrepancies are not known.

### Two-Mode Expansion Approximation

In order to extract some reactor parameters from the measured coherence function, it is desirable to use the two-mode rather than the multi-mode approximation. This arises from the fact that the two-mode approximation adequately describes the coherence function below and including the null or sink frequency. The two-mode approximation is written

$$R^{(k, l)}(x_i, x_j, \omega) = \quad (5.11)$$

$$\left[ \frac{C_{00} \psi_0^{(k)}(x_i) \psi_0^{(l)}(x_j)}{\omega_0^2 + \omega^2} + \frac{C_{11} \psi_1^{(k)}(x_i) \psi_1^{(l)}(x_j)}{\omega_1^2 + \omega^2} \right] /$$

$$\left\{ \frac{C_{00} [\psi_0^{(k)}(x_i)]^2}{\omega_0^2 + \omega^2} + \frac{C_{11} [\psi_1^{(k)}(x_i)]^2}{\omega_1^2 + \omega^2} \right\}$$

$$\times \left[ \frac{C_{00} [\psi_0^{(l)}(x_j)]^2}{\omega_0^2 + \omega^2} + \frac{C_{11} [\psi_1^{(l)}(x_j)]^2}{\omega_1^2 + \omega^2} \right]^{\frac{1}{2}}.$$

Cross-source terms  $C_{01}$  and  $C_{10}$  do not appear in equation (5.11) because the reactor models are symmetric about the centerline. As a result of this symmetry, the integrand in equation (5.4) is an odd function (for

$n = 0, m = 1$  or  $n = 1, m = 0$ ) thereby yielding zero upon integration. It should also be observed that the two-mode expansion approximation in equation (5.11) produces real coherence functions even with asymmetric detector locations. Therefore, only null frequencies and not sink frequencies are predicted.

As will be demonstrated later in this chapter, a necessary condition for the extraction of some reactor parameters by the two-mode expansion approximation is that the measured coherence function exhibits a sink or null frequency. The detector pair placement and reactor characteristics which are necessary for the occurrence of this sink or null frequency have only been studied in a qualitative manner. Therefore, a quantitative description of the null frequency conditions is undertaken in order to establish criteria on core characteristics and detector pair placement which are necessary for the inference of the eigenvalue separation, neutron generation time, and the effective delayed neutron fraction.

### Null Frequency Conditions

In order to understand the physical significance of a null frequency it is informative to investigate the shape of the two-mode expansion approximation of the cross-covariance (equation (3.29)) for short detector gate times

$$C^{(2,2)}(x_i, x_j, \tau) = \sum_{\det-i}^{(2)}(x_i) \sum_{\det-i}^{(2)}(x_j) \quad (5.12)$$

$$\times \left[ \frac{C_{00} \psi_0^{(2)}(x_i) \psi_0^{(2)}(x_j) e^{\omega_0 \tau}}{-2\omega_0} + \frac{C_{11} \psi_1^{(2)}(x_i) \psi_1^{(2)}(x_j) e^{\omega_1 \tau}}{-2\omega_1} \right],$$

$$\tau \geq 0.$$

From equation (5.12) it is seen that the cross-covariance is the sum of two exponentially varying terms. The first term on the right-hand side of equation (5.12) is always positive because  $C_{00}$  and the fundamental thermal group eigenfunctions are everywhere positive. The second term on the right-hand side may be positive or negative depending on the detector pair locations. This comes about because, even though  $C_{11}$  is always positive, the first harmonic thermal eigenfunction may be positive or negative. In fact, if the two detectors are located on opposite sides of the core centerline, the second term will always be negative.

Consider the case of symmetrically placed detectors where

$$\psi_0^{(2)}(x_i) = \psi_0^{(2)}(x_j) \quad (5.13)$$

and

$$\psi_1^{(2)}(x_i) = -\psi_1^{(2)}(x_j) . \quad (5.14)$$

Equation (5.12) may therefore be written

$$C^{(2,2)}(x_i, -x_i, \tau) = \sum_{\text{det-i}}^{(2)}(x_i) \sum_{\text{det-j}}^{(2)}(x_j) \quad (5.15)$$

$$\times \left\{ \frac{C_{00} [\psi_0^{(2)}(x_i)]^2 e^{\omega_0 \tau}}{-2\omega_0} - \frac{C_{11} [\psi_1^{(2)}(x_i)]^2 e^{\omega_1 \tau}}{-2\omega_1} \right\} ,$$

$$\tau \geq 0 .$$

The behavior of the cross-covariance for small lag times ( $\tau \leq 10$  ms) is of particular interest in reactors which have a relatively small eigenvalue separation (in this case, both the SHA Core 35A' and ARK). If

the detectors are located in appropriate symmetric places, the cross-covariance will increase for very small lag times and then turn over and decrease for larger lag times.<sup>20,110,116,117</sup> If it is assumed that the slowing down time is very small, the reason for this behavior is that

$$\frac{C_{11}[\psi_1^{(2)}(x_i)]^2}{-2\omega_1} > \frac{C_{00}[\psi_0^{(2)}(x_i)]^2}{-2\omega_0} . \quad (5.16)$$

If the condition of equation (5.16) holds for the particular reactor model and detector placements, the lag time where the slope of the cross-covariance is zero (call it  $\tau_0$ ) is seen to satisfy the condition

$$\frac{d}{d\tau} C^{(2,2)}(x_i, -x_i, \tau) \Big|_{\tau=\tau_0} = 0 = \sum_{\text{det}-i}^{(2)}(x_i) \sum_{\text{det}-j}^{(2)}(x_j) \quad (5.17)$$

$$\times \left\{ \frac{C_{11}[\psi_1^{(2)}(x_i)]^2 e^{\omega_1 \tau_0}}{2} - \frac{C_{00}[\psi_0^{(2)}(x_i)]^2 e^{\omega_0 \tau_0}}{2} \right\}, \tau_0 \cong 0 .$$

Evaluating  $\tau_0$  from equation (5.17) yields

$$\tau_0 = \frac{\ln a^{(2)}(x_i)}{\omega_0 - \omega_1} , \quad (5.18)$$

where

$$a^{(2)}(x_i) \equiv \frac{C_{11}[\psi_1^{(2)}(x_i)]^2}{C_{00}[\psi_0^{(2)}(x_i)]^2} . \quad (5.19)$$

From equation (5.18), it may be reasoned that, if  $a^{(2)}(x_i)$  is less than one (making the logarithm negative), no increase in the cross-covariance

will be seen with small lag times. Also, it may be reasoned that, as the eigenvalue separation decreases,  $\tau_0$  will increase. Generally speaking, in reactors with small eigenvalue separations the terms  $C_{00}$  and  $C_{11}$  are about equal and, therefore, it depends on the ratio of  $\psi_1^{(2)}(x_i)$  to  $\psi_0^{(2)}(x_i)$  in determining the sign of  $\ln a^{(2)}(x_i)$ .

$a^{(2)}(x_i)$  is plotted in Figures 58 and 59 for the SHA Core 35A' and ARK, respectively, using lambda and modified omega eigenfunction expansions. It is apparent from the figures that, for all symmetric detector locations outside the graphite decoupling region in the ARK and about 20 cm outside the poly decoupling region in the SHA Core 35A', a  $\tau_0$  exists (at least if the two-mode model is valid).  $\tau_0$  for the SHA Core 35A', with detectors located near the edge, has a value of about 1.5 ms and for the ARK, with detectors just outside the fuel region, a value of about 2.3 ms.

Depending on the value of  $a^{(2)}(x_i)$ , the cross-covariance ( $C^{(2,2)}(x_i, -x_i, \tau)$ ) will have different values at  $\tau = 0$ . If  $a^{(2)}(x_i)$  is equal to  $\omega_1/\omega_0$ , the cross-covariance will have an initial value of zero, increase up to  $\tau_0$ , and thereafter decrease for larger values of  $\tau$ .

Looking at the null frequency condition of the two-mode coherence function approximation of equation (5.11), for symmetric detector locations

$$R^{(2,2)}(x_i, -x_i, \omega) \Big|_{\omega=\omega_{\text{null}}} = 0 \quad (5.20)$$

$$= \frac{C_{00} [\psi_0^{(2)}(x_i)]^2}{\omega_0^2 + \omega_{\text{null}}^2} - \frac{C_{11} [\psi_1^{(2)}(x_i)]^2}{\omega_1^2 + \omega_{\text{null}}^2} .$$

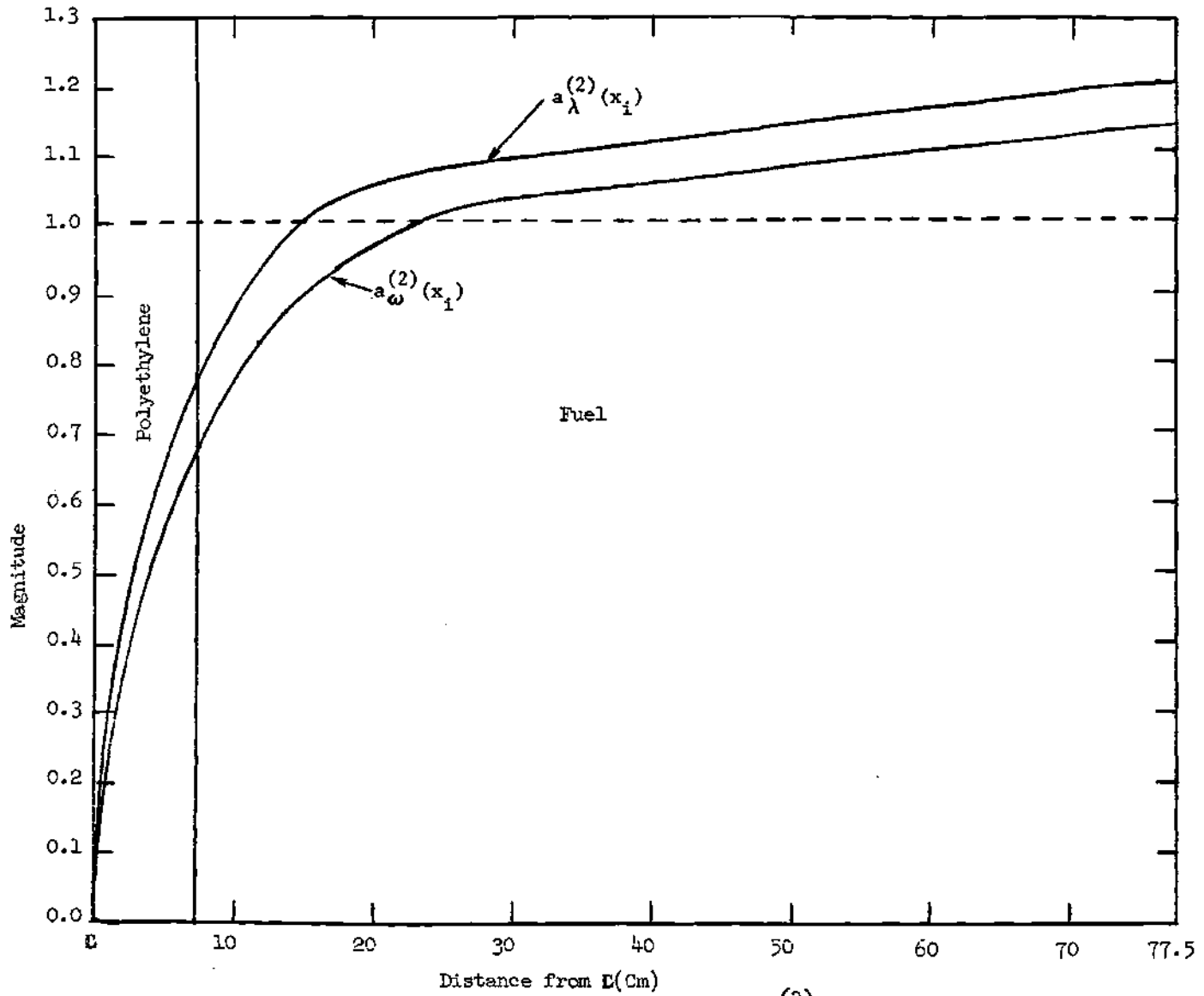


Figure 58. Spatial Weighting Function  $a^{(2)}(x_1)$ —SHA Core 35A'

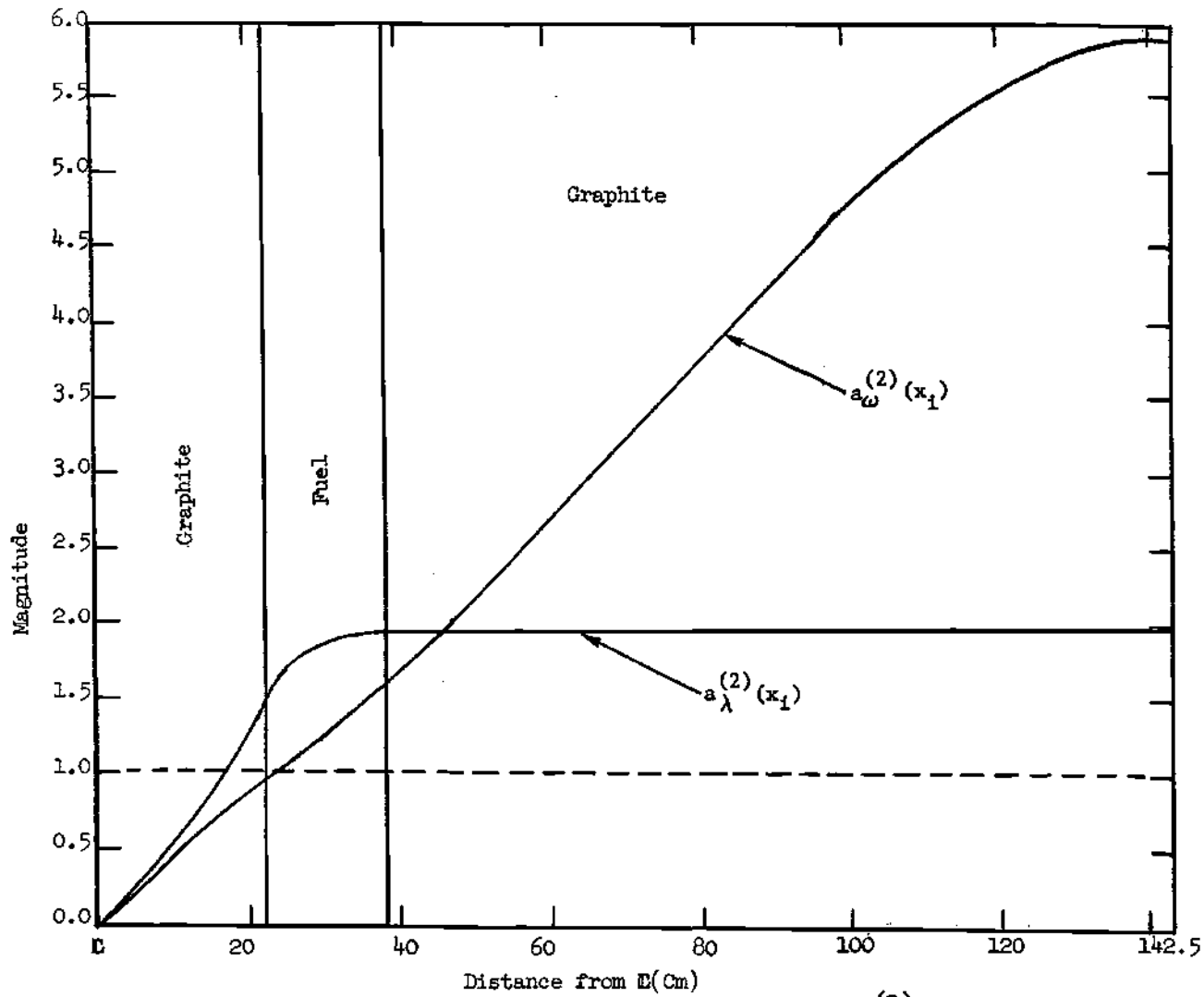


Figure 59. Spatial Weighting Function  $a^{(2)}(x_i)$ —ARK

From equation (5.20), the null frequency condition may be obtained

$$\omega_{\text{null}}^2 = \frac{\omega_1^2 - a^{(2)}(x_1)\omega_0^2}{a^{(2)}(x_1) - 1}, \quad (5.21)$$

where  $a^{(2)}(x_1)$  is required to fall within the limits

$$1 < a^{(2)}(x_1) \leq (\omega_1/\omega_0)^2. \quad (5.22)$$

It is observed that, if  $a^{(2)}(x_1)$  is less than one, only inflection points will be manifest in the coherence function curve.

It is of interest to note the relationship between  $\tau_0$  and  $\omega_{\text{null}}$ . The closer the spatial weighting term  $a^{(2)}(x_1)$  is to unity, the smaller  $\tau_0$  and the larger  $\omega_{\text{null}}$  become. The opposite is true as  $a^{(2)}(x_1)$  increases. If  $a^{(2)}(x_1)$  is kept constant, then as the reactor becomes more loosely coupled  $\tau_0$  increases and  $\omega_{\text{null}}$  decreases. This was observed indirectly by Nagy and Danofsky<sup>26</sup> as they varied the graphite decoupling region in an Argonaut type reactor at Iowa State University.

For asymmetric detector locations, the two-mode approximation is similar to the symmetric situation but with a different relation for the spatial weighting term

$$\omega_{\text{null}}^2 = \frac{\omega_1^2 - a^{(2)}(x_1, x_j)\omega_0^2}{a^{(2)}(x_1, x_j) - 1}, \quad (5.23)$$

where

$$a^{(2)}(x_i, x_j) \equiv \frac{-C_{11} \psi_1^{(2)}(x_i) \psi_1^{(2)}(x_j)}{C_{00} \psi_0^{(2)}(x_i) \psi_0^{(2)}(x_j)} . \quad (5.24)$$

The conditions on  $a^{(2)}(x_i, x_j)$  are

$$1 < a^{(2)}(x_i, x_j) \equiv (w_1/w_0)^2 . \quad (5.25)$$

In these two-mode approximations, only null frequencies (zero coherence) and not sink frequencies (minimum coherence) are generated for asymmetric detector locations. As seen in the exact solution, this is not the case in actual fact. However, the two-mode approximation will be fairly good when the phase angles are small (as in the SHA Core 35A' example, but not in the ARK model).

#### Reactor Parameter Extraction Methods

Methods by which the eigenvalue separation, effective delayed neutron fraction, and neutron generation time may be extracted from interpretation of the measured coherence function are developed in the next two sections. The relation between the methods using the coherence function and MCC is also demonstrated. As stated earlier, a necessary condition for these methods to be applicable is that the measured coherence function exhibit a sink or null frequency which can be associated with the interference of the first two decay modes.

Eigenvalue Separation. The first eigenvalue separation is defined as the difference between the reciprocal of the first and fundamental lambda eigenvalues

$$\Delta(1/K_1) \equiv (1/\lambda_1 - 1/\lambda_0) . \quad (5.26)$$

Assume that the relation

$$\omega_m = \frac{1 - \bar{\beta} - 1/\lambda_m}{\Lambda_{mm}} , \quad m = 0, 1 , \quad (5.27)$$

is valid.  $\omega_m$  is the  $m^{\text{th}}$  order modified omega eigenvalue,  $\lambda_m$  is the  $m^{\text{th}}$  order lambda eigenvalue, and  $\Lambda_{mm}$  is a quantity related to the neutron generation time (see equation (C.10)). How well the relation in equation (5.27) holds depends on the extent of departure of the lambda modes from the finality property, as mentioned earlier. Equation (5.27) will be a good approximation in the case of the SHA Core 35A', but not too good for the ARK. It should be noted that, for the point reactor case, equation (5.27) reduces to the familiar equation relating the prompt neutron decay constant ( $\omega_0$ ) to the effective multiplication constant

$$\omega_0 = \frac{1 - \bar{\beta} - 1/\lambda_0}{\Lambda_{00}} = \frac{\frac{K_{\text{eff}} - 1}{K_{\text{eff}}} - \bar{\beta}}{\Lambda_{00}} = \frac{K_{\text{eff}}(1 - \bar{\beta}) - 1}{\ell} , \quad (5.28)$$

where  $\ell$  is the thermal neutron lifetime.

If the reactor is relatively loosely coupled and if the  $\omega_0 \bar{V}^{-1}$  and  $\omega_1 \bar{V}^{-1}$  operators are small relative to the absorption operator, then to a good approximation

$$\Lambda_{00} \cong \Lambda_{11} . \quad (5.29)$$

Once again the validity of the approximation in equation (5.29) depends on the finality properties of the lambda modes.

The extent or lack of validity of the above assumptions is readily demonstrated in Tables 9 and 10.  $\lambda_m$  and  $\omega_m$  are the calculated lambda and modified omega eigenvalues using the method of Appendix F. The assumptions stated in equations (5.27) and (5.29) are excellent in the SHA Core 35A', but only fair in the ARK.

Using the above assumptions, a relation between the eigenvalue separation and the modified omega eigenvalues can be derived

$$\begin{aligned} \Delta(1/K_1) &\equiv 1/\lambda_1 - 1/\lambda_0 \cong (1-\bar{\beta} - \omega_1 \Lambda_{11}) - (1-\bar{\beta} - \omega_0 \Lambda_{00}) \quad (5.30) \\ &\cong (\omega_0 - \omega_1) \Lambda_{00} = (\omega_1 - \omega_0) \left( \frac{\bar{\beta} + 1/\lambda_0 - 1}{\omega_0} \right) \\ &= \left( \bar{\beta} - \frac{K_{\text{eff}}^{-1}}{K_{\text{eff}}} \right) \left( \frac{\omega_1 - \omega_0}{\omega_0} \right) = (\bar{\beta} - \rho) \left( \frac{\omega_1 - \omega_0}{\omega_0} \right). \end{aligned}$$

For symmetrically located thermal neutron detectors located within a symmetric reactor, the low frequency asymptote of the two-mode expansion approximation of the coherence function (equation (5.11)) is

$$R^{(2,2)}(x_i, -x_i, \omega_{\text{small}}) \cong \quad (5.31)$$

$$\frac{\frac{C_{00} [\psi_0^{(2)}(x_i)]^2}{\omega_0^2} - \frac{C_{11} [\psi_1^{(2)}(x_i)]^2}{\omega_1^2}}{\frac{C_{00} [\psi_0^{(2)}(x_i)]^2}{\omega_0^2} + \frac{C_{11} [\psi_1^{(2)}(x_i)]^2}{\omega_1^2}}$$

(continued)

$$= \frac{(\omega_1/\omega_0)^2 - a^{(2)}(x_1)}{(\omega_1/\omega_0)^2 + a^{(2)}(x_1)}, \quad \omega_{\text{small}} \ll |\omega_0| < |\omega_1|.$$

Table 9. Calculated Terms for Some Expansion Modes of the SHA Core 35A'

m	$(k_{\text{eff}})_m$	$\Lambda_{mm}$ ( $\mu\text{s}$ )	$\omega_m$ ( $\text{sec}^{-1}$ )	$\omega_m^\lambda$ ( $\text{sec}^{-1}$ )
0	0.9998	69	-115	-116
1	0.9938	68	-205	-206
2	0.8426	85	-2172	-2289
3	0.8270	83	-2601	-2614
4	0.6577	111	-4237	-4759
5	0.6391	107	-5173	-5350

The following notations apply to the column headings in both Tables 9 and 10.

$(k_{\text{eff}})_m \equiv \lambda_m$  = calculated lambda eigenvalue (Appendix F)

$$\Lambda_{mm} \equiv \frac{\langle \vec{\psi}_m^\lambda, \vec{V}^{-1} \vec{\psi}_m^\lambda \rangle}{\langle \vec{\psi}_m^\lambda, \vec{M} \vec{\psi}_m^\lambda \rangle}$$

$\omega_m$  = calculated modified omega mode eigenvalue (Appendix F)

$$\omega_m^\lambda \equiv \frac{1 - \bar{\beta} - 1/\lambda_m}{\Lambda_{mm}}$$

Table 10. Calculated Terms for Some Expansion Modes of the ARK

m	$(k_{\text{eff}})_m$	$\Lambda_{mm}$ ( $\mu\text{s}$ )	$\omega_m$ ( $\text{sec}^{-1}$ )	$\omega_m^\lambda$ ( $\text{sec}^{-1}$ )
0	1.0000	148	-42.2	-54.1
1	0.9573	113	-351	-466
2	0.3624	663	-618	-2666
3	0.3381	477	-724	-4120
4	0.1127	1883	-977	-4185
5	0.1066	1379	-1252	-6083

Equation (5.31) may be rearranged to give the following expression

$$\frac{\omega_1 - \omega_0}{\omega_0} = \sqrt{\frac{a^{(2)}(x_i) [1 + R^{(2,2)}(x_i, -x_i, \omega_{\text{small}})]}{1 - R^{(2,2)}(x_i, -x_i, \omega_{\text{small}})}} - 1. \quad (5.32)$$

Combining equations (5.32) and (5.30), an expression for the eigenvalue separation is obtained

$$\Delta(1/K_1) = (\bar{\beta} - \rho) \left\{ \sqrt{\frac{a^{(2)}(x_i) [1 + R^{(2,2)}(x_i, -x_i, \omega_{\text{small}})]}{1 - R^{(2,2)}(x_i, -x_i, \omega_{\text{small}})}} - 1 \right\}. \quad (5.33)$$

In a similar manner, Rydin et al.<sup>20</sup> have derived an expression for  $\Delta(1/K_1)$  in terms of the MCC (see Appendix A)

$$\Delta(1/K_1) = (\bar{\beta} - \rho) \left\{ \sqrt{\frac{a^{(2)}(x_i) [1 + \text{MCC}(x_i, -x_i, T_{\text{plateau}})]}{1 - \text{MCC}(x_i, -x_i, T_{\text{plateau}})}} - 1 \right\}, \quad (5.34)$$

where  $T_{\text{plateau}}$  is defined as the value of  $T$  when

$$\left| \frac{1 - e^{-\omega T_{\text{plateau}}}}{\omega T_{\text{plateau}}} \right| \ll 1, \quad n = 0, 1. \quad (5.35)$$

The equivalence between the coherence function and modified coefficient of correlation method of measuring the eigenvalue separation is observed in equations (5.33) and (5.34). It is apparent from equations (5.33) and (5.34) and by the correlation function method of Rydin et al.<sup>20</sup> that, by measuring the noise characteristics in reactors with small eigenvalue separations,  $\Delta(1/K_1)$  may be inferred if  $\bar{\beta}$ ,  $\rho$ , and  $a^{(2)}(x_i)$  are known. The same type of analysis may be carried out for asymmetrical detector locations by replacing  $a^{(2)}(x_i)$  by  $a^{(2)}(x_i, x_j)$ . The accuracy of this latter method will be reduced somewhat because the two-mode expansion approximation does not admit imaginary components of the coherence function.

As mentioned in the previous paragraph, in order to obtain  $\Delta(1/K_1)$  from noise measurements either in the time or frequency domain (equations (5.34) and (5.33)), the values of  $\bar{\beta}$ ,  $\rho$ , and  $a^{(2)}(x_i)$  must be known. (It is assumed that  $R(x_i, x_j, \omega_{\text{small}})$  and  $\text{MCC}(x_i, x_j, T_{\text{plateau}})$  are measurable.)  $\bar{\beta}$  is usually calculated using a static diffusion theory computer program and  $\rho$  is measured using the standard relationship

$$\rho = \bar{\beta} \left( 1 - \frac{\omega_0}{\omega_0^{\text{critical}}} \right), \quad (5.36)$$

where  $\omega_0^{\text{critical}}$  is the critical prompt neutron decay constant and  $\omega_0$  is the subcritical prompt neutron decay constant. The prompt decay constants may be obtained in frequency domain noise measurements by locating one detector at the core center and observing the break frequency in the CPSD curve. A similar procedure may be carried out in the time domain to obtain the prompt decay constants. The spatial weighting term  $a^{(2)}(x_i)$  may either be numerically calculated from its definition (equation (5.19)) or may be inferred from noise experiments from the following equations

$$a^{(2)}(x_i) = \frac{1}{1 - 2(\omega_0/\omega_{\text{null}})^2 \left[ \frac{R^{(2,2)}(x_i, -x_i, \omega_{\text{small}})}{1 - R^{(2,2)}(x_i, -x_i, \omega_{\text{small}})} \right]} \quad (5.37)$$

derived using equations (5.21) and (5.31), or

$$a^{(2)}(x_i) = \left[ \frac{1 + \text{MCC}(x_i, -x_i, T_{\text{plateau}})}{1 - \text{MCC}(x_i, -x_i, T_{\text{plateau}})} \right] \left[ \frac{1 - \text{MCC}(x_i, -x_i, T_{\text{small}})}{1 + \text{MCC}(x_i, -x_i, T_{\text{small}})} \right]^2, \quad (5.38)$$

where  $T_{\text{small}}$  implies that

$$|T_{\text{small}} \omega_n| \ll 1, \quad n = 0 \text{ or } 1. \quad (5.39)$$

Equation (5.38) was obtained by observing that, in the two-mode approximation

$$\text{MCC}(x_i, -x_i, T_{\text{plateau}}) = \frac{(\omega_1/\omega_0)^2 - a^{(2)}(x_i)}{(\omega_1/\omega_0)^2 + a^{(2)}(x_i)}, \quad (5.40)$$

and

$$\text{MCC}(x_i, -x_i, T_{\text{small}}) = \frac{(\omega_1/\omega_0) - a^{(2)}(x_i)}{(\omega_1/\omega_0) + a^{(2)}(x_i)}. \quad (5.41)$$

Using the experimentally inferred values of  $a^{(2)}(x_i)$  is preferred when not very much is known about the system.

Of course, if it is possible to extract  $\omega_1$  from the noise data, as done by Burke et al.,<sup>20</sup> then equation (5.30) may be used directly to determine  $\Delta(1/K_1)$

$$\Delta(1/K_1) = (\bar{\beta} - \rho) \left( \frac{\omega_1 - \omega_0}{\omega_0} \right). \quad (5.42)$$

However, it is not always possible to determine  $\omega_1$  with any great accuracy.

#### Effective Delayed Neutron Fraction and Neutron Generation Time.

Combining equations (5.33) with (5.36) and (5.34) with (5.36) yields the following relationships

$$\bar{\beta} = \frac{\Delta(1/K_1)}{(\omega_0/\omega_0^{\text{critical}}) \left\{ \sqrt{\frac{a^{(2)}(x_i) [1 + R^{(2,2)}(x_i, -x_i, \omega_{\text{small}})]}{1 - R^{(2,2)}(x_i, -x_i, \omega_{\text{small}})}} - 1 \right\}}, \quad (5.43)$$

and

$$\bar{\beta} = \frac{\Delta(1/K_1)}{(\omega_0/\omega_0^{\text{critical}}) \left\{ \sqrt{\frac{a^{(2)}(x_i) [1 + \text{MCC}(x_i, -x_i, T_{\text{plateau}})]}{1 - \text{MCC}(x_i, -x_i, T_{\text{plateau}})}} - 1 \right\}}. \quad (5.44)$$

The eigenvalue separation in the numerator of equations (5.43) and (5.44) may be calculated using any static diffusion theory code (e.g., EXTERMINATOR) without prior knowledge of  $\bar{\beta}$ . However, it is difficult to calculate the eigenvalue separation accurately when this value is small.<sup>152</sup> The denominators of equations (5.43) and (5.44) are entirely experimentally determined quantities. As a consequence of this,  $\bar{\beta}$  may be determined independently of  $\Lambda_{00}$ , the neutron generation time, using either equation (5.43) or (5.44).

Once  $\bar{\beta}$  has been determined, it is an easy matter to determine  $\Lambda_{00}$  by use of the equation

$$\Lambda_{00} = \bar{\beta}/\omega_0 . \quad (5.45)$$

Therefore,  $\bar{\beta}$  and  $\Lambda_{00}$  may be determined independently of each other using a combination of analytical and experimental techniques.

#### Discussion

It was shown that, if the measured coherence function exhibits a null or sink frequency and if the two( $\omega$  or  $\lambda$ ) mode approximation can describe well the overall shape of the measured coherence function, then much quantitative insight may be gained into the reactor dynamic characteristics. It has been assumed that the measured and exact solution of the coherence function demonstrates good agreement. This is a good assumption for the cores studied, as will be seen in the next chapter. The two-mode approximation was particularly well suited for the coupled cores studied. However, in general the two-mode method will not produce good results. The advantage of the two-mode method over the exact solution

lies in the observation that the insight does come in a quantitative rather than a qualitative sense. That is, in the two-mode method, relatively simple mathematical relations were developed which establish the reactor and detector conditions needed to describe the coherence function and to extract the reactor parameters.

The multi-mode expansion approximation of the exact  $|R^{(2,2)}(x_i, x_j, \omega)|$  was excellent for all detector pair locations and frequencies studied in the SHA Core 35A', but only fair in the ARK. The same conclusion held for the two-mode approximations, but in this case the detector locations must be outside the decoupling regions and the frequency must be less than or equal to the sink or null frequency. The  $2\omega$  mode approximation was much better than the  $2\lambda$  mode in the ARK. Modal approximations of  $|R^{(1,1)}(x_i, x_j, \omega)|$  and  $|R^{(1,2)}(x_i, x_j, \omega)|$ , as in the exact solution, were very similar with the modal approximations of  $|R^{(2,2)}(x_i, x_j, \omega)|$ .

Multi-mode computations of the various phase angles were very poor. The reason for this is not understood. It may have to do with the fact that the phase angles are generally small, as seen in the last chapter, and therefore difficult to predict with modal approximations. If there is any appreciable error in the construction of the eigenfunctions, it is magnified in the phase calculations. This comes about because the phase, in the modal approximation, results from a difference of terms rather than a sum.

The two-mode approximations result in real rather than complex coherence functions for asymmetrically located detectors. Although this is certainly a deficiency of the method, it does not result in very large errors in estimating the exact  $|R^{(2,2)}(x_i, x_j, \omega)|$  because the phase was

generally small up to and including the sink or null frequency. Because this method produced real coherence functions for all detector locations, only null and not sink frequencies were predicted.

The shape of the exact  $|R^{(2,2)}(x_i, x_j, \omega)|$  for various core and detector conditions was easily interpreted using a two-mode expansion approximation. It was seen from equation (5.11) or (5.20) that sink or null frequencies may be pictured as resulting from the interference effects of the fundamental and first harmonic prompt neutron decay modes. These decay modes are excited by the particular spatial distribution of the stochastic source and core coupling characteristics. The relative weight of each mode is a function of the locations of the detectors. The two-mode approximation of the coherence function absolute value for symmetrically placed detectors takes on the form

$$|R^{(2,2)}(x_i, -x_i, \omega)| = \frac{\left| \frac{\omega_1^2 + \omega^2}{\omega_0^2 + \omega^2} - a^{(2)}(x_i) \right|}{\left| \frac{\omega_1^2 + \omega^2}{\omega_0^2 + \omega^2} + a^{(2)}(x_i) \right|} . \quad (5.46)$$

It was seen (equation (5.22)) that it was necessary that the spatial weighting term,  $a^{(2)}(x_i)$ , have a value greater than one in order to predict a null frequency. For the two coupled core reactor models studied, this requirement implied that the detectors could be placed anywhere except near or within the decoupling regions. Also, according to equation (5.46), as  $a^{(2)}(x_i)$  increased (for larger detector separations),  $\omega_{\text{null}}$  decreased. Finally, if  $\Delta(1/K_1)$  increased ( $\omega_1/\omega_0$  increased) so did  $\omega_{\text{null}}$  for some given detector pair arrangement. All these quantitative observa-

tions were entirely consistent with the qualitative conclusions using the exact solution.

The reason why  $|R^{(2,2)}(x_1, -x_1, \omega)|$  decreased with increasing detector separation below  $\omega_{\text{null}}$  and increased with increasing separation above  $\omega_{\text{null}}$  may also be easily explained using the two-mode approximation.

Suppose that  $x_j > x_i$ . The ratio of the coherence functions at these two detector separations is

$$\frac{|R^{(2,2)}(x_1, -x_1, \omega)|}{|R^{(2,2)}(x_j, -x_j, \omega)|} = \frac{\left| \frac{\omega_1^2 + \omega^2}{\omega_0^2 + \omega^2} - a^{(2)}(x_i) \right| \left| \frac{\omega_1^2 + \omega^2}{\omega_0^2 + \omega^2} + a^{(2)}(x_j) \right|}{\left| \frac{\omega_1^2 + \omega^2}{\omega_0^2 + \omega^2} - a^{(2)}(x_j) \right| \left| \frac{\omega_1^2 + \omega^2}{\omega_0^2 + \omega^2} + a^{(2)}(x_i) \right|} \quad (5.47)$$

Remembering that  $a^{(2)}(x_i) < a^{(2)}(x_j)$  for the reactor models studied and that both spatial weighting terms are near unity, it is apparent that the ratio in equation (5.47) is greater than one below  $\omega_{\text{null}}$  and less than one above  $\omega_{\text{null}}$ . These results are also consistent with the exact solution observations. The same type of reasoning may be applied to asymmetrically located detectors.

Methods have been developed, using the two-mode approximations, whereby the eigenvalue separation, effective delayed neutron fraction, and neutron generation time may be inferred by proper interpretation of the measured coherence function or modified coefficient of correlation. The accuracy in determining  $\Delta(1/k_1)$  depends on how well the  $2\lambda$  mode approximation describes the measured coherence function. This accuracy tends to increase the more loosely coupled the core becomes. The accuracy

of the  $\bar{\beta}$  and  $\Lambda_{00}$  determinations appear to be poor for either very tightly or very loosely coupled cores. In other words, there appears to be an optimum eigenvalue separation with regard to the accuracy of the  $\bar{\beta}$  and  $\Lambda_{00}$  determinations.

## CHAPTER VI

## INTERPRETATION OF THE NOISE EXPERIMENTS

To verify the validity of the theoretical development and to provide measured coherence functions for the reactor parameter extraction, noise data from two separate nuclear laboratories were used. Frequency domain measurements of the coherence function for the tightly coupled ARK reactor were carried out by Seifritz and Albrecht<sup>28</sup> at the Institut für Neutronenphysik und Reaktortechnik, Kernforschungszentrum Karlsruhe, West Germany. Time domain noise measurements were undertaken by Burke et al.<sup>20</sup> on several loosely coupled cores including the SHA Core 35A' at Knolls Atomic Power Laboratory (KAPL) in Schenectady, New York, as part of a space-time kinetics program.<sup>29</sup>

Because time domain data were not available for the ARK reactor, it was necessary to Fourier transform the KAPL data to compare characteristics of the two reactors in the frequency domain. This chapter is concerned with the method used to Fourier transform the KAPL noise data, the results of this procedure, and the values of several reactor parameters which may be inferred from these noise measurements.

Fast Fourier Transformation Procedure and Results

The experimental arrangement used to take the SHA Core 35A' noise data consisted of two boron trifluoride detector banks located at opposite ends of the reactor which were connected to a multiscaler set in the time

mode. Conventional low-noise amplifier systems were used, with one  $\mu$ s double-delay-line pulse differentiation. Discriminator windows were adjusted to detect approximately 95% of the pulse-height distribution with the lower level set about four times higher than the maximum observable system-noise pulses.

Time histories for the two detectors were recorded by a 4096-channel multiscaler time analyzer (2048 channels for each detector) and written on magnetic tape. Pulses from both detectors were fed to 10 Mc scalers for a fixed detection time interval or gate time (T), which was varied from one ms to 100 ms. The storage time between gates was 40  $\mu$ s. Count losses were minimized (held to less than 1%) by maintaining the detector count rate below 2000 cps. Some 20 to 40 time histories were obtained for a given run and were identified on tape by a unique tag word. Separate runs were usually made using 1, 3, 10, and 100 ms gate times at one stationary subcritical condition. Measurements were repeated for several slightly subcritical positions.

Reactor noise data were obtained for four different cores, each bisected by a decoupling region consisting of a few inches of polyethylene. Core 38B was constructed with SHA-II type fuel<sup>105,106</sup> and had a four inch polyethylene decoupling region. Cores 35A, 35A', and 39 were constructed with SHA-I type fuel<sup>105,106</sup> and had 4, 5, and 3 inch decoupling regions, respectively.

Data tapes generated by the analyzer were then stored in a different format by the KAPL CDC-6600 computer. The CDC-6600 has a 60 bit word length and writes on tape in physical records of 512 words each. The con-

tents of the CDC tapes were copied onto separate tapes and sent to Georgia Tech for frequency analysis.<sup>118</sup> A FORTRAN IV program using UNIVAC-1108 NTRAN<sup>119</sup> options was constructed to read the CDC data tape and convert to UNIVAC-1108 36 bit word form. The average detector count rate for each run was computed and subtracted from the raw data. This left only the fluctuating portion which was added channel for channel for all the data dumps within a run. The composite of 4096 channels of noise data were Fast Fourier Transformed (FFT) using a program written by J. M. Reynolds.<sup>120</sup> A detailed description of the FFT method presented by Reynolds<sup>121</sup> is reproduced in Appendix G.

The FFT routine produced detector averages, variances, APSD, CPSD, transfer function magnitude and phase, coherence function, and auto- and cross-covariances on all SHA core data (over 10 million data words) in about one hour of UNIVAC-1108 computing time.<sup>150</sup> To obtain the correlation functions and spectral densities by conventional means would have taken nearly 40 hours on the UNIVAC-1108.<sup>34</sup> The relatively small FFT computation time strongly suggests the possibilities of on-line use. This has already been undertaken by Kryter<sup>122</sup> and recently applied to the determination of the void fraction in fuel salt in the Molten-Salt Reactor Experiment at Oak Ridge National Laboratory.<sup>123,124</sup>

Results of the KAPL data computations for the absolute value of the modified coherence function are given in Figure 60 for the four SHA cores. The modified coherence function is similar to the coherence function except the mean detector count rates have not been subtracted from the APSD's in the denominator. Detector gate times used in the FFT analysis

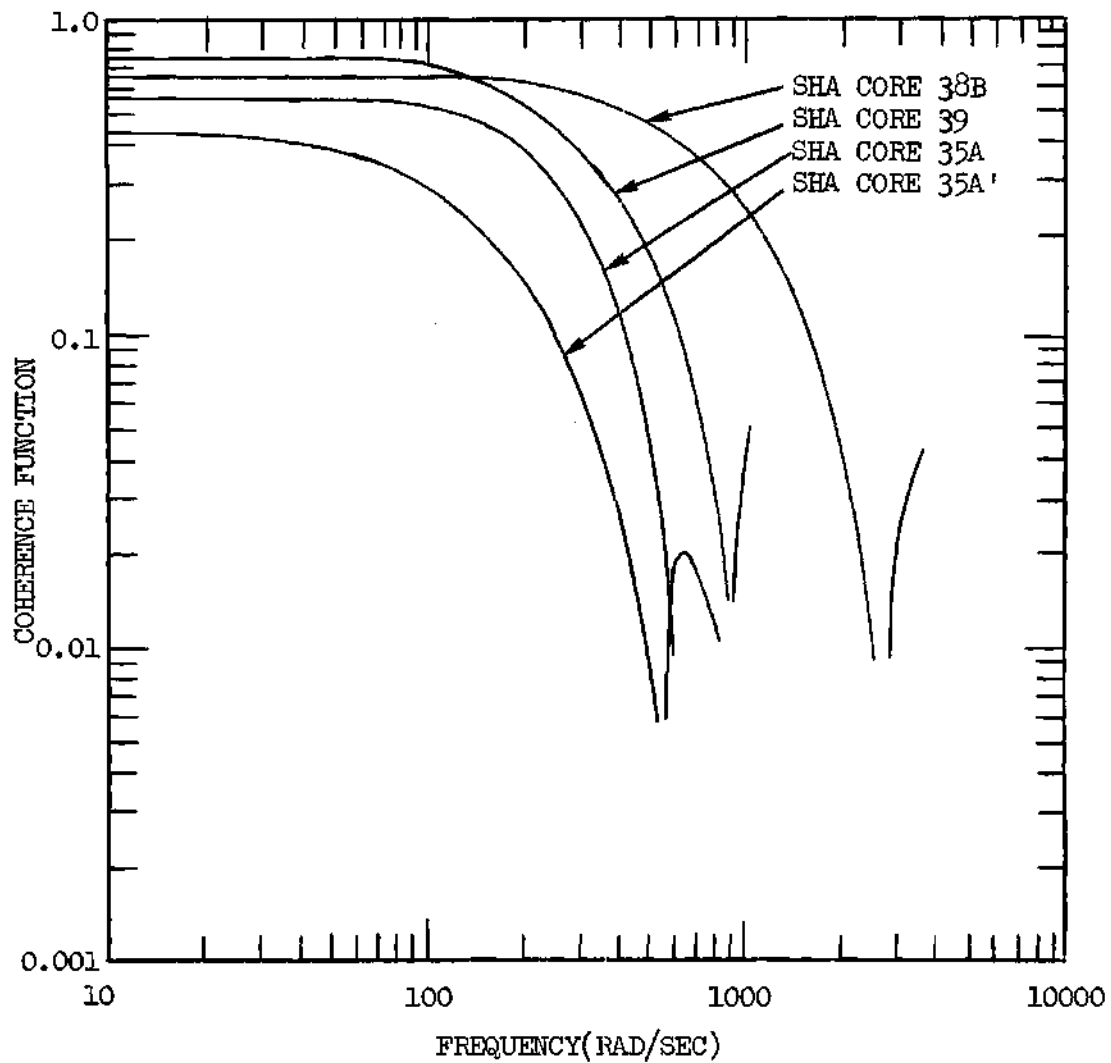


Figure 60. Measured  $|MR(x_1, -x_1, \omega)|$  for Several SHA Cores-  
 $x_1 = -77.5$  cm

were 3 ms. From Figure 60 it is seen that, for SHA cores with type-I fuel (cores 39, 35A, and 35A'), as the width of the polyethylene decoupler is increased (eigenvalue separation decreased) the null frequency and low frequency coherence function decrease in accordance with equations (5.21) and (5.31), respectively.

### Reactor Parameter Extraction and Results

To extract reactor parameters from the digital SHA noise results, it was necessary to investigate the two-mode expansion approximation of the modified coherence function for symmetrically located, point, thermal neutron detectors

$$MR^{(2,2)}(x_1, -x_1, T, \omega) \cong \quad (6.1)$$

$$\left[ \frac{C_{00} [\psi_0^{(2)}(x_1)]^2 G'_{00}(T)}{\omega_0^2 + \omega^2} - \frac{C_{11} [\psi_1^{(2)}(x_1)]^2 G'_{11}(T)}{\omega_1^2 + \omega^2} \right] \Big/ \left[ \bar{D}_1 \text{DFT} \left[ \frac{\Delta(T, \tau)}{T} \right] + \frac{C_{00} [\psi_0^{(2)}(x_1)]^2 G'_{00}(T)}{\omega_0^2 + \omega^2} + \frac{C_{11} [\psi_1^{(2)}(x_1)]^2 G'_{11}(T)}{\omega_1^2 + \omega^2} \right]$$

where

$$G'_{00}(T) \equiv \frac{2(\omega_0 T + 1 - e^{-\omega_0 T})}{(\omega_0 T)^2}, \quad (6.2)$$

$$G'_{11}(T) \equiv \frac{2(\omega_1 T + 1 - e^{-\omega_1 T})}{(\omega_1 T)^2}, \quad (6.3)$$

and  $\text{DFT}\left[\frac{\Delta(\mathbf{T}, \tau)}{T}\right]$  is the digital Fourier transform<sup>34</sup> of the trivial detector response correlation function  $\frac{\Delta(\mathbf{T}, \tau)}{T}$  (see equation (3.9)).  $\text{DFT}\left[\frac{\Delta(\mathbf{T}, \tau)}{T}\right]$  has a value of one for frequencies below the Nyquist frequency.<sup>34</sup> Using this fact and performing some algebraic manipulations, the modified coherence function may be expressed in simpler form

$$\text{MR}^{(2,2)}(x_i, -x_i, T, \omega) \cong \left[ \frac{(\omega_1^2 + \omega^2)}{(\omega_0^2 + \omega^2)} - a^{(2)}(x_i, T) \right] \left[ \left( \frac{\text{NR}}{1 - \text{NR}} \right) \left[ \frac{\omega_1^2 + \omega^2}{\omega_0^2} + \left( \frac{\omega_1^2 + \omega^2}{\omega_1^2} \right) a^{(2)}(x_i, T) \right] + \frac{(\omega_1^2 + \omega^2)}{(\omega_0^2 + \omega^2)} + a^{(2)}(x_i, T) \right], \quad (6.4)$$

where NR, the trivial noise ratio, is defined as

$$\text{NR} \equiv \frac{\bar{D}_i}{\bar{D}_i + \frac{C_{00} G_{00}^i(T) [\psi_0^{(2)}(x_i)]^2}{\omega_0^2} + \frac{C_{11} G_{11}^i(T) [\psi_1^{(2)}(x_i)]^2}{\omega_1^2}} \quad (6.5)$$

and the combination spatial and detector gate interval weighting function,  $a^{(2)}(x_i, T)$ , is defined

$$a^{(2)}(x_i, T) \equiv a^{(2)}(x_i) \frac{G_{11}^i(T)}{G_{00}^i(T)} = \frac{C_{11} [\psi_1^{(2)}(x_i)]^2 G_{11}^i(T)}{C_{00} [\psi_0^{(2)}(x_i)]^2 G_{00}^i(T)}. \quad (6.6)$$

The trivial noise ratio is evaluated by finding the high to low frequency asymptote ratio of the APSD. The APSD's for the four SHA cores are presented in Figure 61 together with the NR value for each. It should be noted that the modified coherence and the coherence functions would be

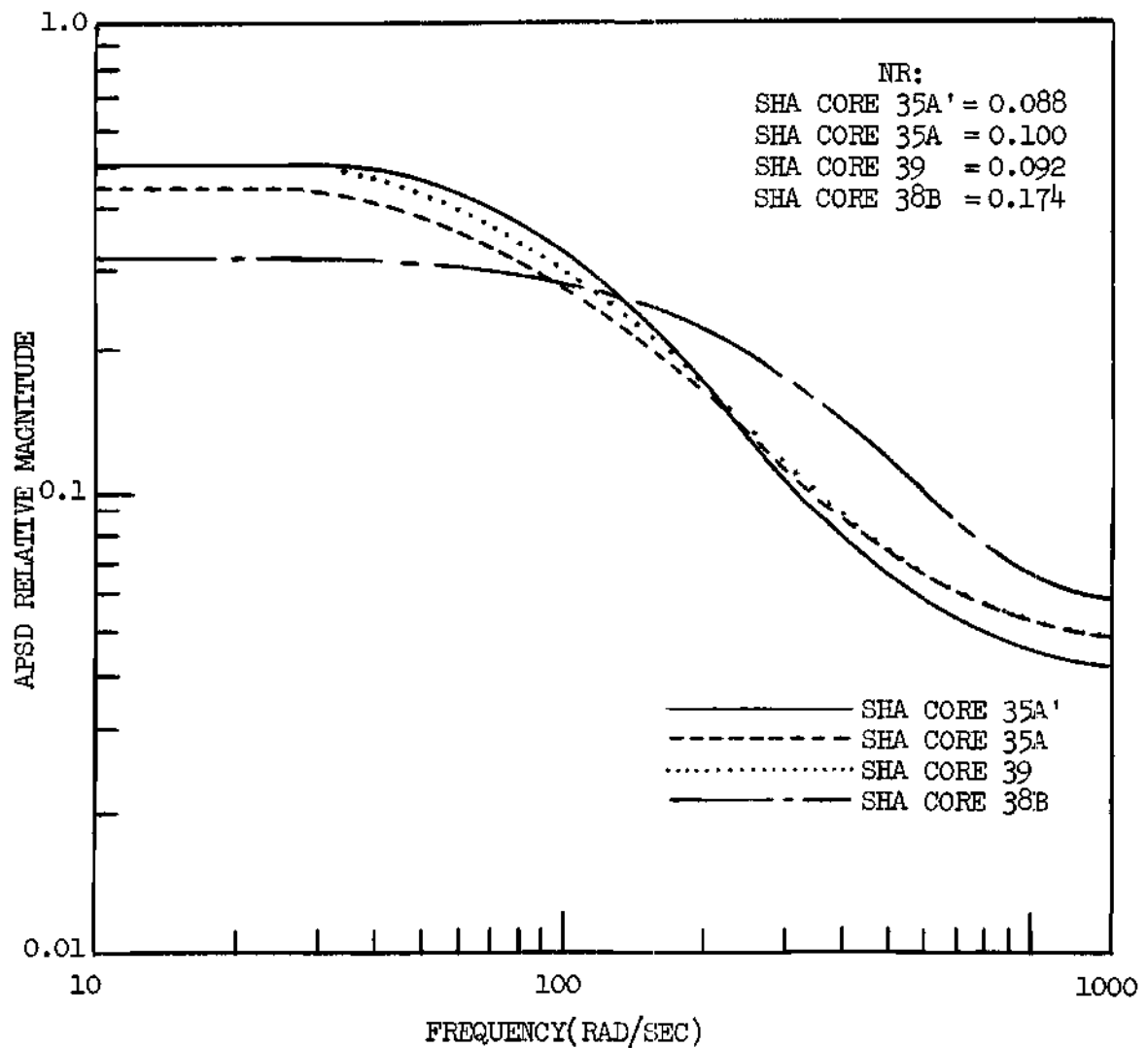


Figure 61. Measured Values of the APSD's and Noise Ratios for Several SHA Cores

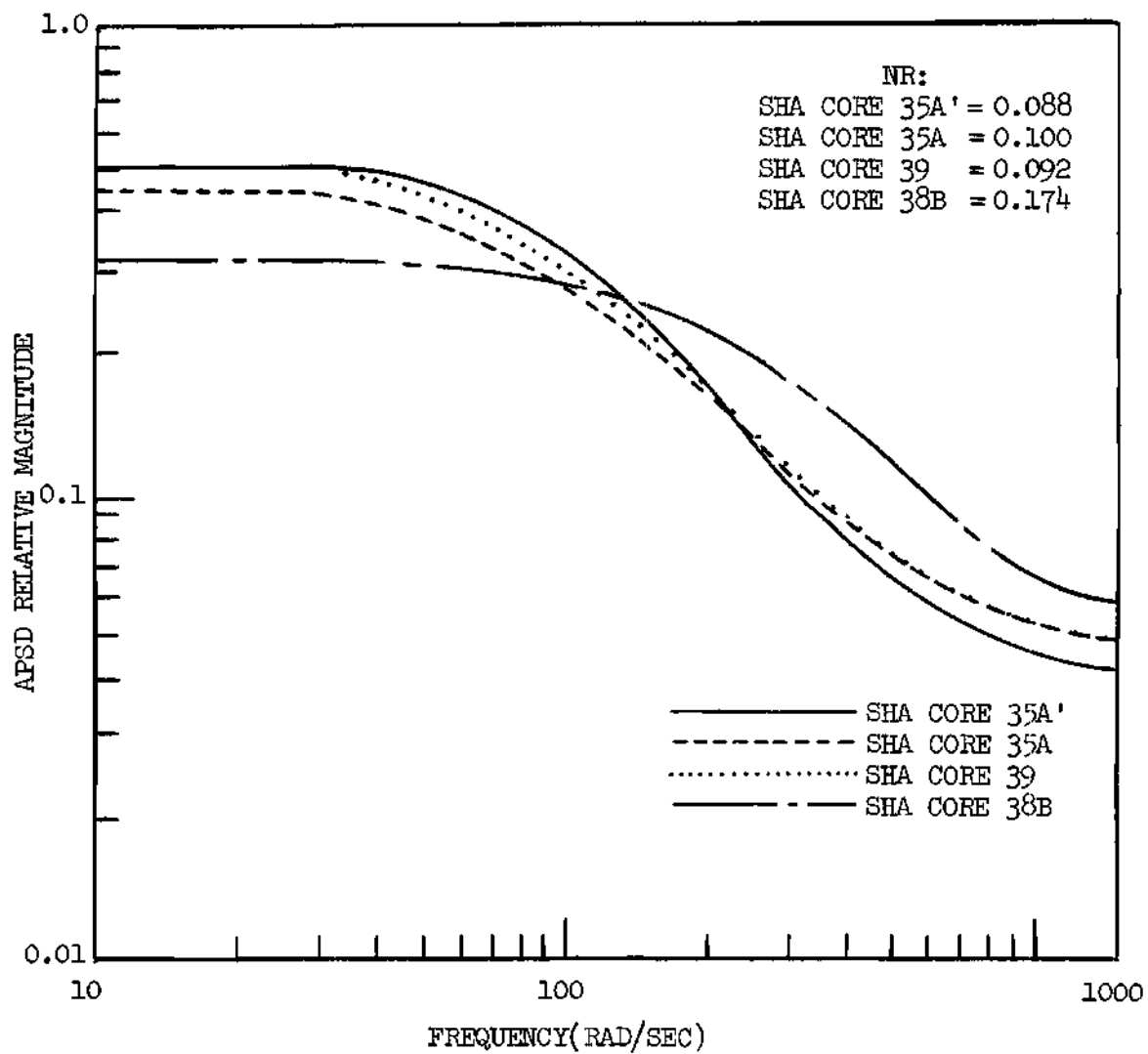


Figure 61. Measured Values of the APSD's and Noise Ratios for Several SHA Cores

identical if the trivial noise ratio was zero and the detector gate times were small (i.e.,  $|\omega_0 T| < |\omega_1 T| \ll 1$ ). The trivial noise ratio tends to have a degrading effect on the extent of coupling between the two detectors.

Using the values of the modified coherence function at low frequencies and the conditions at the null frequency, expressions for  $a^{(2)}(x_i, T)$  and  $\Delta(1/K_1)$  may be obtained in a manner similar to that presented in Chapter V

$$a^{(2)}(x_i, T) = \frac{1}{1 - 2(\omega_0/\omega_{\text{null}})^2 \left[ \frac{MR^{(2,2)}(x_i, -x_i, T, \omega_{\text{small}})}{1 - NR - MR^{(2,2)}(x_i, -x_i, T, \omega_{\text{small}})} \right]}}, \quad (6.7)$$

and

$$\Delta(1/K_1) = (\bar{\beta} - \rho) \left\{ \sqrt{\frac{a^{(2)}(x_i, T) [1 - NR + MR^{(2,2)}(x_i, -x_i, T, \omega_{\text{small}})]}{1 - NR - MR^{(2,2)}(x_i, -x_i, T, \omega_{\text{small}})}} - 1 \right\}. \quad (6.8)$$

It should be noted that the method developed in the last chapter for extracting reactor parameters is directly applicable to the analog ARK data,<sup>28</sup> but must be modified as shown in equations (6.7) and (6.8) to be useful for the digital KAPL data. The reason for this is because, in the analog techniques, the detector response intervals (T) are inherently small. Another way of saying this in the frequency domain is that the detector's response curve is flat up to high frequencies. In addition, the manner in which the ARK data were presented<sup>28</sup> accounted for the subtraction of  $\bar{D}_1$  (trivial detection rate) from the APSD. Therefore the normal coherence function can be used directly for the ARK cal-

culations, but the modified coherence function must be used for the SHA calculations.

Measured and exact solutions of the absolute value of the coherence function for two thermal neutron detectors symmetrically located in the graphite reflector near the edge of the core region for the ARK are presented in Figure 62. Measured and exact values agree well with each other for frequencies below and including the null frequency, but not well above the null frequency. One possible reason for this higher frequency disagreement may be due to the inability of the one-dimensional exact solution to take into account higher order axial buckling of the axial flux shape. (Of course the same will be true of the modal approximations.)

A similar graph for the SHA Core 35A<sup>1</sup> could not be undertaken because of the inability of the exact solution to take into account the detection time intervals and the noise ratio needed for an exact and experimental comparison. However, because of the good low frequency agreement between the exact solution and experimental results in the ARK, it is conjectured that the exact solution would be valid for the SHA noise data if they were taken by analog techniques. Once this reasoning is accepted, it is easily concluded that the two mode approximation is valid for the SHA digital noise results.

A summary of the noise results, both calculational and experimental, for the four SHA cores and the ARK, is presented in Table 11. The descriptions and methods used in arriving at the results of Table 11a are given in Table 11b.

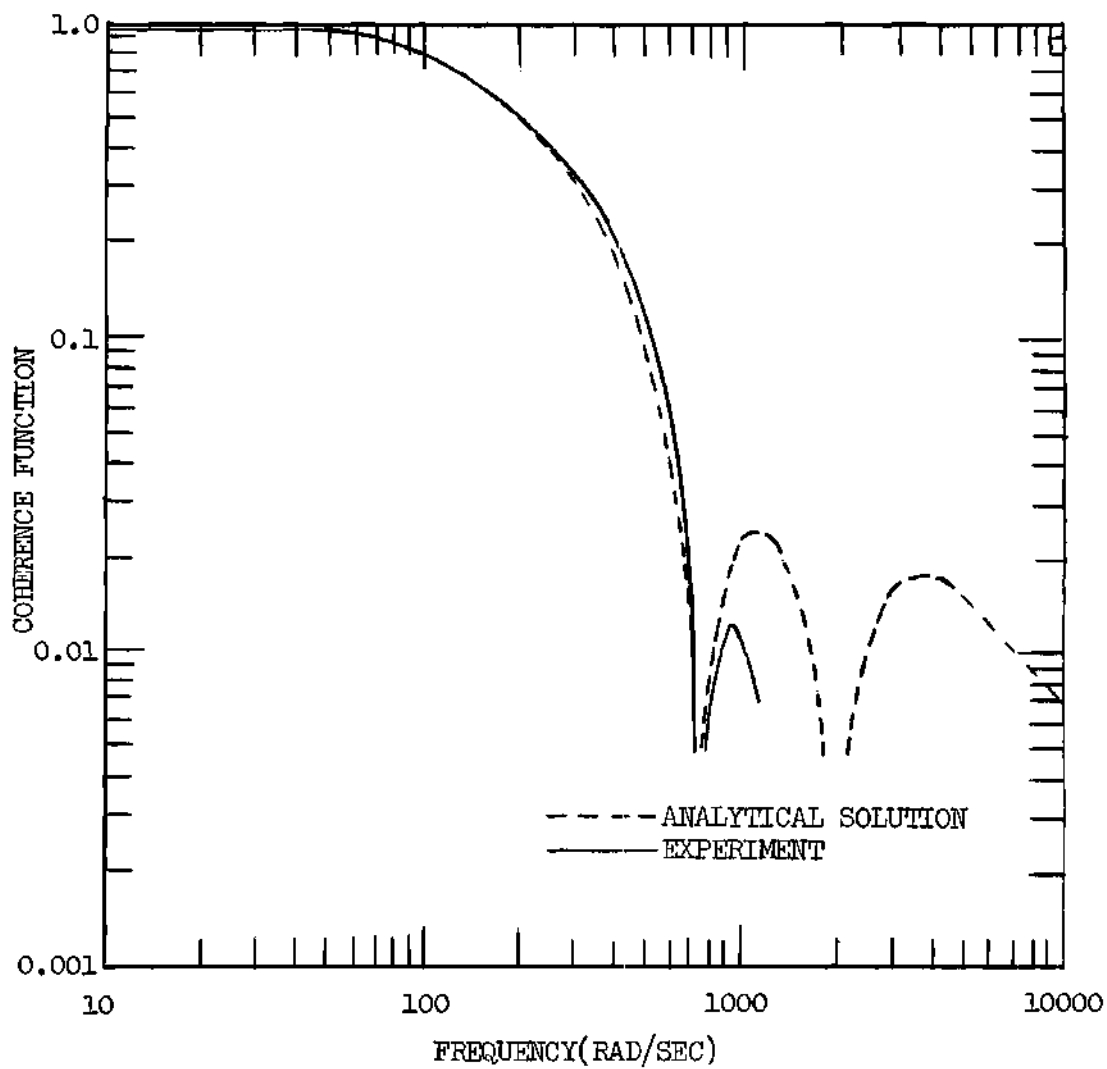


Figure 62. Exact and Measured Values of  $|R^{(2,2)}(x_1, -x_1, \omega)|$  -  
 $ARK-x_1 = -42.5$  cm

Table 11. Summary of the Noise Results (Section a)

	SHA Core 35A'	SHA Core 35A	SHA Core 39	SHA Core 38B	ARK	Comment #
$\rho$ , % $\Delta K/K$	-0.043	-0.043	-0.043	-0.086	0.00	1
$MR^{(2,2)}(x_i, x_j, T, \omega_{small})$ or $R^{(2,2)}(x_i, x_j, \omega_{small})$	0.41	0.56	0.75	0.66	0.942	2
$\omega_0$ , $sec^{-1}$	-127	-112	-130	-330	-42	3
$\omega_1$ , $sec^{-1}$	-200	-250	-360	-850	-351	4
$(\omega_{null})_{calc}$ , $sec^{-1}$	450	610	660	1920	1000	5
$(\omega_{null})_{meas}$ , $sec^{-1}$	520	600	900	2500	730	6
NR	0.088	0.100	0.092	0.174	0.013	7
$a_{\omega}^{(2)}(x_i, T)$ or $a_{\omega}^{(2)}(x_i)$	1.09	--	--	--	2.00	8
$a_{\lambda}^{(2)}(x_i, T)$ or $a_{\lambda}^{(2)}(x_i)$	1.03	--	--	--	2.00	9
$a_{exp}^{(2)}(x_i, T)$ or $a_{exp}^{(2)}(x_i)$	1.11	1.13	1.25	1.16	1.12	10
$\Delta(1/K_1)_{calc}$ , % $\Delta K/K$	0.59	--	--	--	4.30	11
$\Delta(1/K_1)\omega$ , % $\Delta K/K$	0.57	--	--	--	4.60	12
$\Delta(1/K_1)\lambda$ , % $\Delta K/K$	0.53	--	--	--	4.60	13
$\Delta(1/K_1)_{exp}$ , % $\Delta K/K$	0.58	0.99	2.15	1.93	3.28	14
$\Delta(1/K_1)_{MCC}$ , % $\Delta K/K$	0.48	0.79	1.78	1.44	--	15
$\Delta(1/K_1)_{meas}$ , % $\Delta K/K$	0.52	0.97	1.46	1.36	4.71	16
$\bar{\beta}$ calc	0.0078	0.0078	0.0078	0.0078	0.0076	17
$\bar{\beta}$ exp	0.0079	--	--	--	0.0084	18
$\Lambda_{\omega}$ , $\mu s$	69	--	--	--	156	19
$\Lambda_{\lambda}$ , $\mu s$	69	--	--	--	148	20
$\Lambda_{exp}$ , $\mu s$	62	--	--	--	200	21

Table 11. Continued (Section b)

- 
17. Effective delayed neutron fractions for the SHA cores given in Reference 20 and for the ARK in Reference 107.
  18. Inferred  $\bar{\beta}$  using equation (5.43) for the ARK and its equivalent for the SHA Core 35A'.
  - 19&20. Generation times,  $\Lambda_{00}$ , calculated using equation (C.10) for the modified omega and lambda modes, respectively.
  21. Experimentally inferred generation times using equation (5.45) with observed  $\omega_0$ s of comment #3.
- 

Some of the predicted conclusions of the previous chapters are clearly indicated in Table 11. As the eigenvalue separation increases (SHA Core 35A' < 35A < 39) for a given type of core and detector separation, so does the measured low frequency coherence function and null frequency. In addition, the accuracy in the ability to infer experimentally the eigenvalue separation, effective delayed neutron fraction, and generation time decreases with increasing  $\Delta(1/K_1)$ .

The noise ratio (NR) is much smaller in the ARK than in any SHA core. This is most likely due to the good statistics and the inherently short equivalent gate times (T) which were involved in the analog measurements. However, analog measurements generally take much longer to perform than digital. It should again be mentioned that the NR was already taken into account in the presentation of the coherence function results of Seifritz and Albrecht.<sup>28</sup>

Experimentally determined values of the spatial weighting term,  $a^{(2)}(x_i, T)$  or  $a^{(2)}(x_i)$ , agree well with the calculated values in the SHA

Core 35A<sup>1</sup>, but not in the ARK. The calculated values for the ARK case are probably better than the experimentally determined values. The reason for this may be seen upon inspection of equation (5.37). When the low frequency coherence function is near unity (as in the ARK case), the accuracy in determining  $a^{(2)}(x_1)$  experimentally therefore decreases.

There tends to be good agreement between the several methods of determining  $\Delta(1/K_1)$  for eigenvalue separations below 1%  $\Delta K/K$ . Above this value, agreement is not very good. Assuming that the correlation function method,  $\Delta(1/K_1)_{\text{meas}}$  is the better method (since it is the most direct in using the physical observables,  $\omega_0$  and  $\omega_1$ ), then it appears that the  $\Delta(1/K_1)_{\text{MCC}}$  method is better than any of the coherence function methods presented in this work when  $\Delta(1/K_1)$  is greater than about 1%  $\Delta K/K$ .

### Discussion

The methods which were developed for extracting reactor parameters from noise data have been applied in this chapter with general success. For analog noise data, the methods developed in the last chapter could be used directly. However, for the digital noise data, these methods had to be modified somewhat.

Several of the observations about the nature of the coherence function discussed in the previous chapters were confirmed by the measurements. Specifically, it was found that the null frequency and low frequency coherence function increase as the eigenvalue separation increases. Also, the accuracy in inferring the eigenvalue separation, effective delayed neutron fraction, and neutron generation time from noise data decreases with increasing  $\Delta(1/K_1)$ . Finally, it was observed that the phase was zero

for the symmetrically placed detectors used in the measurements.

It was found that, in the digital coherence function noise methods, care must be exercised in keeping the spatial weighting term greater than one and the trivial noise ratio small. The trivial noise ratio is a measure of the trivial correlation to total correlation of a detector. The best way to satisfy the above two requirements is to keep the detection time interval ( $T$ ) short. The 1 ms data of the KAPL data were not useful, however, because of the low statistical accuracy. This could have been alleviated if more noise records were taken at this channel time width.

The experimentally determined spatial weighting functions could be evaluated well only for loosely coupled cores. Otherwise it is more advantageous to calculate them directly from the definitions. There is, however, one exception to this rule. When the detectors are located in places where the fundamental and first harmonic eigenfunctions are small (i.e., near the core edges), the calculation of the spatial weighting function will be subject to rather large error. In these cases, the experimentally determined spatial weighting is best to use for the extraction of the reactor parameters.

It appears that the best method to use to determine the eigenvalue separation from noise data is the correlation function approach of Reference 20 (i.e.,  $\Delta(1/K_1)_{\text{meas}}$ ). Using this method, the fundamental and first harmonic prompt decay constants ( $\omega_0$  and  $\omega_1$ ) are inferred from the auto- and cross-covariances and used to calculate  $\Delta(1/K_1)$  directly from equation (5.30). However, it is not always very easy to determine  $\omega_1$

from the noise data. The accuracy of this determination decreases as the eigenvalue separation increases. Nevertheless, with certain detector locations, it may be possible to accurately extract  $\omega_1$  from noise data even for tightly coupled cores.

Assuming that the best value of the eigenvalue separation is given by  $\Delta(1/K_1)_{\text{meas}}$ , it appears that the MCC method of Reference 20 is superior to the coherence function methods (i.e.,  $\Delta(1/K_1)_\omega$ ,  $\Delta(1/K_1)_\lambda$ , and  $\Delta(1/K_1)_{\text{exp}}$ ) when  $\Delta(1/K_1)$  is greater than about 1%  $\Delta K/K$ . The good agreement of the MCC method with  $\Delta(1/K_1)_{\text{meas}}$  in this range of eigenvalue separations may be fortuitous however. That is, there is no reason in principle why  $\Delta(1/K_1)_{\text{exp}}$  and  $\Delta(1/K_1)_{\text{meas}}$  should not be identical (within experimental error), because they both were obtained entirely from experimental observables. (It is noted that  $\Delta(1/K_1)_{\text{MCC}}$ ,  $\Delta(1/K_1)_\omega$ , and  $\Delta(1/K_1)_\lambda$  were obtained from a combination of experimental observables and computed quantities. In these cases,  $\Delta(1/K_1)_{\text{MCC}}$  of Reference 20 was most likely better because the reactor modeling was better.<sup>152,153</sup>) It would have been of interest to obtain  $\Delta(1/K_1)$  using the MCC method of equations (5.34) and (5.38) and compared it to the  $\Delta(1/K_1)_{\text{meas}}$  and  $\Delta(1/K_1)_{\text{exp}}$  values. In this case, the three different methods would have been on an equal footing.

In order to extract  $\bar{\beta}$  and  $\Lambda_{00}$  from noise measurements, it is necessary to numerically compute  $\Delta(1/K_1)$ . This becomes more difficult as the eigenvalue separation becomes small. It should also be pointed out that, conversely, when the eigenvalue separation becomes large, though it is easy to compute  $\Delta(1/K_1)$ , the accuracy of the  $\bar{\beta}$  and  $\Lambda_{00}$

determinations will be poor. This happens because the two-mode approximation is not valid for large  $\Delta(1/K_1)$ .

## CHAPTER VII

## CONCLUSIONS

The purpose of this work was to develop and apply methods through which some dynamic parameters of coupled core reactors could be inferred from noise measurements. In the process of the investigation, it was necessary to construct an exact, one-dimensional, two-group solution of the neutron noise coherence function. This exact solution was used to see how the shape of the coherence function changed with varying core and detector conditions when experimental results were not available. The exact solution agreed well with what data were available. A qualitative understanding of the nature of the coherence function was gained using this exact solution.

Methods used to extract the reactor parameters were derived from the techniques of modal approximations. A specific case of the modal method, called the two-mode approximation, was used in this work. The two-mode approximations of the coherence function agreed well with the exact solution. Criteria on detector and core conditions needed for accurate inference of the reactor parameters were established using the two-mode method. In addition, the two-mode approximations yield some quantitative insight into the nature of the coherence function for varying detector and core conditions.

Starting with a general formulation of the covariance,<sup>6,31</sup> the interrelation between several common time and frequency domain noise

techniques was demonstrated. These techniques contained the space- and energy-dependence in a continuous form, embodied in the Green's or transfer function. Modal approximations of the noise techniques were shown to arise from the particular modal form which the Green's or transfer function was approximated. Since the objectives of this work were to develop methods to infer some global reactor parameters and to maintain the capability of extension to two-dimensional, multiregion reactors, the lambda and modified omega eigenfunctions were used to approximate the space- and energy-dependence of the Green's function. The point reactor noise formulations result when only the first term in the modal expansion is retained. The same amount of information is contained in both the frequency and time domain noise techniques.

An exact solution of the coherence function was constructed by solving for the two-group Green's function exactly in a one-dimensional system. It was observed that the shape of the coherence function is a complicated function of the frequency dependent mean free path length between the two detectors and the spatial distribution of the stochastic source. The frequency dependence comes about through the Fourier transform of the time derivative in the neutron kinetics equations. This  $\omega/v$  term acts as a frequency dependent  $1/v$  absorber added to the static destruction operator (i.e., the absorption and leakage operators) in the Green's function defining equations. This type of frequency dependence is also manifest in the modal approximations of the coherence function, although it is of a less obvious nature. In this case, the  $\omega/v$  term affects the shape of the expansion modes which Gozani refers to as the kinetic distortion.<sup>125,154</sup>

A number of interesting characteristics of the coupled core coherence function were explained using the exact solution and/or the modal approximations. The rather peculiar behavior of the absolute value of the coherence function at some frequencies called the sink or null frequencies, which are sometimes observed in coupled core measurements, was adequately explained using modal expansion approximations. Null frequencies are observed when detectors are symmetrically located and sinks come about for asymmetrically placed detectors. Sinks or nulls were seen to arise from the interference effects of the prompt neutron decay modes. These decay modes are excited by the stochastically time varying inherent neutron noise source. Their relative influence on the detectors are dependent on the spatial distribution of the source, the location of the detectors, and the degree of core coupling. The lowest frequency sink or null was ascribed to the interference of the fundamental and first harmonic prompt decay modes and the next lowest to the interference of the fundamental and second harmonic, etc. When both detectors were placed in or close to the decoupling region of the coupled cores studied, low order sinks or nulls were no longer observed in the exact solution of the coherence function. In addition, as the detector separation was increased, the low order sink or null frequency decreased asymptotically. These observations were simply explained using the two-mode approximations of the coherence function. Also, it was noted that the time domain equivalent of a null frequency is a short rise in the cross-covariance for short lag times.

Using qualitative arguments in conjunction with the exact solution,

the technique of determining the local thermal neutron lifetimes proposed by Ackermann<sup>19</sup> was demonstrated to be valid only when the local neutron leakage is small. Because the leakage is small in the center portion of large regions, the Ackermann method will be valid there.

The coherence function phase angle, computed using the exact solution, tends to be smaller at any given frequency in loosely coupled cores than in tightly coupled ones. The reason for this most likely resides in the fact that the magnitude of  $\omega/v$  relative to the destruction operator is generally greater for tightly than for loosely coupled cores. It is the magnitude of  $\omega/v$  relative to the destruction operator that determines the magnitude of the phase for a given frequency.

It was observed in both the modal approximations and exact solution that the magnitude of the low frequency (below the sink or null frequency) coherence function decreases with decreasing eigenvalue separation. Also, it was seen that the magnitude of the low frequency coherence function decreased with increasing detector separations, and the magnitude increased with increasing detector separations at high frequencies (above the sink or null frequency). These effects can be explained by either the contribution of the  $\omega/v$  absorption term or the relative contributions of the expansion modes.

Methods were developed and applied whereby the inference of the eigenvalue separation ( $\Delta(1/K_1)$ ), effective delayed neutron fraction ( $\bar{\beta}$ ), and independently the neutron generation time ( $\Lambda_{00}$ ) from noise data was possible subject to certain core and detector placement conditions. The overriding condition was that the measured coherence function exhibit a

sink or null frequency or the equivalent for time domain measurements. A spatial weighting function,  $a^{(2)}(x_1)$ , was defined using the two-mode approximation, whose purpose was to indicate what core and detector placement conditions were necessary for the extraction of the reactor parameters. It was concluded theoretically that  $\Delta(1/K_1)$ ,  $\bar{\beta}$ , and  $\Lambda_{00}$  can only be accurately inferred in loosely coupled cores for detectors located external to the decoupling region. However, it was also concluded that it would be difficult to infer  $\bar{\beta}$  and  $\Lambda_{00}$  if the reactor was too loosely coupled.

The noise methods were applied to extract  $\Delta(1/K_1)$ ,  $\bar{\beta}$ , and  $\Lambda_{00}$  from coherence function measurements on coupled core, zero power reactors at Knolls Atomic Power Laboratory<sup>20</sup> and the Karlsruhe Research Center.<sup>28</sup> Results obtained using these methods compared favorably with time domain experimental interpretations and with direct calculations. From the experimental results (see Table 11), it appears that the accuracy in determining  $\bar{\beta}$ ,  $\Delta(1/K_1)$ , and  $\Lambda_{00}$  decreases with increasing eigenvalue separation. The reason for this most likely stems from the fact that the two-mode approximation of the coherence function (or the time domain equivalent) becomes worse for increasing eigenvalue separation. It was concluded from the results of the experiments and calculations that the best method to obtain reactor parameters by noise analysis is by using the lag time correlation method of Rydin et al.<sup>20</sup>

## CHAPTER VIII

## RECOMMENDATIONS

Since this work was only concerned with one-dimensional (1D) models, it would be of interest to extend the analysis to more realistic 2D models. Investigations of this nature would shed light on the effect of the transverse dimension on the noise calculations. Although it is difficult in general to generate the higher order 2D modes,<sup>126</sup> it is relatively straightforward to calculate the fundamental and first harmonic lambda and modified omega modes using static diffusion theory codes (e.g., EXTERMINATOR-II<sup>89</sup>) for symmetric coupled core reactors. The method of proceeding would be first to compute the 2D flux. This flux is the 2D fundamental lambda eigenfunction and  $k_{eff}$  is the fundamental lambda eigenvalue  $\lambda_0$ . The 2D fundamental modified omega mode would be obtained by reducing the production operator by a factor of  $(1-\bar{\beta})$  and adding negative absorption in the form  $w/v$  until the same  $k_{eff}$  as the lambda calculation is attained. Of course, for subcritical systems,  $k_{eff}$  will be less than one. The first harmonic 2D modes (both  $\lambda$  and  $\omega$ ) would be calculated using the same procedure as above, but only using a quarter of the reactor.<sup>152</sup> That is, zero flux boundary conditions on all sides of the quarter section would be established. The computed flux shapes would be the first harmonic modes and the  $k_{eff}$  of this quarter section would be the first harmonic lambda eigenvalue  $\lambda_1$ . It should be noted that it may be possible to generate the higher 1D or 2D modes for symmetric or asymmetric reactor

models using EXTERMINATOR-II<sup>89</sup> because of the negative flux option in this code, which was used by Johnson and Macdonald.<sup>86,87</sup>

It would also be of interest to check the accuracy of the 1D eigenvector and eigenvalue computations using schemes other than the critical determinate method<sup>127,128</sup> presented in this work. The problem of round-off errors on the zero-crossing of the determinate could be avoided by using a static diffusion theory code such as EXTERMINATOR-II<sup>89</sup> (iterating to find the zero crossings in both the symmetric and asymmetric reactor case), or by using a Wieland iteration scheme,<sup>129,130</sup> or by use of the Stabilized March Technique.<sup>126,131</sup> Using these schemes may also help in eliminating the poor phase angle calculations involved in modal approximations.

The methods presented in this work may be easily extended to asymmetric 1D reactor models. Although no experimental noise data are yet available from asymmetric reactors, it would be appropriate to undertake some calculations for such reactor models in order to give the experimentalist a better idea of how to perform some experiments. Better phase information would be forthcoming from such asymmetric reactor experiments.

Several interesting theoretical studies could be undertaken. Instead of starting with the diffusion equation, one could proceed from the one-group Telegrapher's equation,<sup>87</sup> use a two-mode expansion approximation, and reduce to the two-node form. From an analysis along these lines, not only could the coupling coefficients but also the time distribution function could be calculated a priori.<sup>27,28</sup>

If the 2D modal approximation methods are undertaken, an appropriate

2D exact solution of the neutron noise should be constructed to serve as a standard of comparison. The 1D exact solution presented in this work cannot be easily extended to 2D systems. However, Danofsky<sup>132</sup> has used the space-time kinetics computer code WIGL2<sup>133</sup> to solve for the 1D coherence function exactly in a coupled core reactor. The same type of procedure could be used to solve for the 2D coherence function exactly using the 2D space-time kinetics program TWIGL<sup>134</sup> or some other standard 2D space-time kinetics program. It would be interesting to see if these 2D, exact, finite difference codes would predict the higher order sink or null frequencies.

In the line of experimental work, both the GTRR and AGN 201 at Georgia Tech could be used to obtain useful noise data both in the frequency and time domains. It would be of particular interest to vary the split core configurations in the GTRR for various subcritical conditions. This could be accomplished on the GTRR (a CP-5 type reactor) because of the high photoneutron source which is fairly uniformly distributed and of high intensity even in the far subcritical region. Interpretation of the detector effects using the two-mode expansion techniques for various subcritical conditions may help to clarify some of the related problems being encountered in the fast reactor work.<sup>135</sup> Correlation between fast and thermal neutron detectors may yield additional information on the variation of neutron lifetime in different regions of the reactor.

In the work presented here, it was shown how the effective delayed neutron fraction ( $\bar{\beta}$ ) could be determined independently from the neutron generation time ( $\Lambda_{00}$ ) with noise measurements. However, in this procedure

it was necessary to numerically calculate the eigenvalue separation ( $\Delta(1/K_1)$ ). It was demonstrated that the accuracy in the determination of  $\bar{\beta}$  was optimum for a certain value of  $\Delta(1/K_1)$ , but decreased for larger and smaller values of  $\Delta(1/K_1)$ . The problem of calculating  $\Delta(1/K_1)$  in the  $\bar{\beta}$  determination could be avoided by using the Ackermann<sup>19</sup> method of determining the thermal neutron lifetime ( $l$ ) independently of  $\bar{\beta}$ . In this case,  $l$  could be determined entirely by experimental means and  $\bar{\beta}$  could be determined from the expression  $\bar{\beta} = l\omega_0^{\text{critical}}$ , where  $\omega_0^{\text{critical}}$  is the experimentally observed critical prompt neutron decay constant. In this method,  $\bar{\beta}$  could also be obtained entirely from experimental observables. This may be of some importance in determining the fraction of plutonium present in a breeder reactor.

Finally, it may be possible to infer the value of the capture to fission ratio ( $\alpha$ ) from noise measurements by a modification of the Ackermann<sup>19</sup> method. Measurement of the global  $\alpha$  in a fast breeder reactor would certainly be very desirable.

**APPENDICES**

## APPENDIX A

## BASIC RELATIONS OF RANDOM NOISE THEORY

Average or Mean

Suppose that one has an infinite number of identical reactors which are monitored by an infinite number of identical detectors. Designate the  $i^{\text{th}}$  detector response rate in the  $k^{\text{th}}$  reactor at time  $t$  by  $D_{ik}(t)$ . The ensemble average of the detectors response rates at time  $t$  is

$$\langle D_i(t) \rangle \equiv \lim_{N \rightarrow \infty} \frac{\sum_{k=1}^N D_{ik}(t)}{N} . \quad (\text{A.1})$$

For ergodic, stationary processes, the time average or mean can be substituted for the ensemble average

$$\langle D_i \rangle = \bar{D}_i \equiv \lim_{R \rightarrow \infty} \frac{\int_0^R dt D_{ik}(t)}{R} . \quad (\text{A.2})$$

$R$  is the record length of the measurement.

Variance

The variance of the  $i^{\text{th}}$  detector response rate assuming ergodic, stationary processes is defined as

$$\sigma^2(D_i, D_i) \equiv \lim_{R \rightarrow \infty} \frac{\int_0^R dt [D_i(t) - \bar{D}_i]^2}{R} = \overline{D_i^2} - \bar{D}_i^2 . \quad (\text{A.3})$$

### Covariance

This function is defined in a manner similar to the variance, but with two rather than one detector

$$\sigma^2(D_i, D_j) \equiv \lim_{R \rightarrow \infty} \frac{\int_0^R dt [D_i(t) - \bar{D}_i][D_j(t) - \bar{D}_j]}{R} = \overline{D_i D_j} - \bar{D}_i \bar{D}_j \quad (A.4)$$

The quantity  $\overline{D_i D_j}$  is usually called the time averaged product density.<sup>6</sup>

### Modified Coefficient of Correlation

This is a quantity originally defined by Harris et al.,<sup>59</sup> which is in effect a rationalized covariance

$$MCC(D_i, D_j) \equiv \frac{\sigma^2(D_i, D_j)}{\sqrt{[\sigma^2(D_i, D_i) - \bar{D}_i][\sigma^2(D_j, D_j) - \bar{D}_j]}} \quad (A.5)$$

The modified coefficient of correlation tends to measure the global or reactor wide departure from Poisson because the local variations are divided out. It is for this reason that it is well suited for coupled core noise investigations.

### Auto-Covariance

The auto-covariance and variance are closely related

$$\begin{aligned} C(D_i, D_i, \tau) &\equiv \lim_{R \rightarrow \infty} \frac{\int_0^R dt [D_i(t) - \bar{D}_i][D_i(t+\tau) - \bar{D}_i]}{R} & (A.6) \\ &= \lim_{R \rightarrow \infty} \frac{\int_0^R dt [D_i(t) D_i(t+\tau)]}{R} - \bar{D}_i^2 \end{aligned}$$

(continued)

$$= \overline{D_i(t) D_i(t+\tau)} - \bar{D}_i^2, \quad \tau \geq 0,$$

$$C(D_i, D_i, \tau) \equiv \overline{D_i(t-\tau) D_i(t)} - \bar{D}_i^2, \quad \tau \leq 0,$$

where  $\tau$  is the detector lag (or lead) time.

### Cross-Covariance

The cross-covariance is closely related to the covariance

$$C(D_i, D_j, \tau) \equiv \overline{D_i(t) D_j(t+\tau)} - \bar{D}_i \bar{D}_j, \quad \tau \geq 0, \quad (\text{A.7})$$

$$C(D_i, D_j, \tau) \equiv \overline{D_i(t-\tau) D_j(t)} - \bar{D}_i \bar{D}_j, \quad \tau \leq 0.$$

### Auto-Correlation Function

This function is just the auto-covariance with the square of the mean detector rate added to it

$$\phi(D_i, D_i, \tau) \equiv C(D_i, D_i, \tau) + \bar{D}_i^2. \quad (\text{A.8})$$

### Cross-Correlation Function

In a similar manner, the cross-correlation function is the cross-covariance with the product of the mean rates added to it

$$\phi(D_i, D_j, \tau) \equiv C(D_i, D_j, \tau) + \bar{D}_i \bar{D}_j. \quad (\text{A.9})$$

Auto-Power-Spectral-Density

Fourier transformation of the auto-covariance yields the APSD

$$\hat{\Phi}(D_i, D_i, \omega) \equiv \int_{-\infty}^{\infty} d\tau C(D_i, D_i, \tau) e^{-j\omega\tau} . \quad (\text{A.10})$$

Cross-Power-Spectral-Density

Fourier transformation of the cross-covariance yields the CPSD

$$\hat{\Phi}(D_i, D_j, \omega) \equiv \int_{-\infty}^{\infty} d\tau C(D_i, D_j, \tau) e^{-j\omega\tau} . \quad (\text{A.11})$$

Coherence Function

This function, originally defined in coupled core noise analysis work by Albrecht and Seifritz,<sup>27</sup> is a type of rationalized CPSD

$$R(D_i, D_j, \omega) \equiv \frac{\hat{\Phi}(D_i, D_j, \omega)}{\sqrt{[(\hat{\Phi}(D_i, D_i, \omega) - \bar{D}_i)] [\hat{\Phi}(D_j, D_j, \omega) - \bar{D}_j]}} . \quad (\text{A.12})$$

The coherence function serves the same purpose in the frequency domain as the modified coefficient of correlation does in the time domain.

## APPENDIX B

## MODAL EXPANSION APPROXIMATIONS OF SPACE-ENERGY-TIME

## REACTOR KINETICS

Many of the approximate solution methods used in space-energy-time reactor kinetics may be used to good advantage in space- and energy-dependent noise work as is indicated in Chapter II. This appendix is concerned with a review of a particular special case of the more general method of weighted residuals; that of the modal expansion approximations to the space-energy-time reactor kinetics. This presentation follows along the lines of Chapter I in Reference 30.

The time dependent neutron balance equation may be written (using standard notation)<sup>30</sup>

$$\begin{aligned} \frac{1}{v} \frac{\partial F}{\partial t}(\mathbf{r}, E, \vec{\Omega}, t) = & - \vec{\Omega} \cdot \nabla F(\mathbf{r}, E, \vec{\Omega}, t) - \sum_T(\mathbf{r}, E, t) F(\mathbf{r}, E, \vec{\Omega}, t) \quad (B.1) \\ & + Q(\mathbf{r}, E, \vec{\Omega}, t) + (1-\bar{\beta}) \frac{\chi_p(E)}{4\pi} \int_0^\infty dE' v \sum_f(\mathbf{r}, E', t) \int_{\Omega'} F(\mathbf{r}, E', \vec{\Omega}', t) d\vec{\Omega}' \\ & + \int_0^\infty dE' \int_{\Omega'} d\vec{\Omega}' \sum_s(\mathbf{r}; E', \vec{\Omega}' \rightarrow E, \vec{\Omega}; t) F(\mathbf{r}, E', \vec{\Omega}', t) \\ & + \sum_{m=1}^M \lambda_m \frac{\chi_m(E)}{4\pi} C_m(\mathbf{r}, t) . \end{aligned}$$

$F(\mathbf{r}, E, \vec{\Omega}, t)$  is the product of the neutron velocity and neutron distribution function. The term on the left-hand side of equation (B.1) denotes the

time rate of change of the neutron distribution function in the differential phase space  $d\mathbf{r}d\mathbf{E}d\vec{\Omega}$ . The terms on the right-hand side of equation (B.1) represent the leakage, removal, external source, fission, in-scattering and delayed neutron rates in the differential phase space, respectively.

Because the balance equation is extremely difficult to solve except for very simple reactor models, the time-dependent multi-group diffusion equation approximation is usually involved. This approximation may be written in matrix form<sup>30</sup>

$$[\nabla \cdot \vec{D}(\mathbf{r}, t) \nabla - \vec{R}_a(\mathbf{r}, t) - \vec{R}_s(\mathbf{r}, t) + \vec{S}(\mathbf{r}, t) + (1 - \beta) \vec{\chi}_p \vec{F}^T(\mathbf{r}, t)] \vec{\Phi}(\mathbf{r}, t) \quad (\text{B.2})$$

$$+ \sum_{m=1}^M \lambda_m \vec{\chi}_m C_m(\mathbf{r}, t) + \vec{Q}(\mathbf{r}, t) = \vec{V}^{-1} \frac{\partial}{\partial t} \vec{\Phi}(\mathbf{r}, t)$$

and

$$\beta_m \vec{F}^T(\mathbf{r}, t) \vec{\Phi}(\mathbf{r}, t) - \lambda_m C_m(\mathbf{r}, t) = \frac{\partial}{\partial t} C_m(\mathbf{r}, t), \quad m = 1, \dots, M \quad (\text{B.3})$$

$\vec{\Phi}(\mathbf{r}, t)$  is the space- and time-dependent  $G \times 1$  ( $G$  is the number of energy groups) column vector of group fluxes,  $\vec{\chi}_p$  and  $\vec{\chi}_m$  are column vectors of prompt fission and precursor decay neutron spectra, respectively, and  $\vec{F}^T(\mathbf{r}, t)$  is a row vector with elements  $\nu^{(g)} \Sigma_f^{(g)}(\mathbf{r}, t)$ .  $\vec{Q}(\mathbf{r}, t)$  is a vector of group sources. The  $G \times G$  matrices  $\vec{D}(\mathbf{r}, t)$ ,  $\vec{R}_a(\mathbf{r}, t)$ ,  $\vec{R}_s(\mathbf{r}, t)$ , and  $\vec{V}^{-1}$  are diagonal with elements  $D^{(g)}(\mathbf{r}, t)$ ,  $\Sigma_a^{(g)}(\mathbf{r}, t)$ ,  $\Sigma_s^{(g)}(\mathbf{r}, t)$ , and  $1/V^{(g)}$ , respectively ( $g$  represents the particular energy group), while  $\vec{S}(\mathbf{r}, t)$  is a  $G \times G$  matrix with elements  $\Sigma^{(g'-g)}(\mathbf{r}, t)$  (representing the scattering cross section from group  $g'$  to  $g$ ).  $C_m(\mathbf{r}, t)$  represents the delayed neutron

concentration of the  $m^{\text{th}}$  delayed group. The remaining notation is standard.

### Modal Expansion Approximations

Modal expansion techniques may be characterized as those procedures by which the number of independent variables in a problem is reduced by means of an expansion in known functions of one or more of the independent variables. The general theory of this technique has been discussed in some detail.<sup>115,136-138</sup>

The time-synthesis modal approximation of the space-energy-time dependent neutron flux and precursor concentrations is constructed by assuming a finite expansion of known shape vectors  $\vec{\psi}_n(\mathbf{r})$ , multiplied by unknown time dependent scalar expansion coefficients  $a_n(t)$ . (This is called the group collapsed method.<sup>30</sup>)

$$\vec{\Phi}(\mathbf{r}, t) = \sum_{n=0}^N a_n(t) \vec{\psi}_n(\mathbf{r}) + \vec{R}(\mathbf{r}, t) . \quad (\text{B.4})$$

$\vec{R}(\mathbf{r}, t)$  is the residual vector which is the difference between the true flux and the modal approximation. The manner used to reduce the weighted residual to zero will determine the method of approximation.<sup>136</sup> Equation (B.4) is substituted into equations (B.2) and (B.3), the former is pre-multiplied by a known weighting vector  $\vec{W}_\ell^T(\mathbf{r})$  and the latter by  $\vec{W}_\ell^T(\mathbf{r})\vec{\chi}_m$ , and both integrated over the volume of the reactor. The Gx1 vector transpose  $\vec{W}_\ell^T(\mathbf{r})$  is an arbitrary weighting vector. When the above procedure of weighting and integrating is carried out, the following set of equations results from the requirement that the weighted residual is zero in an

integral sense, for  $N$  different weighting functions  $\vec{W}_n(\mathbf{r})$ .

$$\begin{aligned} \sum_{n=0}^N [-A_{ln}(t)a_n(t) + (1-\beta)F_{ln}a_n(t)] + \sum_{m=1}^M \lambda_m C_{m,\ell}(t) + Q_\ell(t) & \quad (B.5) \\ = \sum_{n=0}^N \tau_{ln} \frac{d}{dt} a_n(t), & \quad \ell = 0, 1, \dots, N, \end{aligned}$$

and

$$\beta_m \sum_{n=0}^N F_{m,ln}(t)a_n(t) - \lambda_m C_{m,\ell}(t) = \frac{d}{dt} C_{m,\ell}(t), \quad (B.6)$$

$$m = 1, 2, \dots, M; \quad \ell = 0, 1, \dots, N,$$

where

$$A_{ln}(t) \equiv \int_{\text{reactor}} d\mathbf{r} \vec{W}_\ell^T(\mathbf{r}) [\nabla \cdot \vec{D}(\mathbf{r}, t) \nabla - \vec{K}_a(\mathbf{r}, t) - \vec{K}_s(\mathbf{r}, t) + \vec{S}(\mathbf{r}, t)] \vec{\psi}_n(\mathbf{r}), \quad (B.7)$$

$$F_{ln}(t) \equiv \int_{\text{reactor}} d\mathbf{r} \vec{W}_\ell^T(\mathbf{r}) \vec{\chi}_p \vec{F}(\mathbf{r}, t) \vec{\psi}_n(\mathbf{r}), \quad (B.8)$$

$$F_{m,ln}(t) \equiv \int_{\text{reactor}} d\mathbf{r} \vec{W}_\ell^T(\mathbf{r}) \vec{\chi}_m \vec{F}(\mathbf{r}, t) \vec{\psi}_n(\mathbf{r}), \quad (B.9)$$

$$\tau_{ln} \equiv \int_{\text{reactor}} d\mathbf{r} \vec{W}_\ell^T(\mathbf{r}) \vec{V}^{-1} \vec{\psi}_n(\mathbf{r}), \quad (B.10)$$

$$C_{m,\ell}(t) \equiv \int_{\text{reactor}} d\mathbf{r} \vec{W}_\ell^T(\mathbf{r}) \vec{\chi}_m C_m(\mathbf{r}, t), \quad (B.11)$$

$$Q_\ell(t) \equiv \int_{\text{reactor}} d\mathbf{r} \vec{W}_\ell^T(\mathbf{r}) \vec{Q}(\mathbf{r}, t). \quad (B.12)$$

Equations (B.5) and (B.6) are coupled ordinary differential equations, which are solved for  $a_n$  and  $C_{m,\ell}$ . The neutron flux is constructed from equation (B.4). Although the residue  $R(r,t)$  is not zero at every point in space and time, its spatially weighted integral is zero.

The choice of expansion and weighting vectors is an important aspect of the application of the modal expansion techniques. Several types of modes which have been used will be described. Only eigenvector type expansion and weighting vectors will be discussed here. It has been observed<sup>136</sup> that, when the expansion vectors are eigenvectors of the time-dependent diffusion operator and the weighting vectors are the adjoint eigenvectors, the first order variation of the Lagrangian functional is zero. Before proceeding some operators are defined

$$\vec{L}(r) \equiv -\nabla \cdot \vec{D}(r) \nabla + \vec{K}_a(r) + \vec{K}_s(r) - \vec{S}(r) , \quad (B.13)$$

$$\vec{M}(r) \equiv \vec{\chi}_p \vec{F}^T(r) . \quad (B.14)$$

Note that the time dependence of the material properties has been removed.

### Natural Modes

The eigenvectors of the time-independent neutron and precursor balance operator (assuming an  $\exp(\alpha_n t)$  time dependence for the flux and precursors), referred to as the natural modes, satisfy

$$\begin{bmatrix} [(1-\bar{\beta})\vec{M}(r) - \vec{L}(r)] & \lambda_1 \vec{X}_1 & \dots & \dots & \lambda_M \vec{X}_M \\ \beta_1 \vec{F}^T(r) & -\lambda_1 & \dots & \dots & 0 \\ \vdots & \vdots & \ddots & \ddots & \vdots \\ \vdots & \vdots & \vdots & \ddots & \vdots \\ \beta_M \vec{F}^T(r) & 0 & \dots & \dots & -\lambda_M \end{bmatrix} \begin{bmatrix} \vec{\Psi}_n^\alpha(r) \\ C_{1,n}(r) \\ \vdots \\ \vdots \\ C_{M,n}(r) \end{bmatrix} \quad (\text{B.15})$$

$$= \begin{bmatrix} \bar{V}^{-1} & 0 & \dots & \dots & 0 \\ 0 & 1 & \dots & \dots & 0 \\ \vdots & \ddots & \ddots & \ddots & \vdots \\ \vdots & \vdots & \ddots & \ddots & \vdots \\ \vdots & \vdots & \vdots & \ddots & \vdots \\ 0 & 0 & \dots & \dots & 1 \end{bmatrix} \alpha_n \begin{bmatrix} \vec{\Psi}_n^\alpha(r) \\ C_{1,n}(r) \\ \vdots \\ \vdots \\ C_{M,n}(r) \end{bmatrix}$$

where  $\vec{\Psi}_n^\alpha(r)$  is a  $G \times 1$  column eivenvector of the group fluxes. Equation (B.15) may be written

$$\vec{H}(r) \vec{\xi}_n(r) = \alpha_n \vec{T} \vec{\xi}_n(r) \quad (\text{B.16})$$

The natural modes satisfy a useful biorthogonality property

$$\begin{aligned} \langle \vec{\xi}_k^+, \vec{T} \vec{\xi}_n \rangle &= 0 ; & k \neq n \\ &\neq 0 ; & k = n , \end{aligned} \quad (\text{B.17})$$

where the adjoint eigenvector satisfies the adjoint equation

$$\vec{H}^+(r) \vec{\xi}_k^+(r) = \alpha_k \vec{T} \vec{\xi}_k^+(r) , \quad (\text{B.18})$$

and  $\vec{H}^+(\mathbf{r})$  is the Hermitian adjoint of  $\vec{H}(\mathbf{r})$ .

Note that equations (B.2) and (B.3) may be rewritten in a compact form (considering time independent material properties but a time dependent source)

$$\vec{H}(\mathbf{r})\vec{\gamma}(\mathbf{r},t) + \vec{Q}'(\mathbf{r},t) = \vec{I} \frac{\partial}{\partial t} \vec{\gamma}(\mathbf{r},t) . \quad (\text{B.19})$$

Because of the orthogonality property, the time-synthesis equations are decoupled

$$\frac{d}{dt} a'_n(t) = \alpha_n a'_n(t) + \frac{\langle \vec{\xi}_n^+, \vec{Q}'(\mathbf{r},t) \rangle}{\langle \vec{\xi}_n^+, \vec{I} \vec{\xi}_n \rangle} \quad (\text{B.20})$$

when  $\vec{\xi}_n^+(\mathbf{r})$  is taken as the weighting vector. Here  $a'_n(t)$  is a column vector of the  $a_n(t)$  and the  $C_{m,n}(t)$  of equations (B.5) and (B.6). The significant feature of equation (B.20) is the absence of modal coupling. This property is referred to as finality.<sup>115</sup>

### Omega Modes

The eigenvectors of the neutron balance operator (assuming an  $\exp(\omega_n t)$  time dependence for the flux and ignoring delayed neutrons) which satisfy the equation

$$[\vec{M}(\mathbf{r}) - \vec{L}(\mathbf{r})] \vec{\psi}_n^{\omega}(\mathbf{r}) = \omega_n \vec{V}^{-1} \vec{\psi}_n^{\omega}(\mathbf{r}) , \quad (\text{B.21})$$

are known as the omega modes. These vectors are biorthogonal with respect to  $\vec{\psi}_n^{\omega+}(\mathbf{r})$  which satisfies the equation

$$[\vec{M}(\mathbf{r}) - \vec{L}(\mathbf{r})] \vec{\psi}_n^{\omega+}(\mathbf{r}) = \omega_n \vec{V}^{-1} \vec{\psi}_n^{\omega+}(\mathbf{r}) . \quad (\text{B.22})$$

The biorthogonality relation

$$\begin{aligned} \langle \vec{\psi}_k^{\omega+}, \vec{V}^{-1} \vec{\psi}_n^{\omega+} \rangle &= 0 ; & k \neq n \\ &\neq 0 ; & k = n , \end{aligned} \quad (\text{B.23})$$

leads to some simplification in equations (B.5) and (B.6) but does not decouple the different modal equations (i.e., does not lead to finality).

#### Lambda Modes

The eigenvectors of the static neutron balance operator are called the lambda modes

$$\vec{L}(\mathbf{r}) \vec{\psi}_n^{\lambda}(\mathbf{r}) = \frac{1}{\lambda_n} \vec{M}(\mathbf{r}) \vec{\psi}_n^{\lambda}(\mathbf{r}) , \quad (\text{B.24})$$

which have the biorthogonality property

$$\begin{aligned} \langle \vec{\psi}_k^{\lambda+}, \vec{M} \vec{\psi}_n^{\lambda} \rangle &= 0 ; & k \neq n \\ &\neq 0 ; & k = n , \end{aligned} \quad (\text{B.25})$$

where  $\vec{\psi}_k^{\lambda+}(\mathbf{r})$  satisfies the equation

$$\vec{L}(\mathbf{r}) \vec{\psi}_k^{\lambda+}(\mathbf{r}) = \frac{1}{\lambda_k} \vec{M}^+(\mathbf{r}) \vec{\psi}_k^{\lambda+}(\mathbf{r}) . \quad (\text{B.26})$$

These vectors do not have the property of finality.

### Discussion

If the magnitude effects of the delayed neutrons are neglected (i.e., use prompt neutron flux behavior only), and it is assumed that the material properties of the reactor do not vary with time, equations (B.2) and (B.3) may be written as one equation

$$[(1-\bar{\beta})\vec{M}(r) - \vec{L}(r)]\vec{\Phi}(r,t) + \vec{Q}(r,t) = \vec{V}^{-1} \frac{\partial}{\partial t} \vec{\Phi}(r,t) \quad (\text{B.27})$$

which is similar to equation (B.19), but without the delayed neutron components. The eigenvectors of the above neutron balance operator can be thought of as the prompt neutron natural modes or the modified omega modes of equation (B.21)

$$[(1-\bar{\beta})\vec{M}(r) - \vec{L}(r)]\vec{\psi}_n^w(r) = \omega_n \vec{V}^{-1} \vec{\psi}_n^w(r) . \quad (\text{B.28})$$

These modified omega modes have the biorthogonality and finality properties. The significance of this fact is demonstrated in Appendix C where it is shown that the Green's response function may be approximated by a modal expansion using the modified omega modes.

## APPENDIX C

## MODAL EXPANSION APPROXIMATION OF THE GREEN'S FUNCTION

The two-group, space-dependent Green's function used in this work is the solution to the following matrix boundary value problem<sup>21,139</sup>

$$[(1-\bar{\beta})\vec{M}(r) - \vec{L}(r)]\vec{g}(r,r',t) = \vec{V}^{-1} \frac{\partial}{\partial t} \vec{g}(r,r',t) \quad (C.1)$$

$$+ \delta(t)\vec{\delta}(r-r') , \quad t \cong 0 ,$$

$$\vec{g}(\text{boundaries},r',t) = \vec{0} , \quad (C.2)$$

$$\vec{g}(r,r',t) = \vec{0} , \quad t < 0 . \quad (C.3)$$

The double arrowed quantities represent  $2 \times 2$  matrices with  $\vec{M}$ ,  $\vec{L}$ ,  $\vec{V}^{-1}$ ,  $\vec{\delta}$ , and  $\vec{g}$  representing the production, destruction matrix operators and reciprocal velocity, Dirac delta and Green's function matrices, respectively. The Green's function (also called the impulse response function) is defined as the neutron flux at point  $r$  and time  $t$  resulting from one neutron introduced at point  $r'$  and time  $t = 0$ .

It is assumed that the Green's function can be approximated by a finite series expansion<sup>127,140</sup>

$$\vec{g}(\mathbf{r}, \mathbf{r}', t) = \sum_{n=0}^N a_n(t) \vec{\psi}_n(\mathbf{r}) \vec{\psi}_n^{\dagger T}(\mathbf{r}') + \vec{R}(\mathbf{r}, \mathbf{r}', t) . \quad (\text{C.4})$$

The arrows represent vector quantities, and the symbol  $\dagger T$  indicates the adjoint transpose. The residual  $\vec{R}(\mathbf{r}, \mathbf{r}', t)$  is the difference between the finite series expansion and the true solution.<sup>102,136</sup>  $\vec{\psi}_n(\mathbf{r})$  and  $\vec{\psi}_n^{\dagger T}(\mathbf{r}')$  are known expansion and weighting vector functions, respectively, and  $a_n(t)$  is an unknown time dependent scalar (group collapsing is used). In this work, two different types of expansion and weighting vector functions will be used, the modified omega (really the natural modes for equation (C.1)), and the lambda eigenvectors (see Appendix B). Using these two types of eigenvectors in equation (C.4), substituting into equation (C.1), and making use of the respective eigenvalue equations yields

$$\sum_{n=0}^N a_n^\omega(t) \omega_n \vec{V}^{-1} \vec{\psi}_n^\omega(\mathbf{r}) \vec{\psi}_n^{\dagger T \omega}(\mathbf{r}') \quad (\text{C.5})$$

$$+ [(1-\bar{\beta})\vec{M}(\mathbf{r}) - \vec{L}(\mathbf{r}) - \vec{V}^{-1} \frac{\partial}{\partial t}] \vec{R}^\omega(\mathbf{r}, \mathbf{r}', t)$$

$$= \vec{V}^{-1} \sum_{n=0}^N \dot{a}_n^\omega(t) \vec{\psi}_n^\omega(\mathbf{r}) \vec{\psi}_n^{\dagger T \omega}(\mathbf{r}') + \delta(t) \vec{\delta}(\mathbf{r}-\mathbf{r}')$$

$$\sum_{n=0}^N a_n^\lambda(t) [1 - \bar{\beta} - 1/\lambda_n] \vec{M} \vec{\psi}_n^\lambda(\mathbf{r}) \vec{\psi}_n^{\dagger T \lambda}(\mathbf{r}') \quad (\text{C.6})$$

$$+ [(1-\bar{\beta})\vec{M}(\mathbf{r}) - \vec{L}(\mathbf{r}) - \vec{V}^{-1} \frac{\partial}{\partial t}] \vec{R}^\lambda(\mathbf{r}, \mathbf{r}', t)$$

$$= \vec{V}^{-1} \sum_{n=0}^N \dot{a}_n^\lambda(t) \vec{\psi}_n^\lambda(\mathbf{r}) \vec{\psi}_n^{\dagger T \lambda}(\mathbf{r}') + \delta(t) \vec{\delta}(\mathbf{r}-\mathbf{r}') .$$

The method of weighted residuals consists of arbitrarily choosing a function and requiring the weighted integral of the residual to vanish.<sup>136</sup> Multiplying equations (C.5) and (C.6) by the transpose adjoint eigenvectors (modified omega and lambda, respectively), integrating over the reactor volume and making use of the biorthogonality property, and employing an inner product notation results in the following equations

$$a_m^\omega(t)\omega_m - \dot{a}_m^\omega(t) = \delta(t) / \langle \vec{\psi}_m^\omega, \vec{V}^{-1} \vec{\psi}_m^\omega \rangle, \quad m = 0, 1, \dots, N \quad (C.7)$$

$$a_m^\lambda(t) [1 - \bar{\beta} - \frac{1}{\lambda_m}] \langle \vec{\psi}_m^\lambda, \vec{M} \vec{\psi}_m^\lambda \rangle = \vec{\psi}_m^{+T\lambda}(r') \quad (C.8)$$

$$= \sum_{n=0}^N \dot{a}_n^\lambda(t) \langle \vec{\psi}_m^\lambda, \vec{V}^{-1} \vec{\psi}_n^\lambda \rangle = \vec{\psi}_n^{+T\lambda}(r')$$

$$+ \delta(t) \vec{\psi}_m^{+T\lambda}(r'), \quad m = 0, 1, \dots, N.$$

It should be noted from equations (C.7) and (C.8) that, for the particular neutron balance operator used in this presentation (i.e., neglecting delayed neutron time effects), the modified omega modes have the property of finality,<sup>115</sup> but the lambda modes do not (see Appendix B). Because of this, equation (C.7) is of a simpler form than equation (C.8). Equation (C.8) may be cast into the following form

$$a_m^\lambda(t) [1 - \bar{\beta} - \frac{1}{\lambda_m}] \vec{\psi}_m^{+T\lambda}(r') = \sum_{n=0}^N \dot{a}_n^\lambda(t) \Lambda_{mn} \vec{\psi}_n^{+T\lambda}(r') \quad (C.9)$$

$$+ \delta(t) \vec{\psi}_m^{+T\lambda}(r') / \langle \vec{\psi}_m^\lambda, \vec{M} \vec{\psi}_m^\lambda \rangle,$$

where  $\Lambda_{mn}$ , a quantity analogous to the familiar neutron generation time is defined as

$$\Lambda_{mn} \equiv \frac{\langle \vec{\psi}_m^\lambda, \vec{V}^{-1} \vec{\psi}_n^\lambda \rangle}{\langle \vec{\psi}_m^\lambda, \vec{M} \vec{\psi}_m^\lambda \rangle}. \quad (\text{C.10})$$

Upon some amount of reflection, it may be observed that, if the  $\omega_n \vec{V}^{-1}$  operator is small relative to the  $\vec{L}(r)$  operator in the moderator region and small relative to the  $\vec{M}(r) - \vec{L}(r)$  operator in the fuel region, then the lambda modes approximately have the finality property. Assuming that the above condition is satisfied, equation (C.9) becomes decoupled

$$a_m^\lambda(t) \left[ \frac{1 - \bar{\beta} - 1/\lambda_m}{\Lambda_{mn}} \right] - \dot{a}_m^\lambda(t) = \delta(t) / \langle \vec{\psi}_m^\lambda, \vec{V}^{-1} \vec{\psi}_m^\lambda \rangle, \quad (\text{C.11})$$

$$m = 0, 1, \dots, N.$$

Equations (C.7) and (C.11) have the same form and will consequently have similar solutions

$$a_m^\omega(t) = e^{\omega_m t} / \langle \vec{\psi}_m^\omega, \vec{V}^{-1} \vec{\psi}_m^\omega \rangle, \quad (\text{C.12})$$

$$a_m^\lambda(t) = e^{\left[ \frac{1 - \bar{\beta} - 1/\lambda_m}{\Lambda_{mn}} \right] t} / \langle \vec{\psi}_m^\lambda, \vec{V}^{-1} \vec{\psi}_m^\lambda \rangle. \quad (\text{C.13})$$

## APPENDIX D

## DERIVATION OF THE POINT REACTOR COVARIANCE

Assuming point detectors, equation (3.22) may be rewritten

$$\begin{aligned}
 \sigma^2(r_i, r_j, T) &= \frac{1}{T^2} \int_{\text{reactor}} dr' \int_0^T dt_2 \int_0^T dt_1 VW(t_1, t_2) & (D.1) \\
 &\times \sum_{\text{det-i}} (r_i) \frac{\int_{\text{reactor}} dr' \psi_0(r') \psi_0(r') \omega_0(t_1 - t_0)}{\int_{\text{reactor}} dr' \psi_0(r') \psi_0(r')} \psi_0(r_i) \psi_0(r') \\
 &\times \lambda_p \bar{v}_p^2 \sum_f^{(2)} (r') \bar{\phi}^{(2)}(r') \\
 &\times \sum_{\text{det-j}} (r_j) \frac{\int_{\text{reactor}} dr' \psi_0(r') \psi_0(r') \omega_0(t_2 - t_0)}{\int_{\text{reactor}} dr' \psi_0(r') \psi_0(r')} \psi_0(r_j) \psi_0(r')
 \end{aligned}$$

Define the detector efficiency as the ratio of detection rate to fission rate

$$\epsilon_i \equiv \frac{\int_{\text{reactor}} dr' \sum_f^{(2)} (r') \psi_0(r') \psi_0(r_i)}{\int_{\text{reactor}} dr' \psi_0(r') \psi_0(r_i)} = \frac{\int_{\text{reactor}} dr' \psi_0(r') \psi_0(r_i)}{\int_{\text{reactor}} dr' \psi_0(r') \psi_0(r_i)} \quad (D.2)$$

$$\epsilon_j \equiv \frac{\sum (r_j) \psi_0(r_j)}{\sum_f \overline{\sum_f^{(z)}} \int_{\text{reactor}} dr' \psi_0(r')} , \quad (\text{D.3})$$

where the average thermal neutron fission cross section is

$$\overline{\sum_f^{(z)}} \equiv \frac{\int_{\text{reactor}} dr \sum_f^{(z)} (r') \psi_0(r')}{\int_{\text{reactor}} dr' \psi_0(r')} . \quad (\text{D.4})$$

Next assume that the detector efficiencies are equal ( $\epsilon_1 = \epsilon_j = \epsilon$ ), then substituting the above definitions into equation (D.1) and performing the spatial integrations

$$\begin{aligned} \sigma^2(r_i, r_j, T) &= \frac{1}{T^2} \int_0^T dt_2 \int_0^T dt_1 VW(t_1, t_2) \\ &\times \chi_{\theta}^2 \nu_p^2 \left( \nu \overline{\sum_f^{(z)}} \right)^2 P \left( e^{\omega_0(t_1-t_0)} e^{\omega_0(t_2-t_0)} \right) , \end{aligned} \quad (\text{D.5})$$

where  $P$  is the reactor power level

$$P \equiv \int_{\text{reactor}} dr' \psi_0(r') \sum_f^{(z)} (r') \overline{\sum_f^{(z)}} (r') \psi_0(r') \left[ \frac{\int_{\text{reactor}} dr' \psi_0(r')}{\int_{\text{reactor}} dr' [\psi_0(r')]^2} \right]^2 . \quad (\text{D.6})$$

Computing the time integrations in equation (D.5)

$$\sigma^2(r_i, r_j, T) = \frac{\chi_a \bar{v}_p^2}{\omega_0} P \left[ \frac{\bar{\nu}_f^{(z)}}{\omega_0 T} \right]^2 \left( \omega_0 T + 1 - e^{-\omega_0 T} \right). \quad (D.7)$$

The fission rate probability  $\bar{\nu}_f^{(z)}$  may be expressed in another form<sup>34</sup>

$$\bar{\nu}_f^{(z)} = \frac{K_{eff}}{\bar{v}_p \ell}. \quad (D.8)$$

Substitution of equation (D.8) into (D.7) leads to the final form of the covariance

$$\sigma^2(r_i, r_j, T) = P \left( \frac{\epsilon K_{eff}}{\ell} \right)^2 \chi_a \frac{1}{\omega_0} \left[ \frac{\omega_0 T + 1 - e^{-\omega_0 T}}{(\omega_0 T)^2} \right]. \quad (D.9)$$

## APPENDIX E

EXACT SOLUTION OF THE GREEN'S FUNCTION  
IN ONE-DIMENSIONAL REACTOR GEOMETRY

The two-group, one-dimensional prompt Green's function is the solution to the matrix boundary value problem (see Appendix C)

$$[(1-\bar{\beta})\vec{M}(x) - \vec{L}(x)] \vec{g}(x, x', t) = \vec{v}^{-1} \frac{\partial}{\partial t} \vec{g}(x, x', t) + \delta(t) \vec{\delta}(x-x') \quad (\text{E.1})$$

$$t \geq 0 ,$$

$$\vec{g}(\text{boundaries}, x', t) = \vec{0} , \quad (\text{E.2})$$

$$\vec{g}(x, x', t) = \vec{0} , \quad t < 0 . \quad (\text{E.3})$$

The matrix terms in equations (E.1) - (E.3) are the one-dimensional analogies of those in equations (C.1) - (C.3).

Explicit forms of the above matrix operators for the model at hand are

$$\vec{M}(x) = \begin{bmatrix} 0 & \sum_f^{(2)} (x) \\ 0 & 0 \end{bmatrix} , \quad (\text{E.4})$$

$$\vec{L}(x) = \begin{bmatrix} -\frac{\partial}{\partial x} D^{(1)}(x) \frac{\partial}{\partial x} + D^{(1)}(x) B_T^2 + \sum^{(1,2)}(x) + \sum^{(1)}(x) \\ -\sum^{(1,2)}(x) \\ 0 \\ -\frac{\partial}{\partial x} D^{(2)}(x) \frac{\partial}{\partial x} + D^{(2)}(x) B_T^2 + \sum^{(2)}(x) \end{bmatrix}, \quad (E.5)$$

$$\vec{V}^{-1} = \begin{bmatrix} 1/v^{(1)} & 0 \\ 0 & 1/v^{(2)} \end{bmatrix}, \quad (E.6)$$

$$\vec{\delta}(x-x') = \begin{bmatrix} \delta(x-x') & 0 \\ 0 & 0 \end{bmatrix}, \quad (E.7)$$

$$\vec{g}(x, x', t) = \begin{bmatrix} g^{(1,1)}(x, x', t) & g^{(1,2)}(x, x', t) \\ g^{(2,1)}(x, x', t) & g^{(2,2)}(x, x', t) \end{bmatrix}. \quad (E.8)$$

It is assumed that only thermal neutrons cause fissions and that the fission produces one or more fast neutrons (i.e., no thermal neutrons produced). The latter condition dictates the form of equation (E.7).

Fourier transforming equations (E.1) - (E.3) results in two equations

$$[(1-\beta)\vec{M}(x) - \vec{L}(x) - \hat{i} \omega \vec{V}^{-1}] \vec{g}(x, x', \omega) = \vec{\delta}(x-x'), \quad (E.9)$$

$$\vec{g}(\text{boundaries}, x', \omega) = \vec{0}, \quad (E.10)$$

together with the usual continuity of flux and current at the region interfaces. The imaginary number  $\sqrt{-1}$  is designated as  $\hat{i}$ .

An alternate form of equations (E.9) and (E.10), not involving the Dirac delta, which is more amenable to numerical computation is<sup>139</sup>

$$[(1-\bar{\beta})\vec{M}(x) - \vec{L}(x) - \hat{i} \omega \vec{V}^{-1}] \vec{g}(x, x', \omega) = \vec{0}, \quad x \neq x', \quad (\text{E.11})$$

$$\lim_{\epsilon \rightarrow 0} [\vec{g}(x'+\epsilon, x', \omega) - \vec{g}(x'-\epsilon, x', \omega)] = \vec{0}, \quad (\text{E.12})$$

$$\lim_{\epsilon \rightarrow 0} \left[ \frac{\partial}{\partial x} \vec{g}(x'+\epsilon, x', \omega) - \frac{\partial}{\partial x} \vec{g}(x'-\epsilon, x', \omega) \right] = \begin{bmatrix} 1/D^{(1)}(x') & 0 \\ 0 & 0 \end{bmatrix}, \quad (\text{E.13})$$

$$\lim_{\epsilon \rightarrow 0} [\vec{g}(x_{\text{int}}+\epsilon, x', \omega) - \vec{g}(x_{\text{int}}-\epsilon, x', \omega)] = \vec{0}, \quad (\text{E.14})$$

$$\lim_{\epsilon \rightarrow 0} \left[ \vec{D}(x_{\text{int}}+\epsilon) \frac{\partial}{\partial x} \vec{g}(x_{\text{int}}+\epsilon, x', \omega) - \vec{D}(x_{\text{int}}-\epsilon) \frac{\partial}{\partial x} \vec{g}(x_{\text{int}}-\epsilon, x', \omega) \right] = \vec{0}, \quad (\text{E.15})$$

$$\vec{g}(\text{boundaries}, x', \omega) = \vec{0}, \quad (\text{E.16})$$

where  $\vec{D}$  is a diagonal matrix of group diffusion coefficients and  $x_{\text{int}}$  represents the interface locations. Equations (E.11) - (E.15) establish the conditions that the Green's response function flux and current are continuous everywhere except at the source location, where the current is discontinuous.

Because no thermal source has been assumed (see equation (E.7)), it is necessary to compute only the left-half of the Green's function matrix

(equation (E.8)). As a consequence of this fact only the Green's function vector

$$\vec{g}(x, x', \omega) = \begin{bmatrix} g^{(1,1)}(x, x', \omega) \\ g^{(2,1)}(x, x', \omega) \end{bmatrix}, \quad (\text{E.17})$$

need be computed. With this simplification, equations (E.11) - (E.16) become vector equations.

The method of solution follows along the lines presented by No-dean<sup>141</sup> which in turn is a modification of the critical determinate method for finding analytic solutions of the group fluxes.<sup>127</sup> It should be noted that, if equations (E.11) - (E.16) were cast into finite difference form, they would be identical to the complex fluxes used by Macdonald<sup>87</sup> in his space- and energy-dependent noise work.

The Green's function response vector has an analytical solution of the form,

$$\vec{g}(x, x', \omega) = \sum_{i=1}^4 e^{a_{ij}(\omega)x} \vec{A}_{ij}(x'), \quad j = 1, 2, \dots, N_R + 1, \quad (\text{E.18})$$

where  $N_R$  is the number of material regions.  $a_{ij}(\omega)$  is a known or calculated complex (real and imaginary) constant which is dependent on the frequency ( $\omega$ ) and the material properties of the region.  $\vec{A}_{ij}(x')$  is a complex coefficient vector which is dependent on the source location ( $x'$ ) and the material properties of the region. It is computed by a matrix inversion scheme described below.

The four  $a_{ij}(\omega)$  constants are the roots of the characteristic

equation which result when equation (E.18) is substituted into equation (E.11) for each region

$$\begin{aligned}
 D_j^{(1)} D_j^{(2)} [a_{ij}(\omega)]^4 - \left\{ \left[ D_j^{(2)} \left( D_j^{(1)} B_T^2 + \sum_j^{(1,2)} + \sum_j^{(1)} + \frac{\hat{i}\omega}{v^{(1)}} \right) \right] \right. \\
 \left. + D_j^{(1)} \left[ D_j^{(2)} B_T^2 + \sum_j^{(2)} + \frac{\hat{i}\omega}{v^{(2)}} \right] \right\} [a_{ij}(\omega)]^2 \\
 - (1-\bar{\beta}) \sum_{f_j}^{(2)} \sum_j^{(1,2)} = 0, \quad j = 1, 2, \dots, N_{R+1}.
 \end{aligned} \quad (E.19)$$

Parenthesis superscripts indicate the energy group and the subscripts indicate the region. Since equation (E.19) is fourth order, there are four independent values of  $a_{ij}(\omega)$  for each region ( $j$ ) and frequency ( $\omega$ ).

Because the diffusion equation is coupled in energy, the coefficient vector is partially redundant

$$\vec{A}_{ij}(x') = A_{ij}(x') \begin{bmatrix} K_{ij}(\omega) \\ 1 \end{bmatrix}, \quad (E.20)$$

where  $K_{ij}$  is a known energy coupling term.

Substitution of equation (E.18) into the boundary, source, and interface equations (E.12) - (E.16) results in a vector equation

$$\vec{Z}(\omega) \vec{A}(x') = \vec{\Delta}. \quad (E.21)$$

$\vec{Z}(\omega)$  is a  $4 \cdot N_{R+1}$  block diagonal square matrix containing all the calculated interface, source, and boundary conditions (i.e., with elements

like  $K_{ij}(\omega) e^{a_{ij}(\omega)x_{int}}$ .  $\vec{\Delta}$  is a  $4 \cdot N_{R+1}$  long column vector with one element equal  $1/D^{(1)}(x')$ , arising from the source condition, and the rest of the elements equal to zero. The coefficient vector  $\vec{A}(x')$  was calculated by Gauss forward elimination, back substitution scheme. Special care was taken to avoid round off error in this type of procedure. In order to minimize this error, row and column pivoting was performed at each forward elimination step. With this process finished, all the terms necessary to calculate the Green's function response vector from equation (E.18) were specified.

## APPENDIX F

## GENERATION OF THE EIGENVALUES AND EIGENVECTORS

The two different types of expansion modes used in the modal approximation of the coherence function are the modified omega and lambda eigenvectors (see Appendix B). The modified omega eigenvectors for a two-group, one-dimensional reactor model are solutions to the following eigenvalue equation with boundary and interface conditions

$$[(1-\bar{\beta})\bar{M}(x) - \bar{L}(x) - \omega_n \bar{V}^{-1}] \bar{\Psi}_n^\omega(x) = \bar{0}, \quad (\text{F.1})$$

$$\bar{\Psi}_n^\omega(\text{boundaries}) = \bar{0}, \quad (\text{F.2})$$

$$\lim_{\epsilon \rightarrow 0} [\bar{\Psi}_n^\omega(x_{\text{int}}+\epsilon) - \bar{\Psi}_n^\omega(x_{\text{int}}-\epsilon)] = \bar{0}, \quad (\text{F.3})$$

$$\lim_{\epsilon \rightarrow 0} \left[ \bar{D}(x_{\text{int}}+\epsilon) \frac{d}{dx} \bar{\Psi}_n^\omega(x_{\text{int}}+\epsilon) - \bar{D}(x_{\text{int}}-\epsilon) \frac{d}{dx} \bar{\Psi}_n^\omega(x_{\text{int}}-\epsilon) \right] = \bar{0}, \quad (\text{F.4})$$

$$n = 0, 1, 2, \dots,$$

where  $x_{\text{int}}$  represents the interface locations. The matrix operators for the model at hand are identical with those in Appendix E.

The lambda eigenvectors for the same reactor model are solutions to the following eigenvalue equation with boundary and interface conditions

$$\left[ \vec{L}(x) - \frac{1}{\lambda_n} \vec{M}(x) \right] \vec{\Psi}_n^\lambda(x) = \vec{0} , \quad (\text{F.5})$$

$$\vec{\Psi}_n^\lambda(\text{boundaries}) = \vec{0} , \quad (\text{F.6})$$

$$\lim_{\epsilon \rightarrow 0} \left[ \vec{\Psi}_n^\lambda(x_{\text{int}} + \epsilon) - \vec{\Psi}_n^\lambda(x_{\text{int}} - \epsilon) \right] = \vec{0} , \quad (\text{F.7})$$

$$\lim_{\epsilon \rightarrow 0} \left[ \vec{D}(x_{\text{int}} + \epsilon) \frac{d}{dx} \vec{\Psi}_n^\lambda(x_{\text{int}} + \epsilon) - \vec{D}(x_{\text{int}} - \epsilon) \frac{d}{dx} \vec{\Psi}_n^\lambda(x_{\text{int}} - \epsilon) \right] = \vec{0} , \quad (\text{F.8})$$

$$n = 0, 1, 2, \dots .$$

The marked similarity of equations (F.1) - (F.4) and (F.5) - (F.8) with equations (E.11) - (E.16) should be noted. Because of this similarity the method of solution follows along somewhat the same lines as that presented in Appendix E. Solution methodology is that of Betancourt.<sup>128</sup>

The eigenvectors have analytical solutions of the form

$$\vec{\Psi}_n^\omega(x) = \sum_{i=1}^4 e^{a_{ijn}^\omega x} \vec{A}_{ijn}^\omega , \quad (\text{F.9})$$

$$\vec{\Psi}_n^\lambda(x) = \sum_{i=1}^4 e^{a_{ijn}^\lambda x} \vec{A}_{ijn}^\lambda , \quad j = 1, 2, \dots, N_R , \quad (\text{F.10})$$

$$n = 0, 1, \dots ,$$

where  $N_R$  is the number of material regions and  $n$  is the modal expansion number (i.e.,  $n=0$  is the fundamental,  $n=1$  is the first harmonic, etc.).

$a_{ijn}^\omega$  and  $a_{ijn}^\lambda$  are known or calculated real or complex constants which are dependent on the eigenvalues and the material properties of the region.

$\vec{A}_{ijn}^{\omega}$  and  $\vec{A}_{ijn}^{\lambda}$  are unknown coefficient vectors which depend on the eigenvalues and material properties of the region also and are evaluated by a matrix inversion scheme.

The four  $a_{ijn}^{\omega}$  and  $a_{ijn}^{\lambda}$  constants are roots of the characteristic equations which result when equations (F.9) and (F.10) are substituted into (F.1) and (F.5), respectively, for each region.

$$D_j^{(1)} D_j^{(2)} (a_{ijn}^{\omega})^4 - \left[ D_j^{(2)} \left( D_j^{(1)} B_T^2 + \sum_j^{(1,2)} + \sum_j^{(1)} + \frac{\omega_n}{v^{(1)}} \right) \right. \\ \left. + D_j^{(1)} \left( D_j^{(2)} B_T^2 + \sum_j^{(2)} + \frac{\omega_n}{v^{(2)}} \right) \right] (a_{ijn}^{\omega})^2 - (1-\beta) \sum_{fj}^{(2)} \sum_j^{(1,2)} = 0, \quad (F.11)$$

$$D_j^{(1)} D_j^{(2)} (a_{ijn}^{\lambda})^4 - \left[ D_j^{(2)} \left( D_j^{(1)} B_T^2 + \sum_j^{(1,2)} + \sum_j^{(1)} \right) \right. \\ \left. + D_j^{(1)} \left( D_j^{(2)} B_T^2 + \sum_j^{(2)} \right) \right] (a_{ijn}^{\lambda})^2 - \frac{\sum_{fj}^{(2)} \sum_j^{(1,2)}}{\lambda_n} = 0, \quad (F.12)$$

$$j = 1, 2, 3, \dots, N_R,$$

$$n = 0, 1, \dots$$

Superscripts in parentheses indicate the average group and subscripts indicate the region. Since equations (F.11) and (F.12) are fourth order, there are four independent values of  $a_{ijn}^{\omega}$  and  $a_{ijn}^{\lambda}$  for each region (j) and each eigenvalue ( $\omega_n$  or  $\lambda_n$ ).

Because the diffusion equation is coupled in energy, the coefficient

vectors are partially redundant

$$\vec{A}_{ijn}^{\omega} = A_{ijn}^{\omega} \begin{bmatrix} K_{ijn}^{\omega} \\ 1 \end{bmatrix}, \quad (\text{F.13})$$

$$\vec{A}_{ijn}^{\lambda} = A_{ijn}^{\lambda} \begin{bmatrix} K_{ijn}^{\lambda} \\ 1 \end{bmatrix}, \quad (\text{F.14})$$

where the constants  $K_{ijn}^{\omega}$  and  $K_{ijn}^{\lambda}$  are known coupling terms.

Substitution of equations (F.9) and (F.10) into the boundary and interface equations (F.2) - (F.4) and (F.6) - (F.8), respectively, results in the following vector equations

$$\vec{Z}_n^{\omega} \vec{A}_n^{\omega} = \vec{0}, \quad (\text{F.15})$$

$$\vec{Z}_n^{\lambda} \vec{A}_n^{\lambda} = \vec{0}, \quad n = 0, 1, \dots \quad (\text{F.16})$$

$\vec{Z}_n^{\omega}$  and  $\vec{Z}_n^{\lambda}$  are  $4 \cdot N_R$  block diagonal square matrices containing all the calculated interface and boundary conditions (i.e., with elements like

$K_{ijn}^{\omega} e^{a_{ijn}^{\omega} x_{int}}$ ).  $\vec{A}_n^{\omega}$  and  $\vec{A}_n^{\lambda}$  are  $4 \cdot N_R$  long column vectors of coefficient elements  $A_{ijn}^{\omega}$  and  $A_{ijn}^{\lambda}$ . Since equations (F.15) and (F.16) are homogeneous, the only non-trivial solutions for  $\vec{A}_n^{\omega}$  and  $\vec{A}_n^{\lambda}$  result when the determinants of  $\vec{Z}_n^{\omega}$  and  $\vec{Z}_n^{\lambda}$  are zero

$$|\vec{Z}_n^{\omega}| = 0, \quad (\text{F.17})$$

$$|\vec{Z}_n^{\lambda}| = 0, \quad n = 0, 1, \dots \quad (\text{F.18})$$

In the standard example given in Lamarsh,<sup>127</sup>  $K_{\text{eff}} = \lambda_0$  is set equal to unity and the reactor width is varied until the critical determinant is found (i.e., when equation (F.18) is satisfied for  $n = 0$ ). By proceeding in this manner the critical dimensions of the reactor are found. The approach in this work was different. Here, reactor dimensions and material were known, and it was desired to find the eigenvalues which produce the critical determinates of equations (F.17) and (F.18). The real eigenvalue spectra ( $\omega_0, \omega_1, \dots; \lambda_0, \lambda_1, \dots$ ) were calculated by varying  $\omega_n$  and  $\lambda_n$  from their initial values for each  $n$  until equations (F.17) and (F.18), respectively, were satisfied (e.g., the Regula False method<sup>142</sup>). Upon calculation of each eigenvalue, a Gauss forward elimination and back substitution process was carried out on equations (F.15) and (F.16) to find the coefficient vectors. Special care was taken to avoid round off error in this type of procedure. In order to minimize this error, row and column pivoting was performed at each forward elimination step, using Univac-1108 double precision. With this process completed, all the terms necessary to calculate the modified omega eigenvector (equation (F.9)) and the lambda eigenvector (equation (F.10)) were specified.

## APPENDIX G

## FAST FOURIER TRANSFORM\*

The Fast Fourier Transform (FFT) is a general name given to three different, yet conceptually identical computation schemes.<sup>143,144</sup> Any one of them may be employed to quickly calculate the complex discrete Fourier transform (DFT) or its inverse (IDFT). The choice of algorithm is dependent on several factors. However, from the standpoints of programming ease, efficiency, and space required for calculations, the Sande<sup>144</sup> version is probably the best selection.

Application of the FFT to the computation of spectral densities, covariances, and related quantities has been widely discussed.<sup>145-147</sup> Nevertheless, the method seems to have found only limited use among nuclear investigators.<sup>122-124,148</sup> This may be attributed to the fact that articles on the subject are often generalized to the point of being ambiguous to an initiate of the subject.

Discrete Time and Frequency Relationships

The N-point discrete Fourier transform (DFT) is defined by

$$\alpha_K = \frac{1}{N} \sum_{j=0}^{N-1} x_j W^{-jK}, \quad K = 0, 1, \dots, N-1, \quad (G.1)$$

where  $x_j$  is a sample of the process "x" at time  $t \approx j\Delta t$ ,  $\Delta t$  is a constant

---

\* A summary of a talk given by J. M. Reynolds.<sup>121</sup>

sampling interval,  $W = e^{-i \frac{2\pi}{N}}$ ,  $i = \sqrt{-1}$ , and  $\alpha_K$  is the  $K^{\text{th}}$  Fourier coefficient at frequency  $f = K/N\Delta t$ .

Denoting complex conjugation by "\*", one can easily show that, if the  $x_j$ 's are real, then

$$\alpha_K = \alpha_{N-K}^* , \quad K = 1, 2, \dots, N/2-1 . \quad (\text{G.2})$$

This is an indirect manifestation of Nyquist's theorem which states that information at frequencies higher than  $f = (N/2)/N\Delta t = 1/2\Delta t$  can never be resolved from regularly sampled data. If higher frequencies are present in the original data, these are folded or aliased back into the interval  $[0 \leq f < 1/2\Delta t]$ . The effects of aliasing can never be extracted after sampling by digital filtration. Aliasing can only be removed by faster sampling rates or, where applicable, analog filtration of high frequencies before sampling (digitizations).

The Fourier coefficients of equation (G.1) do not realize the fullest amount of information available from the  $N$  data points,  $x_j$ . If one forms a new  $2N$ -point record,  $x_j^{(a)}$ , which has  $N$  zeros appended to the original data, the following  $2N$ -point DFT may be taken

$$A_K^{(a)} = \frac{1}{2N} \sum_{j=0}^{2N-1} x_j^{(a)} W^{-\frac{jK}{2}} , \quad K = 0, 1, \dots, 2N-1 . \quad (\text{G.3})$$

Once again, if the  $x_j$ 's are real, one has

$$A_K^{(a)} = A_{2N-K}^{(a)*} , \quad K = 1, 2, \dots, N-1 . \quad (\text{G.4})$$

As before, the new Fourier coefficients,  $A_K^{(a)}$ , contain unique information over the interval  $[0 \leq f < 1/2\Delta t]$ . However, they occur at frequencies  $f = K/2N\Delta t$  which is half the frequency spacing of the  $\alpha_K$ 's.

Singleton<sup>147</sup> has shown that two real N-point records  $x_j$  and  $y_j$  (possibly sampled "input and output" processes) can be transformed with a single 2N-point DFT. A new complex data record  $z_j^{(a)}$  is formed which has  $x_j^{(a)}$  as its real part and  $y_j^{(a)}$  as the complex part. The result of the DFT is a set of Fourier coefficients  $C_K^{(a)}$  from which one may easily separate the  $A_K^{(a)}$  and  $B_K^{(a)}$  (the Fourier coefficients for  $y_j^{(a)}$ ) by utilizing a symmetry of the type found in equations (G.2) or (G.4). The same principle can be used to obtain the  $A_K^{(a)}$  from an N-point DFT if the even points of  $x_j^{(a)}$  are in the real part of the data vector and the odd points are in the imaginary part. Simple separation and synthesis formulas are used after the DFT to reconstruct the  $A_K^{(a)}$ .

The zero-appended cross-periodogram is defined by

$$CP_K^{(a)} = A_K^{(a)*} B_K^{(a)}, \quad K = 0, 1, \dots, 2N-1, \quad (G.5)$$

If the x and y records had zero average, the forward reduced-bias cross-covariance estimate is

$$CC_\ell^{(f)} = \frac{1}{N-\ell} \sum_{j=0}^{N-1-\ell} x_j y_{j+\ell}, \quad \ell = 0, 1, \dots, N-1. \quad (G.6)$$

and the reduced-bias reverse cross-covariance estimate is

$$CC_{\ell}^{(r)} = \frac{1}{N-\ell} \sum_{j=0}^{N-1-\ell} x_{j+\ell} y_j, \quad \ell = 0, 1, \dots, N-1. \quad (G.7)$$

Defining

$$cc_{\ell} = \sum_{K=0}^{2N-1} CP_K^{(a)} W^{\frac{j\ell}{2}}, \quad \ell = 0, 1, \dots, 2N-1, \quad (G.8)$$

it can then be shown<sup>145</sup> that

$$CC_{\ell}^{(f)} = \frac{2N}{N-\ell} cc_{\ell}, \quad CC_{\ell}^{(r)} = \frac{2N}{N-\ell} cc_{2N-\ell}, \quad \ell = 1, 2, \dots, N-1, \quad (G.9)$$

$$CC_0^{(f)} = CC_0^{(r)} = 2cc_0, \quad cc_N = 0.$$

Equation (G.8) is the inverse DFT (IDFT) of the zero-appended cross-periodogram. Equations (G.6) - (G.9) then relate that the zero-appended cross-periodogram, and an arrangement of the forward and reverse reduced-bias cross-covariances forms a DFT-pair relationship. This "arrangement" shows<sup>149</sup> that the zero-appended cross-periodogram is actually the raw cross-power-spectral-density (CPSD) estimate as tempered by a Bartlett spectral window.<sup>1</sup>

For analysis of noise-like data, it is useful to smooth consecutive raw CPSD estimates so that averages over bands of frequencies can be formed. Statistical accuracy, and one's ability to observe qualitative effects are thereby enhanced. The smoothed estimate is defined by

$$CP_{1,g,h}^{(a)} = \frac{1}{g} \sum_{K=hg}^{(h+1)g-1} CP_K^{(a)}, \quad h = 0, 1, \dots, N/g-1. \quad (G.10)$$

The first subscript of  $CP_{f,g,h}^{(a)}$  is the window type (1 for Bartlett), the second is the number of raw estimates in the smoothed band, and the last is the frequency index of the smoothed band.

Windows other than the Bartlett can be achieved by forming certain linear combinations of Fourier coefficients before the multiplication in quadrature. This produces another type of raw CPSD estimate which is sometimes called a zero-appended, modified cross-periodogram.<sup>145</sup> The more sophisticated windows are sharper than the Bartlett. That is, they contain less leakage energy from adjacent bands. However, when smoothing is conducted, sharper windows give preferential weighting to certain frequencies. The Bartlett suffers less from this problem. Also, the fraction of leakage energy to smoothed band energy becomes competitive with sharper windows when the number of raw estimates in a band is large. For the above reason and also for the sake of computational economy, it was decided to keep the Bartlett window.

When a small assembly (not ensemble) of data records from some stochastic process or processes is available, common sense dictates that it is desirable to use as much data as possible to enhance statistical accuracy. For an assembly of  $M$  pairs of  $N$ -point real data records, the assembly-averaged<sup>121</sup> zero-appended cross-periodogram is

$$\overline{CP}_K^{(a)} = \frac{1}{M} \sum_{g=1}^M CP_{g,K}^{(a)}, \quad K = 0, 1, \dots, N-1, \quad (G.11)$$

where  $CP_{g,K}^{(a)}$  is  $CP_K^{(a)}$  for the  $g^{\text{th}}$  pair of data records. Welch<sup>146</sup> has shown equation (G.11) to be a viable CPSD estimator.

The assembly-averaged forward cross-covariance is defined by Reynolds<sup>121</sup> as

$$\overline{CC}_\ell^{(f)} = \frac{1}{M} \sum_{g=1}^M CC_{g,\ell}^{(f)}, \quad \ell = 0, 1, \dots, N-1, \quad (G.12)$$

where  $CC_{g,\ell}^{(f)}$  is  $CC_\ell^{(f)}$  for the  $g^{\text{th}}$  pair of data records. A similar equation also holds for  $CC_\ell^{(r)}$ .

Since the IDFT (or DFT) is independent of  $g$  summation indices, it is easily shown through equation (G.8) that

$$\overline{cc}_\ell = \sum_{K=0}^{2N-1} \overline{CP}_K^{(a)} W^{\frac{j\ell K}{2}}, \quad \ell = 0, 1, \dots, 2N-1. \quad (G.13)$$

Equation (G.9) can be used to obtain both  $\overline{CC}_\ell^{(f)}$  and  $\overline{CC}_\ell^{(r)}$  from equation (G.13). Since  $\overline{CP}_K^{(a)}$  may be shown to be a good estimator, it is hypothesized that assemblage-averaged covariances are of similar quality, due to the transform-pair relationship of equation (G.13).

Zero-appended auto-periodograms are easily obtained by simply squaring Fourier coefficients from single data records in quadrature. IDFT's may be applied to these to produce auto-covariance estimates. Assembly-averaging and smoothing can be handled in exactly the same manner as is used for twin record analyses.

After assembly averaging of the raw zero-appended auto- and cross-periodograms, smoothing may be conducted to give auto-power-spectral-density (APSD) and CPSD estimates. The results are employed in the calculation of effective assembly-averaged coherence and transfer function gain and phase estimates. The usual formulas<sup>151</sup> are applied here.

The assembly-averaged zero-appended auto- and cross-periodograms can finally be used for computation of assembly-averaged auto- and cross-covariance estimates by application of two IDFT's. One IDFT is needed for the assembly-averaged cross-covariance result, the other for the two sets of assembly-averaged auto-covariance estimates. This latter fact is true because, by definition, zero-appended auto-periodograms and assembly-averaged auto-covariance estimates are both real. Therefore, one zero-appended auto-periodogram is inserted into the real portion of a complex data array, and the other is put in the imaginary part. A single IDFT is applied. The real result is the set of assembly-averaged auto-covariance estimates from one record while the imaginary result is the set of assembly-averaged auto-covariances from the other record.

The best feature of all of this analysis is that it is the potential for great computational speed. Only  $M$  DFT's and two IDFT's are needed to compute so many time and frequency domain statistical estimators from the assembly of  $M$  pairs of data records.

#### Digital Computations and the FFT

There is little here to state concerning general analysis that has not already been mentioned. Figure 63 is a flowchart encapsulation of the facts which have just been presented. However, one point has not been treated. This is that the average extraction of the first flowchart block is very important from two standpoints. The first is that the step must be taken because of the very definition<sup>1</sup> of auto- or cross-covariances. The second reason is that a very strong zero frequency component would cause near-zero frequency distortion due to inescapable spectral window

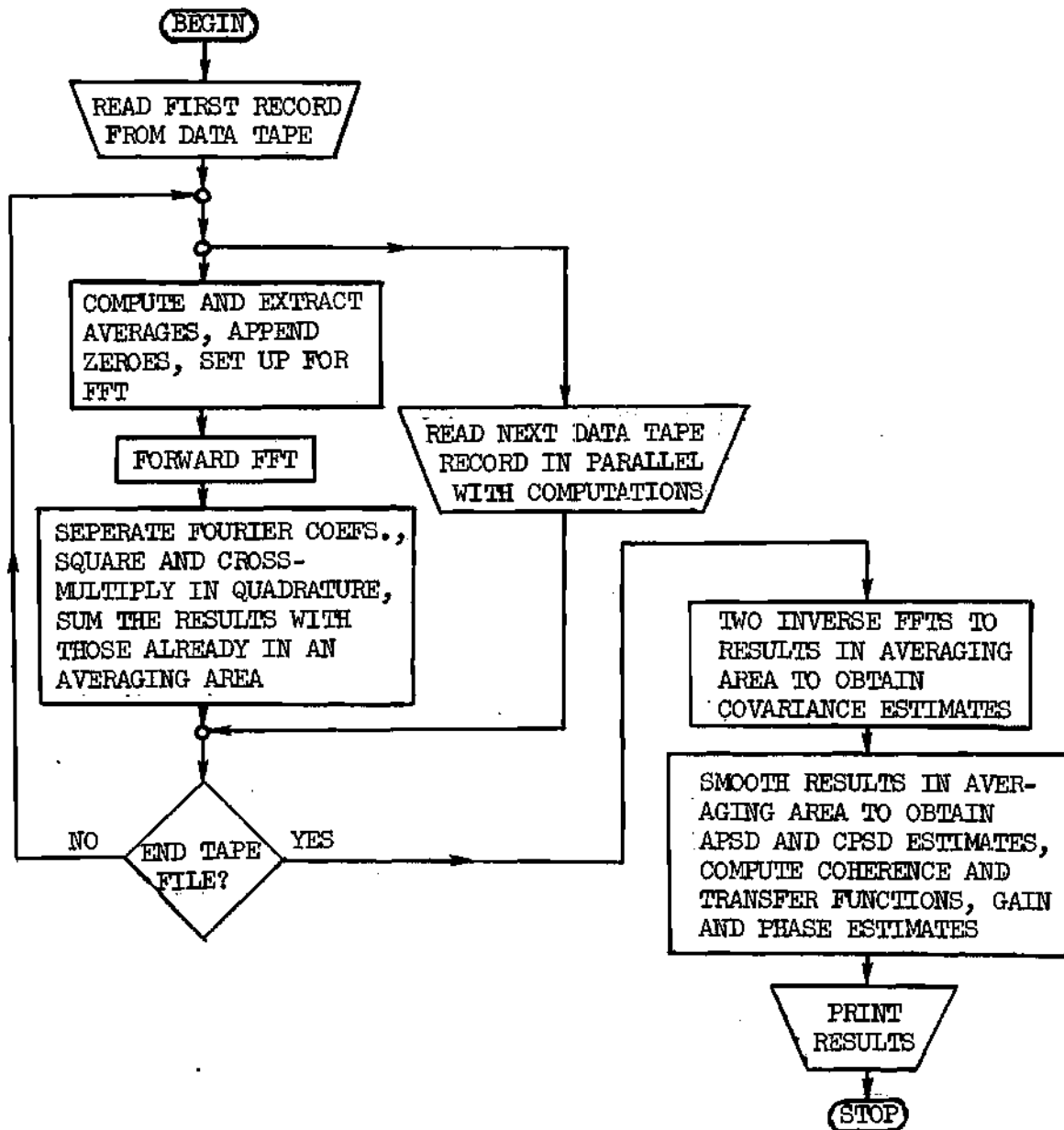


Figure 63. Fast Fourier Transform Flowchart of the KAPL Data

leakage. The stripping of averages performs like a high-pass filter with infinitely sharp DC cut-off.

The Cooley-Tukey<sup>143</sup> and Sande<sup>144</sup> radix-two FFT's both require an operation which places the data in reverse binary order. This occurs after transformation for the latter and before transformation for the former algorithm.

$$16C_4 + 8C_3 + 4C_2 + 2C_1 + C_0 \rightarrow 16C_0 + 8C_1 + 4C_2 + 2C_3 + C_4 \quad (\text{G.14})$$

Natural Binary Order

Reverse Binary Order

$$C_j = 0, 1, \dots, 4 \quad , \quad j = 0, 1, \dots, 4 \quad .$$

Equation (G.14) demonstrates the connotation of reverse binary order. It simply means that the coefficient positions for any index are reversed from their natural positions. For example, consider reverse constructs for the numbers between zero and thirty-one. Equation (G.14) shows that the reverse construct of zero is zero, the reverse construct of twenty-four is three, etc.

Conventionally, one forms reverse constructs by successively right shifting bits ( $C_j$ ) out of the natural index, multiplying these by increasing powers of two, and summing the results. The reverse construct is tested to find if it is less than or equal to the natural index to prevent redundant data swapping. If  $N = 2^P$ ,  $P$  multiply-divide-add-modulus operations are required per operation. This takes about 4.2 seconds of Univac-1108 time for  $N = 2^{14} = 16384$  points. This is just about equal to the time required by the FFT. A better approach is construct a table of  $2^{P/2}$  reverse constructs when  $P$  is even or  $2^{(P+1)/2}$

reverse constructs for  $P$  odd. For the even case, one looks up the reverse constructs for the right and left halves of the overall natural construct and interchanges the position of these values. This produces the overall reverse construct which, of course, is tested to prevent redundant data swapping. For the odd power case, consider that the right half of the overall natural construct is larger (contains  $(P+1)/2$  bits). The right half reverse construct is found directly from the table and multiplied by  $2^{(P-1)/2}$ . The left (smaller) half natural construct is multiplied by two so that its reverse construct can be found in the table. This reverse construct is found and added to the previous reverse construct product. The overall reverse construct then results and is tested to prevent redundant data swapping. Only one set of multiply-divide-add-modulus operations is now required per reverse construct.

Another economy can be gained by noting that all even values in the last  $N/2$  natural constructs have reverse constructs which would produce redundant data swaps. Observation of this and use of table-driven reverse construct generation speeds up data re-ordering by nearly a factor of ten for large powers of two. For example, re-ordering of 16384 data values on the Univac-1108 by this method requires only about 0.5 second.

It should be noted that table-driven data re-ordering, "brute-force" re-ordering, or any of the FFT algorithms can be programmed efficiently in a source language such as FORTRAN IV. However, it may be advisable to use an assembler in the event that the particular compiler is not well optimized.

## APPENDIX H

## PHASE ANGLE INVESTIGATION

The method of investigation presented in this appendix represents an extension and modification of the work of Ackermann et al.<sup>19</sup> The purpose of this appendix is to indicate why the Ackermann method (for inferring the thermal neutron lifetime from measurement of the fast-thermal phase angle) holds for point reactor models, but breaks down when space dependence is included.<sup>111</sup>

Using the same terminology as in Appendix E, equation (E.9) may be written

$$-\left[ \frac{\hat{i}\omega}{\bar{v}(1)} + L^{(1,1)}(x) \right] g^{(1,1)}(x, x', \omega) + (1-\bar{\beta}) \sum_f^{(2)}(x) g^{(2,1)}(x, x', \omega) \quad (\text{H.1})$$

$$= \delta(x-x') ,$$

and

$$\sum^{(1,2)}(x) g^{(1,1)}(x, x', \omega) - \left[ \frac{\hat{i}\omega}{\bar{v}(2)} + L^{(2,2)}(x) \right] g^{(2,1)}(x, x', \omega) \quad (\text{H.2})$$

$$= 0 ,$$

with the appropriate boundary conditions. Making use of the modal expansion approximation of the Green's function (see Appendix C), the fast and thermal complex, frequency dependent, local leakages may be defined

$$Lk^{(1)}(x, x', \omega) = \left[ -\frac{\partial}{\partial x} D^{(1)}(x) \frac{\partial}{\partial x} + D^{(1)}(x) B_T^{\otimes} \right] g^{(1,1)}(x, x', \omega) \quad (H.3)$$

$$= \sum_{n=0}^N \frac{\psi_n^{(1)+}(x')}{(\omega_n - i\omega) \langle \vec{\psi}_n, \vec{V}^{-1} \vec{\psi}_n \rangle} \left[ -\frac{d}{dx} D^{(1)}(x) \frac{d}{dx} \psi_n^{(1)}(x) + D^{(1)}(x) B_T^{\otimes} \psi_n^{(1)}(x) \right], \quad N = 0, 1, 2, \dots,$$

$$Lk^{(2)}(x, x', \omega) = \left[ -\frac{\partial}{\partial x} D^{(2)}(x) \frac{\partial}{\partial x} + D^{(2)}(x) B_T^{\otimes} \right] g^{(2,1)}(x, x', \omega) \quad (H.4)$$

$$= \sum_{n=0}^N \frac{\psi_n^{(2)+}(x')}{(\omega_n - i\omega) \langle \vec{\psi}_n, \vec{V}^{-1} \vec{\psi}_n \rangle} \left[ -\frac{d}{dx} D^{(2)}(x) \frac{d}{dx} \psi_n^{(2)}(x) + D^{(2)}(x) B_T^{\otimes} \psi_n^{(2)}(x) \right], \quad N = 0, 1, 2, \dots$$

Both the fast and thermal local leakages may be computed when the appropriate eigenfunctions are known. The leakages are complicated functions of the (fast) stochastic source distribution, local effects, and in general, are complex (real and imaginary parts). However, for frequencies  $\omega < \omega_0$  (low frequency region), the leakage functions will almost be completely real. This fact becomes very important later in this appendix.

Using the leakage functions in equations (H.1) and (H.2)

$$-\left[\frac{\hat{i}\omega}{v^{(1)}} + \sum^{(1,2)}(x) + \sum^{(1)}(x)\right]g^{(1,1)}(x,x',\omega) - Lk^{(1)}(x,x',\omega) \quad (H.5)$$

$$+ (1-\bar{\beta}) v \sum_f^{(2)}(x) g^{(2,1)}(x,x',\omega) = \delta(x-x'),$$

and

$$\sum^{(1,2)}(x) g^{(1,1)}(x,x',\omega) - \left[\frac{\hat{i}\omega}{v^{(2)}} + \sum^{(2)}(x)\right]g^{(2,1)}(x,x',\omega) \quad (H.6)$$

$$- Lk^{(2)}(x,x',\omega) = 0.$$

Assuming that  $\omega/v^{(1)}$  is small relative to the other terms and solving for the Green's functions in equations (H.5) and (H.6)

$$g^{(1,1)}(x,x',\omega) = \left\{ \delta(x-x') \left[ \sum^{(2)}(x) + \frac{\hat{i}\omega}{v^{(2)}} \right] \right. \quad (H.7)$$

$$+ (1-\bar{\beta}) v \sum_f^{(2)}(x) Lk^{(2)}(x,x',\omega) + \left. \left[ \sum^{(2)}(x) + \frac{\hat{i}\omega}{v^{(2)}} \right] Lk^{(1)}(x,x',\omega) \right\} /$$

$$\left\{ \left[ \sum^{(1,2)}(x) + \sum^{(1)}(x) \right] \left[ \frac{\hat{i}\omega}{v^{(2)}} + \sum^{(2)}(x) \right] \right.$$

$$\left. + \sum^{(1,2)}(x) (1-\bar{\beta}) v \sum_f^{(2)}(x) \right\},$$

and

$$g^{(2,1)}(x,x',\omega) = \left\{ \delta(x-x') \sum^{(1,2)}(x) + \sum^{(1,2)}(x) Lk^{(1)}(x,x',\omega) \right. \quad (H.8)$$

$$+ Lk^{(2)}(x,x',\omega) \left. \left[ \sum^{(1,2)}(x) + \sum^{(1)}(x) \right] \right\} / \left[ \sum^{(1,2)}(x) + \sum^{(1)}(x) \right]$$

(continued)

$$\times \left[ \frac{\hat{i}\omega}{v^{(2)}} + \sum^{(2)}(x) \right] + \sum^{(1,2)}(x) (1-\bar{\beta}) v \sum_f^{(2)}(x) \} .$$

Using the definition of the CPSD

$$\hat{\Phi}^{(k,l)}(x_i, x_j, \omega) = \int_{\text{reactor}} dx' g^{(k,1)}(x_i, x', \omega) \sum_f^{(2)}(x') \hat{\Phi}^{(2)}(x') \quad (\text{H.9})$$

$$\times g^{(l,1)}(x_j, x', \omega) ,$$

and equations (H.7) and (H.8)

$$\hat{\Phi}^{(1,2)}(x_i, x_i, \omega) = \frac{\left[ \sum^{(2)}(x_i) - \frac{\hat{i}\omega}{v^{(2)}} \right] A_\omega(x_i) + B_\omega(x_i)}{\text{DEN}_\omega^{(1,2)}(x_i, x_i)} , \quad (\text{H.10})$$

and

$$\hat{\Phi}^{(2,2)}(x_i, x_j, \omega) = \frac{\delta(x_i, x_j) C(x_i) + D_\omega(x_i) + E_\omega(x_j) + F_\omega(x_i, x_j)}{\text{DEN}_\omega^{(2,2)}(x_i, x_j)} \quad (\text{H.11})$$

$\delta(x_i, x_j)$  is the Kronecker Delta, and  $C(x_i)$  is a real function which is dependent on the thermal flux at  $x_i$ . The functions  $A_\omega(x_i)$ ,  $B_\omega(x_i)$ ,  $D_\omega(x_i)$ ,  $E_\omega(x_j)$ , and  $F_\omega(x_i, x_j)$  are complicated functions of the local leakage and source distribution. They are complex in general, but the imaginary component is much smaller than the real portion for frequencies,  $\omega < \omega_0$ .

$\text{DEN}_\omega^{(1,2)}(x_i, x_i)$  is always real and a weak function of frequency (for

$\omega < \sum^{(2)}(x_i) v^{(2)}$ ), but not a function of the local leakage.

$\text{DEN}_\omega^{(2,2)}(x_i, x_j)$  is also not a function of the local leakage. It should

also be mentioned that, for contiguous or symmetric detector locations, the numerator in equation (H.11) is pure real (at all frequencies) and, therefore, the CPSD will exhibit zero phase at all frequencies.

For the point reactor model which Ackermann<sup>19</sup> assumed (in which case local leakages are zero)  $A_\omega(x_i)$  and  $B_\omega(x_i)$  are pure real functions. In this case, Ackermann showed

$$-\tan [\text{phase of } \hat{\Phi}^{(1,2)}(x_i, x_i, \omega)] = \omega \ell, \quad (\text{H.12})$$

which is easily obtained from equation (H.10) for  $\ell^{-1} = v \sum_{(x_i)}^{(a)}$ , which is the thermal neutron lifetime.

## BIBLIOGRAPHY

1. R. B. Blackman and J. W. Tukey, The Measurement of Power Spectra, Dover Publications, Inc , New York, N. Y., 1958.
2. S. Chandrasekhar, "Stochastic Problems in Physics and Astronomy," Review of Modern Physics, 15, 1, 20 (1943).
3. N. Wiener, Cybernetics, MIT Press, Cambridge, Mass., 1948.
4. W. Marks and W. J. Pierson, "The Power Spectrum Analysis of Ocean-Wave Records," Transactions of the American Geographical Union, 33, 834 (1952).
5. G. P. Wadsworth, et al., "Detection of Reflections on Seismic Records by Linear Operators," Geological Physics, 18, 539 (1953).
6. D. R. Harris, "Neutron Fluctuations in a Reactor of Finite Size," Nuclear Science and Engineering, 21, 369 (1965).
7. E. Fermi, R. P. Feynmann, and F. deHoffmann, "Theory of the Criticality of the Water Boiler and the Determination of the Number of Delayed Neutrons," USAEC Report MDCC-383 (LADC-269), (Dec. 1944).
8. R. P. Feynmann, F. deHoffmann, and R. Serber, "Dispersion of the Neutron Emission in U-235 Fission," Journal of Nuclear Energy, 3, 64 (1956).
9. F. deHoffmann, "Intensity Fluctuations of a Neutron Chain Reactor," USAEC Report MDCC-382 (LADC-256), (Oct. 1946).
10. F. deHoffmann, "Statistical Aspects of Pile Theory," The Science and Engineering of Nuclear Power, C. Goodman, Ed., Vol. II, 116, Addison Wesley Co., Reading, Mass., 1949.
11. B. C. Diven, H. C. Martin, R. F. Taschek, and J. Terrell, "Multiplicities of Fission Neutrons," Physical Review, 101, 1012 (1956).
12. J. D. Orndoff, "Prompt Neutron Periods of Metal Critical Assemblies," Nucl. Sci. Eng., 2, 450 (1957).
13. R. Schröder, "Bestimmung der Reaktorleistung mit Hilfe des Reaktorrauschens," Nukleonik, 4, 227 (1962).

14. Preprints of the Japan - United States Seminar on Nuclear Reactor Noise Analysis, Tokyo, Japan, 1968.
15. E. S. Kenney, "Noise Analysis of Nuclear Reactors with the Use of Gamma Radiation," in Neutron Noise, Waves, and Pulse Propagation, CONF-660206, 399 (1967).
16. W. K. Lehto and J. M. Carpenter, "Determination of Reactor Kinetic Parameters by Photon Observation," Nucl. Sci. Eng., 33, 225 (1968).
17. F. E. LeVert and M. A. Schultz, "Local Power Measurements Using Gamma-Ray Noise," Transactions of the American Nuclear Society, 14, 862 (1971).
18. J. A. Johnson, "Measurement of Pressure-to-Pressure Transfer Functions Through the Phoebus-1A Nuclear Reactor," in Neutron Noise, Waves, and Pulse Propagation, CONF-660206, 271 (1967).
19. N. J. Ackermann, Jr., J. M. Nieto, and P. Akhtar, "Two-Group Reactor Noise Analysis by Langevin's Technique," J. Nucl. Eng., 22, 675 (1968).
20. R. A. Rydin, J. A. Burke, W. E. Moore, and K. W. Seemann, "Noise and Transient Kinetics Experiments and Calculations for Loosely Coupled Cores," Nucl. Sci. Eng., 46, 179 (1971). Also J. A. Burke, W. E. Moore, R. A. Rydin, and K. W. Seemann, "Time Domain Noise Measurements in Loosely Coupled Cores," Dynamics of Nuclear Systems, Univ. of Arizona Press, Tucson, (Mar. 1970).
21. H. Borgwaldt, T. E. Murely, and D. Sanitz, "The Modal Synthesis of Rossi-Alpha Data for Moderator-Reflected Fast Assemblies," in Neutron Noise, Waves, and Pulse Propagation, CONF-660206, 747 (1967).
22. R. A. Hendrickson and G. Murphy, "Cross-Spectral Density Measurements in a Coupled-Core Reactor," Nucl. Sci. Eng., 31, 215 (1968).
23. R. A. Danofsky, "A Space-Dependent Reactor-Noise Formulation Utilizing Modal Expansions," Nucl. Sci. Eng., 36, 28 (1969).
24. R. W. Albrecht and R. A. Danofsky, "Analytical-Experimental Correlations in Space-Dependent Coherences," Trans. Am. Nucl. Soc., 12, 708 (1969).
25. J. M. Betancourt and R. A. Danofsky, "A Space-Dependent Reactor-Noise Formulation Based on the Natural Mode Approximation," Nucl. Sci. Eng., 38, 77 (1969).
26. M. Nagy and R. A. Danofsky, "Cross-Spectral-Density Sink Frequency Behavior for Coupled-Core Argonaut Reactors," Nucl. Sci. Eng., 42, 419 (1970).

27. R. W. Albrecht and W. Seifritz, "Fundamental Properties of the Coherence Function in Symmetrical Two-Node Systems," Nukleonik, 11, 143 (1968).
28. W. Seifritz and R. W. Albrecht, "Measurement and Analysis of the Coupled Core Coherence Function in a Two Node Symmetrical Reactor," Nukleonik, 11, 149 (1968).
29. R. A. Rydin, J. A. Burke, W. E. Moore, and K. W. Seemann, "Space-Time Kinetics Experiments and Calculations for a Loosely Coupled Core," Trans. Am. Nucl. Soc., 13, 698 (1970).
30. W. M. Stacey, Jr., Space-Time Nuclear Reactor Kinetics, Academic Press, New York, N. Y., 1969.
31. H. Borgwaldt and D. Stegemann, "A Common Theory for Neutronic Noise Analysis Experiments in Nuclear Reactors," Nukleonik, 7, 313 (1965).
32. W. Seifritz and D. Stegemann, "Reactor-Noise Analysis," Journal of the International Atomic Energy Agency, Vol. 9, 1, (1971).
33. J. B. Dragt, "Reactor Noise: A Study of Neutronic Fluctuations in Low-Power Nuclear Reactors, with Special Emphasis on Accurate Time-Domain Analysis," Reactor Centrum Nederland, Petten, Report RCN-101, (Oct. 1968).
34. R. E. Uhrig, Random Noise Techniques in Nuclear Reactor Systems, Ronald Press Co., New York, N. Y., 1970.
35. Trans. Am. Nucl. Soc., 14, 853-860 (1971).
36. E. D. Courant and R. K. Wallace, "Fluctuations of the Number of Neutrons in a Pile," Phys. Rev., 72, 1038 (1947).
37. O. R. Frisch and D. J. Littler, "Pile Modulation and Statistical Fluctuations in Piles," Philosophical Magazine, 45, 126 (1953).
38. V. Raievski, "Fluctuations Statistiques du Nombre de Neutrons dans une Pile," Centre a l'Energie Atomique, Report-917, (1958).
39. W. Matthes, "Statistical Fluctuations and Their Correlation in Reactor Neutron Distributions," Nukleonik, 4, 213 (1962).
40. W. Matthes, "Measurement of the Transfer-Function with Statistical Methods," Nukleonik, 8, 21 (1966).
41. W. Matthes, "Theory of Fluctuations in Neutron Fields," Nukleonik, 8, 87 (1966).
42. W. Matthes, "The Concept of Neutron Importance in Reactor Physics," EURATOM - Report 1897e (1964).

43. A. Dalfes, "A Study of Stochastic Kinetics of Nuclear Reactors," Nukleonik, 4, 299 (1962).
44. A. Dalfes, "The Fokker-Planck and Langevin Equations of a Nuclear Reactor," Nukleonik, 5, 348 (1963).
45. A. Dalfes, "The Correlation Function and Power Spectral Density of Nuclear Reactors," Nukleonik, 6, 53 (1964).
46. A. Dalfes, "Some Considerations on Nuclear Reactor Noise," Nukleonik, 7, 426 (1965).
47. A. Dalfes, "The Random Processes of a Nuclear Reactor and Their Detection," Nukleonik, 8, 94 (1966).
48. A. Blaquiere and R. Pachowska, "Le Bruit de Fond des Réacteurs Nucléaires. Un Modèle Radioélectrique Simple," Comptes Rendus, 251, 2918 (1961).
49. A. Blaquiere, J. Cazemajou, and G. Lapique, "L'équation de Fokker-Planck et la Fonction d'autocorrélation des Réacteurs Nucléaires," Compt. Rend., 253, 2226 (1961).
50. A. Blaquiere and R. Pachowska, "Fluctuations d'un Système Dépendent de Plusieurs Paramètres Aléatoires. Application aux Réacteurs Nucléaires," Centre à l'Energie Atomique, Report-2115 (1962).
51. H. Hurwitz, D. B. MacMillian, J. H. Smith, and M. L. Storm, "Kinetics of Low Source Reactor Startups, I and II," Nucl. Sci. Eng., 15, 166 and 187 (1963).
52. B. Kozik, "Korrelationstheorie der Neutronen in Kernreaktoren," Kernenergie, 9, 373 (1966).
53. B. Kozik, "Correlation of Neutrons in Nuclear Reactors Allowing for Space-Energy Distribution," J. Nucl. En., 21, 293 (1967).
54. W. M. Stacey, Jr., "Stochastic Kinetic Theory for a Space- and Energy-Dependent Zero-Power Nuclear Reactor Model," Nucl. Sci. Eng., 36, 389 (1969).
55. L. Pál, "Statistical Fluctuations of Neutron Multiplication," Proceedings of the Second Geneva International Conference on the Peaceful Uses of Atomic Energy, 16, 687 (1958).
56. L. Pál, "Determination of the Prompt Neutron Period from the Fluctuations of the Number of Neutrons in a Reactor," J. Nucl. En. Parts A/B, 17, 395 (1963).

57. H. Borwaldt and D. Sanitz, "Die Impulskorrelation Zweier Neutronendetektoren in Stationären Reaktor," Nukleonik, 5, 239 (1963).
58. G. I. Bell, "On the Stochastic Theory of Neutron Transport," Nucl. Sci. Eng., 21, 390 (1965).
59. D. R. Harris, M. Natelson, J. A. Galey, and E. Schmidt, "Measurements and Detailed Model Analysis of Space-Correlated Reactor Fluctuations," Nucl. Sci. Eng., 40, 173 (1970).
60. M. M. R. Williams, "An Application of Slowing Down Kernels to Thermal Neutron Density Fluctuations in Nuclear Reactors," J. Nucl. En., 21, 321 (1967).
61. M. M. R. Williams, "Probability Distributions in Simple Neutronic Systems Via the Fokker-Planck Equations," J. Nucl. En., 23, 633 (1969).
62. J. S. Cassell and M. M. R. Williams, "Space Dependent Noise Spectra Via the Transport Equation," J. Nucl. En., 23, 575 (1969).
63. J. K. Vaurio and P. J. Januho, "Stochastic Properties of Nuclear Reactors in a Two-Group Model," J. Nucl. En., 23, 419 (1969).
64. V. V. Bulavin, in "Statistical Methods in Experimental Reactor Kinetics," Reactor Centrum Nederland, Petten, Report RCN-98, 301 (1968).
65. V. G. Zolotukhin, A. Mogil'ner, "Distribution of the Counting of a Neutron Detector Placed in a Reactor," Atomnaya Energiya, 10, 379 (1961).
66. V. G. Zolotukhin, A. Mogil'ner, "Distribution of the Number of Counts on a Neutron Detector Placed in a Reactor," Atomnaya Energiya, 15, 11 (1963).
67. J. B. Dragt, "Threefold Correlations and Third Order Moments in Reactor Noise," Nukleonik, 10, 7 (1967).
68. A. Furuhashi, "Analyzing Neutron Count Trios into Two- and Three-Forked Components," Journal of Nuclear Science and Technology, 6, 156 (1969).
69. H. Borgwaldt, "Einheitliche Theorie der Korrelations-Experimente in Nulleistungsreaktoren," Karlsruhe Institute for Nuclear Research - Report-4/66-5 (1966).
70. M. E. Congdon and R. W. Albrecht, "An Adjoint-Weighting in Neutron Fluctuation Analysis with Emphasis on an Effective Detector Efficiency," Nucl. Sci. Eng., 39, 207 (1970).

71. B. F. Zolotar, "Monte Carlo Analysis of Nuclear Reactor Fluctuation Models," Nucl. Sci. Eng., 31, 282 (1968).
72. C. E. Cohn, "A Simplified Theory of Pile Noise," Nucl. Sci. Eng., 7, 472 (1960).
73. C. E. Cohn, "Reflected-Reactor Kinetics," Nucl. Sci. Eng., 13, 12 (1962).
74. W. B. Davenport and W. L. Root, An Introduction to the Theory of Random Signals and Noises, McGraw-Hill, New York, N. Y., 1958.
75. J. L. Doob, "The Brownian Movement and Stochastic Equations," Annals of Mathematics, 43, 351 (1942).
76. M. N. Moore, "The Determination of Reactor Transfer Functions from Measurements at Steady Operation," Nucl. Sci. Eng., 3, 387 (1958) and Nucl. Sci. Eng., 4, 134 (1958).
77. M. N. Moore, "The Power Noise Transfer Function of a Reactor," Nucl. Sci. Eng., 6, 448 (1959).
78. M. N. Moore, "Noise Field of a Reactor," in Noise Analysis in Nuclear Systems, R. Uhrig, Editor, Univ. of Fla. Press (1964).
79. J. R. Sheff, The Cross Correlation of the Neutron Density Fluctuations at Two Points in a Nuclear Reactor, Ph.D. Thesis, Univ. of Washington, 1965.
80. J. R. Sheff and R. W. Albrecht, "Space Dependence of the Reactor-Noise Spectral-Density Function," in Neutron Dynamics and Control, CONF-650413 (1966).
81. J. R. Sheff, "Space-Dependent Cross Spectral Density in a Bare Cube," in Neutron Noise, Waves, and Pulse Propagation, CONF-660206, 623 (1967).
82. J. R. Sheff and R. W. Albrecht, "The Space Dependence of Reactor Noise I and II," Nucl. Sci. Eng., 24, 246 and 26, 207 (1966).
83. H. S. Carslow and J. C. Jaeger, Conduction of Heat in Solids, Oxford Press, London, p. 373, 1959.
84. J. R. Sheff, "Three-Energy-Group Space-Dependent Spectral Densities," Trans. Am. Nucl. Soc., 12, 709 (1969).
85. A. Z. Akcazu and R. K. Osborn, "Application of Langevin's Technique to Space- and Energy-Dependent Noise Analysis," Nucl. Sci. Eng., 26, 13 (1966).

86. R. J. Johnson and R. N. Macdonald, "Calculation of Space-Dependent Effects in Pile-Oscillator and Reactor-Noise Measurements," in Neutron Noise, Waves, and Pulse Propagation, CONF-660206, 649 (1967).
87. R. N. Macdonald, A Method for the Analysis of Modulated Neutron Experiments, Ph.D. Thesis, Georgia Institute of Technology, Atlanta (1966).
88. C. E. Cohn, R. J. Johnson, and R. N. Macdonald, "Calculating Space-Dependent Reactor Transfer Functions Using Static Techniques," Nucl. Sci. Eng., 26, 198 (1966).
89. T. B. Fowler, M. L. Tobias, and D. R. Vondy, "EXTERMINATOR-II: A Fortran IV Code for Solving Multigroup Neutron Diffusion Equations in Two Dimensions," Oak Ridge National Lab.-4078 (1967).
90. M. Otsuka and T. Iijima, "Space-Dependent Formula for Rossi- $\alpha$  Measurements," Nukleonik, 7, 488 (1965).
91. M. Otsuka and K. Saito, "Space-Time Correlations in Neutron Distributions in a Multiplying Medium," J. Nucl. Sci. Technol., 2, 191 (1965).
92. M. Otsuka and K. Saito, "Neutron Fluctuations in a Multi-Point Reactor," J. Nucl. Sci. Technol., 2, 40 (1965).
93. M. Otsuka and K. Saito, "Neutron Fluctuations in a Multiplying Medium," Nucl. Sci. Eng., 24, 412 (1966).
94. S. Ukai, S. Takeda, and S. Yamada, "A Generalized Analysis of Rossi- $\alpha$  Experiment," J. Nucl. Sci. Technol., 2, 355 (1965).
95. A. Furuhashi and G. Inaba, "Eine Korrektur der Formel für die Rossi- $\alpha$  Methode," J. Nucl. Sci. Technol., 3, 305 (1966).
96. R. K. Osborn and S. Yip, "Physical Theory of Neutron Noise in Reactors and Reactorlike Systems," in Noise Analysis in Nuclear Systems, R. Uhrig, Editor, Univ. of Fla. Press, 1 (1964).
97. M. Natelson and R. K. Osborn, "Kinetic Equations for Neutron Distributions," J. Nucl. En., Parts A/B, 19, 619 (1965).
98. M. Natelson, R. K. Osborn, and F. Shure, "Recent Developments in the Analysis of Neutron-Noise Experiments," in Neutron Noise, Waves, and Pulse Propagation, CONF-660206, 669 (1967).
99. R. K. Osborn and A. Z. Akcazu, "Some 'Theorems' on Neutron Fluctuations and Fluctuation Spectra," in Neutron Dynamics and Control, CONF-650413, 531 (1966).

100. M. Natelson, R. K. Osborn, and F. Shure, "Space and Energy Effects in Reactor Fluctuation Experiments," J. Nucl. En., Parts A/B, 20, 557 (1966).
101. R. W. Albrecht and W. Seifritz, "The Information of Neutron Fluctuations," Nucl. Sci. Eng., 41, 417 (1970).
102. E. L. Fuller and D. A. Meneley, "Weighted-Residual Methods in Space-Dependent Reactor Dynamics," Nucl. Sci. Eng., 40, 206 (1970).
103. D. D. Ebert and L. J. Gallaher, "An Analytic Solution of the Space-Dependent Coherence Function," Trans. Am. Nucl. Soc., 14, 195 (1971).
104. D. H. Lennox, B. I. Spinrad, W. N. Kelber, R. H. Armstrong, and W. L. Kolb, "The Argonaut Reactor: A Generalized Reactor Facility for Nuclear Technology Training and Research," 2nd U. N. Intern. Conf. Peaceful Uses At. En., 10, 265 (1958).
105. D. R. Back, et al., "Comparison of Knolls Atomic Power Laboratory Clean Critical and Subcritical Experiments with Calculations," in Exponential and Critical Experiments, Vol. II, p. 391, IAEA, Vienna (1964).
106. M. R. Mendelson, "Monte Carlo Criticality Calculations for Thermal Reactors," Nucl. Sci. Eng., 32, 319 (1968).
107. G. Kussmaul, "Theoretische und Experimentelle Untersuchungen zum Zweipunktreaktor," Institut für Neutronenphysik und Reaktortechnik, Kernforschungszentrum Karlsruhe, Report INR-4/68-17 (Feb. 1968).
108. D. J. McGoff, "FORM: A Fourier Transferred Fast Spectrum Code for the IBM-709," North American Aviation-SR-MEMO-5766 (1960).
109. R. Shudde and J. Dyer, "TEMPEST-II," NAA-AMTD-111 (1961).
110. F. N. McDonnell and M. J. Harris, "Pulsed-Source Experiments in a Reflected Coupled-Core Reactor," Trans. Am. Nucl. Soc., 14, 864 (1971).
111. J. R. Penland, N. J. Ackermann, Jr., and S. H. Hanauer, "Space- and Energy-Dependent Reactor Noise Measurements," Trans. Am. Nucl. Soc., 14, 854 (1971).
112. N. J. Ackermann, J. R. Penland, and S. H. Hanauer, "A Space- and Energy-Dependent, Four-Nodal Point Neutron Fluctuation Theory," Trans. Am. Nucl. Soc., 14, 854 (1971).
113. J. C. Robinson and M. L. Alexander, "Calculation of Reactor Noise Spectra Using a Space-Energy-Dependent Model: Comparison with Experiment," Trans. Am. Nucl. Soc., 14, 856 (1971).

114. D. D. Ebert, J. D. Clement, and W. M. Stacey, Jr., "Coherence Function Analysis in Coupled Cores Using Modal Expansions," Trans. Am. Nucl. Soc., 14, 858 (1971).
115. S. Kaplan, "The Property of Finality and the Analysis of Problems in Reactor Space-Time Kinetics by Various Modal Expansions," Nucl. Sci. Eng., 9, 357 (1961).
116. R. A. Danofsky, "Cross Power Spectral Measurements in the Two-Core University Training Reactor-10," in Noise Analysis in Nuclear Systems, R. Uhrig, Editor, Univ. of Fla. Press, p. 229 (1964).
117. C. D. Kylstra and R. E. Uhrig, "Measurement of the Spatially Dependent Transfer Function," in Noise Analysis in Nuclear Systems, R. Uhrig, Editor, Univ. of Fla. Press, p. 285 (1964).
118. J. A. Burke, Personal Communications, Knolls Atomic Power Laboratory, (Dec. 1970).
119. Programmers Reference Manual for the UNIVAC1108-EXEC8 Executive System, Rich Electronic Computer Center, Georgia Institute of Technology, Atlanta, Ga. (April 1, 1969).
120. J. M. Reynolds, Personal Communications, Atlanta (Nov. 1970).
121. J. M. Reynolds and J. D. Clement, "Efficient Digital Reactor Noise Analysis Through Averaging FFT-Computed Periodograms," Trans. Am. Nucl. Soc., 14, 192 (1971).
122. R. C. Kryter, "On-Line Reactor Noise Spectrum Computation with a Fast Fourier Transform Algorithm," Trans. Am. Nucl. Soc., 12, 291 (1969).
123. J. C. Robinson, "Analytical Determination of the Neutron Flux-to-Pressure Frequency Response: Application to the Molten-Salt Reactor Experiment," Nucl. Sci. Eng., 42, 382 (1970).
124. J. C. Robinson and D. N. Fry, "Experimental Neutron Flux-to-Pressure Frequency Response for the Molten-Salt Reactor Experiment: Determination of Void Fraction in Fuel Salt," Nucl. Sci. Eng., 42, 397 (1970).
125. T. Gozani, "The Concept of Reactivity and its Application to Kinetic Measurements," Nukleonik, 5, 55 (1963).
126. L. R. Foulke, A Modal Expansion Technique for Space-Time Reactor Kinetics, Ph.D. Thesis, MIT (1966).
127. J. R. Lamarsh, Introduction to Nuclear Reactor Theory, Addison-Wesley, Reading, Mass., p. 554, 1966.

128. J. M. Betancourt, Analysis of Coupled Core Reactors Using the Natural Mode Approximation, Ph.D. Thesis, Iowa State Univ. (1968).
129. E. L. Wachspress, Iterative Solution of Elliptic Systems, Prentice-Hall, Inc., Englewood Cliffs, N. J., p. 20, 1966.
130. R. L. Ewen, "MULE - A Fortran Program for the Calculation of Three Types of Overtone Modes," WAPD-TM-369, October 1963.
131. D. R. Edwards and K. F. Hansen, "The Stabilized March Technique Applied to the Diffusion Equation," Nucl. Sci. Eng., 25, 58 (1966).
132. R. A. Danofsky, "Observation of Coupled-Core Characteristics by Noise-Measurement Techniques," Trans. Am. Nucl. Soc., 14, 855 (1971).
133. A. F. Henery and A. V. Volta, "WIGL2 - A Program for the Solution of the One-Dimensional, Two-Group, Space-Time Diffusion Equations Accounting for Temperature, Xenon and Control Feedback," WAPD-TM-532 (Oct. 1965).
134. J. B. Yasinsky, M. Natelson, and L. A. Hageman, "TWIGL - A Program to Solve the Two-Dimensional, Two-Group, Space-Time Neutron Diffusion Equations with Temperature Feedback," WAPD-TM-743 (Feb. 1968).
135. N. J. Ackermann, Jr., A. R. Buhl, and R. C. Kryter, "An Analytical and Experimental Evaluation of Subcriticality Measurements by the Polarity Spectral Coherence Method," Trans. Am. Nucl. Soc., 14, 44 (1971).
136. W. M. Stacey, Jr., Modal Approximations: Theory and an Application to Reactor Physics, MIT Press, Cambridge, Mass., 1967. Also, "A General Modal Expansion Method for Obtaining Approximate Equations for Linear Systems," Nucl. Sci. Eng., 28, 438 (1967).
137. S. Kaplan, "Synthesis Methods in Reactor Analysis," Advances in Nuclear Science and Technology, 3, 233 (1965).
138. S. Kaplan, O. J. Marlowe, and J. Bewick, "Application of Synthesis Techniques to Problems Involving Time Dependence," Nucl. Sci. Eng., 18, 163 (1964).
139. Ivar Stakgold, Boundary Value Problems of Mathematical Physics, MacMillan Co., New York, N. Y., p. 65, 1967.
140. G. Arfken, Mathematical Methods for Physicists, Academic Press, New York, N. Y., p. 595, 1966.

141. W. C. Nodean, The Response of a Coupled Core Reactor to a Localized Oscillation of the Absorption Cross Section, Ph.D. Thesis, Iowa State Univ. (1969).
142. B. Carnahan, H. Luther, and J. Wilkes, Applied Numerical Methods, Wiley and Sons, Inc., New York, N. Y., p. 179, 1969.
143. J. W. Cooley and J. W. Tukey, "An Algorithm for the Machine Calculation of Complex Fourier Series," Mathematics of Computations, 19, 297 (1965).
144. W. M. Gentleman and G. Sande, "Fast Fourier Transforms for Fun and Profit," Joint Computer Conf. AFIPS Proc., 29, 563 (1966).
145. J. W. Cooley, "Applications of the Fast Fourier Transform Method," Proc. IBM Computing Symp. (1966).
146. P. D. Welch, "The Use of Fast Fourier Transform for the Estimation of Power Spectra: A Method Based on Time Averaging Over Short, Modified Periodograms," IEE. Trans. Audio Electroacoustics, AU-15, 70 (1967).
147. R. C. Singleton, "On Computing the Fast Fourier Transform," Commun. ACM, 10, 647 (1967).
148. David S. Gooden and T. F. Parkinson, "Regional-Dependent Reactor Kinetics," Nucl. Sci. Eng., 46, 169 (1971).
149. R. H. Jones, "A Reappraisal of the Periodogram in Spectral Analysis," Technometrics, 7, 531 (1965).
150. D. D. Ebert, J. M. Reynolds, and J. D. Clement, "Coherence Function Measurements and Analyses in Tightly and Loosely Coupled Cores," Trans. Am. Nucl. Soc., 14, 1, 196 (1971).
151. W. E. Schiesser, "Statistical Uncertainty of Frequency Response Determined from Random Signals," TM711-C-2, Weston Instruments, Inc., (1966).
152. R. A. Rydin, Personal Communications, University of Virginia (Nov. 1971).
153. W. M. Stacey, Jr., Personal Communications, Argonne National Laboratory (Dec. 1971).
154. M. M. El-Zeftawy and L. Ruby, "Kinetic Distortion in a TRIGA Reactor with an Asymmetric Reflector," Nucl. Sci. Eng., 45, 335 (1971).

## VITA

David Dean Ebert was born on August 9, 1940 in Watertown, Wisconsin. He attended Watertown High School and graduated in 1958. Mr. Ebert attended the University of Wisconsin where he received a Bachelor of Science degree in Applied Mathematics and Engineering Physics in January, 1963.

In January, 1963 he was employed by the National Aeronautics and Space Administration in Cleveland, Ohio as an aerospace scientist. While at NASA, he worked on the core physics analysis of a tungsten-water nuclear rocket concept.

Mr. Ebert left NASA to attend graduate school at the Georgia Institute of Technology in September of 1963. He received a Master of Science degree in Nuclear Engineering from Georgia Tech in June, 1965. During the summer of 1964, he participated in the Engineering Practice School program at Argonne National Laboratory.

In the fall of 1964, Mr. Ebert began work as an experimental reactor physicist at Knolls Atomic Power Laboratory in Schenectady, New York. He left KAPL in September, 1967 to work on a doctorate in Nuclear Engineering at Georgia Tech. This graduate study was supported by an Atomic Energy Commission Traineeship and a Graduate Research Assistantship. Mr. Ebert also taught a course in modern physics at Georgia State University and supervised a reactor physics laboratory class at Georgia Tech during this time. While pursuing his studies at Georgia Tech, Mr. Ebert worked on his dissertation at Argonne National Laboratory during the summers of

1970 and 1971 under the guidance of Dr. Weston M. Stacey, Jr. The work at ANL was supported in part by the Argonne Center for Educational Affairs.

Mr. Ebert is a member of the American Nuclear Society and the Society of the Sigma Xi.